Aus dem Institut für Biowissenschaften
der Universität Rostock

EFFECT OF TEMPERATURE ON THE ELECTROROTATION BEHAVIOR OF HUMAN RED BLOOD CELLS

Dissertation
zur
Erlangung des akademischen Grades
doctor rerum naturalium (Dr. rer. nat.)
der
Mathematisch-Naturwissenschaftlichen Fakultät
der Universität Rostock

vorgelegt von
Jutiporn Sudsiri
geboren am 01.09.1972 in Trang – Thailand

Rostock, den 15 Januar 2011

urn:nbn:de:gbv:28-diss2011-0121-2

1. Gutachter: Prof. Dr. Dieter G. Weiss
2. Gutachter: Prof. Dr. Christiane Helm
3. Gutachter: Prof. Dr. Monika Fritz

Tag der Verteidigung: 05.07.2011

Table of contents

Table of contents iii

Dedication vi

List of publications vii

List of Abbreviations viii

Zusammenfassung ix

Abstract xi

1. Introduction 1
    - 1.1 The dielectric properties of biological materials 1
    - 1.2 General strategies for modelling the dielectric properties of biological cells 2
    - 1.3 Dielectric techniques 3
    - 1.4 Electrorotation 3
    - 1.5 Model interpretation of ER 5
    - 1.6 Effect of temperature on ER investigation 7
    - 1.7 Influence of temperature on membrane transport 8
    - 1.8 Influences of temperature on activation energy and ion diffusion across membrane 9
    - 1.9 Influences of temperature on cell volume 11
    - 1.10 Relation of cell volume and cell shape changes in HRBCs 13
    - 1.11 Influence of cell volume on cytoplasmic conductivity 15
    - 1.12 Influence of cytoplasmic concentrations on cytoplasmic conductivity 16
    - 1.13 Effect of the solvent on ion mobility at infinite dilution 19
    - 1.14 Proposal 20

2. Theory 22
    - Theoretical calculations of the temperature dependence of ER spectra 22

3. Materials and methods 27
    - 3.1 Preparation of solutions 27
        - 3.1.1 Phosphate Buffer (PB) solutions 27
        - 3.1.2 Measuring solutions 27
        - 3.1.3 DIDS solution 29
    - 3.2 Preparation of red blood cells 29
    - 3.3 Preparation of the cell suspension for ER measurement 30
    - 3.4 Microscopic observation and measurement of cell radii 30
    - 3.5 ER measurements 30
    - 3.6 Interpretation of ER spectra 32
    - 3.7 DIDS treatment 33

3.8 Volume experiments 33
3.9 Hematocrit 33
3.10 Red cell count 33
3.11 Determination of cell water 34

4. Results 35
- 4.1 Measuring solutions 35
  - 4.1.1 Conductivity of solutions 35
  - 4.1.2 Ionic strength of the solutions 36
  - 4.1.3 Equivalent conductivity of solutions 37
  - 4.1.4 Viscosity of solutions 38
  - 4.1.5 A relation of molar conductivity to viscosity 40
- 4.2 ER measurement 41
  - 4.2.1 Effect of external conductivities on the ER spectrum 41
  - 4.2.2 Effect of temperature on ER spectrum 44
  - 4.2.3 The anomalous rotation speed at 15 °C 49
- 4.3 Cell volume and cell water of HRBCs 49
  - 4.3.1 Effect of external media on cell volume and cell water 49
  - 4.3.2 Effect of temperature on cell volume and cell water 52
- 4.4 Influence of cell volume on cytoplasmic conductivity 55
- 4.5 Influence of external media and temperatures on cell shape 62
- 4.6 Cell parameters of HRBCs obtained from the interpretation of the FEM 67

5. Discussion 71
- 5.1 Solutions 71
  - 5.1.1 Conductivity of solutions 71
  - 5.1.2 Ionic strength of the solutions 71
  - 5.1.3 Equivalent conductivity of solutions 71
  - 5.1.4 Viscosity of solutions 72
  - 5.1.5 A relation of molar conductivity to viscosity 73
- 5.2 ER measurement 74
  - 5.2.1 Effect of external conductivities on ER spectrum 74
  - 5.2.2 Effect of temperature on ER spectrum 74
  - 5.2.3 The anomalous rotation speed at 15 °C 76
- 5.3 Cell volume and cell water of HRBCs 77
  - 5.3.1 Effect of external media on cell volume and cell water 77
  - 5.3.2 Effect of temperature on cell volume and cell water 80
- 5.4 Cytoplasmic conductivity of HRBCs 81
  - 5.4.1 Temperature coefficient of cytoplasmic conductivity 83
  - 5.4.2 Cytoplasmic limiting molar conductivity of human red blood cells 84
- 5.5 Influence of external media and temperatures on cell shape 85
- 5.6 Cell parameters of human red blood cells obtained from the interpretation of the FEM 86
  - 5.6.1 Cytoplasmic conductivity 86
  - 5.6.2 Cytoplasmic permittivity 88
  - 5.6.3 Membrane conductivity 88

        5.6.4 Membrane permittivity 89
    5.7 Summary and Conclusions 89

6. Appendix 92
    6.1 An introduction to dielectric theory 92
    6.2 A basic theory of interactions of a spherical particle with an electric field 94
        6.2.1 Effective dipole moment 94
        6.2.2 Theory for particle rotation 96
    6.3 Biological electrolytes 98

7. References 101

8. Acknowledgements 108

Curriculum vitae 110

Selbständigkeitserklärung 115

Dedication

This work is dedicated to my parents, my sun, Puttimeath Chuaibamrung, and my husband Capt. Suriya Chuaibamrung who by the time I finished my studies, were able to understand, encourage and forgive me for spending not so much time with them.

List of Publications

Parts of this thesis were included in the following publications:

Original Papers

1. J. Sudsiri, D. Wachner, J. Donath, and J. Gimsa. 2002. Can molecular properties of human red blood cells be accessed by electrorotation ? Songklanakarin J. Sci. Technol. 24: 785-789
2. J. Sudsiri, D. Wachner, M. Simeonova, J. Donath, and J. Gimsa. 2006. Effect of temperature on the electrorotation behavior of human red blood cells. J. of Technology Malaysia. 44(F): 1-12.
3. J. Sudsiri, D. Wachner, and J. Gimsa.2007. On the temperature dependence of the dielectric membrane properties of human red blood cells. Bioelectrochemistry. 70:134-140.

List of Abbreviations

C_m	membrane capacitance	(F/m^2)
DEP	dielectrophoretic	
DIDS	4,4'- diisothiocyanostilbene-2,2' disulphonate	
d	membrane thickness	(m)
e_0	electronic charge = 1.602×10^{-19}	(C)
ER	electrorotation	
F	Faraday's constant =9.6484×10^4	$(C \cdot mol^{-1})$
f_{c1}	first characteristic frequency of ER peak	
f_{c2}	second characteristic frequency of ER peak	
FEM	finite element model	
Hct	hematocrit	
I	ionic strength of the solutions	$(molL^{-1})$
$\mathrm{Im}\, K^*$	imaginary part of Clausius-Mossotti-Factor	
K^*	Clausius-Mossotti factor	
k_B	Boltzmann's constant = 1.38×10^{-23}	$(J\ K^{-1})$
L	Avogadro's number = 6.022×10^{23}	(mol^{-1})
MCV	mean cell volume	
PCV	packed cell volume	
Q_{10}	temperature coefficient	
R	molar gas constant = 8.3145	$(J\ mol^{-1}\ K^{-1})$
R_1	first ER peak	
R_2	second ER peak	
T_{fric}	hydrodynamic friction	
T_{ER}	electrorotation torque	
u	a mobility of ions	$(m^2\ s^{-1}\ V^{-1})$
Z^i	impedance of cell cytoplasm	Ω
Z^m	impedance of cell membrane	Ω
Z^e	impedance of external medium	Ω
Λ^0	equivalent conductivity at infinite dilution	(Sm^2mol^{-1})
Λ	molar conductivity for individual ion specie	(Sm^2mol^{-1})
$\prod$	osmotic pressure	(Pa)
β	electro-osmotic permeability	$(cm^3\ C^{-1})$
η	viscosity of solution	(mPa.s)
ε	dielectric permittivity relative to free space	(F/m)
ε_0	dielectric permittivity of vacuum =8.854×10^{-12}	(F/m)
δ	dilution coefficient	
ω	angular frequency	(rad/s)
τ	relaxation time	(s)
σ	electrical conductivity	(S/m)
ξ	normalized influential cell radius	

Zusammenfassung

Auf biologische Zellen wirkende Temperatureffekte können die physiologischen Funktionen sowie biochemischen Parameter eines ganzen Organismus beeinflussen. Diese Effekte führen zu Änderungen der chemischen Zusammensetzung und damit der Eigenschaften der Membranen und des Zytoplasmas.

Es war das Ziel dieser Arbeit, den Effekt der Temperatur auf dielektrische Parameter (σ und ε) von roten Blutzellen des Menschen (Human Red Blood Cells, HRBCs) zu untersuchen.

Die Messungen wurden an den Zellen in physiologischen Medien mit Leitfähigkeiten von 0,02 bis 3 S/m und bei Temperaturen zwischen 10 und 35°C durchgeführt. In einer Messkammer wurde zwischen vier Mikrochipelektroden ein elektrisches Wechselstrom-Feld (Frequenzbereich von 10 kHz bis 250 MHZ) etabliert. Die Elektrorotations(ER)-Spektren wurden zuerst mittels einer Lorentz-Anpassung korrigiert.

Folgende Ergebnisse wurden erzielt: Die Kennfrequenzen (f_{c1}, f_{c2}) und die Umdrehungsgeschwindigkeiten (R_1, R2) der ER-Peaks erhöhten sich mit steigender Temperatur. Die erfassten f_{c1}, f_{c2}, R_1 und R_2 wurden mit dem Modell für abgeflachte einschalige Zellen von Gimsa et al. (Biophys. J. (1999) 77:1316-1326) ebenfalls korrigiert und dargestellt. Zieht man die theoretischen Standardtemperatur-Abhängigkeiten für alle Mittelparameter in Betracht, so konnten die experimentell ermittelten Punkte nur für ein schmales Leitfähigkeitband von 0,20 bis 0,50 S/m bei einer Temperaturspanne von 20 bis 25 ^{o}C korrigiert werden. Für andere untersuchte Lösungen und Temperaturen wurden Abweichungen der experimentellen Punkte von den theoretischen Kurven gefunden. Auch konnten Effekte bezüglich des Zellvolumens und -radius aufgrund geänderter Eigenschaften von Medium und Temperaturveränderungen gefunden werden. Es wurde gefunden, dass sich das Zellvolumen und -wasser im Leitfähigkeitsbereich zwischen 0,20 und 0,50 S/m erhöht. Innerhalb dieses Leitfähigkeitsbereiches verformten sich die Zellen des Zellradius nahm zu. Bei Leitfähigkeiten höher als 0,50 S/m nahm das Zellvolumen und -wasser ab. Unter diesen Bedingungen änderten die Zellen ihre normale Form in die Echinozyten-Form, so dass auch hier eine Abnahme des Zellradius festgestellt wurde. Mit steigender Temperatur konnte für alle untersuchten Lösungen eine Zunahme von Zellvolumen und -radius belegt werden. Die Änderungen des Zellvolumens und -wassers führten zu einer Änderung der inneren Jonenkonzentrationen. Die molaren zytoplasmatischen Leitfähigkeiten

wurden auf der Grundlage der Debye-Hückel-Onsager-Relation entsprechend der „Regel für zytoplasmatische Viskosität" von Walden unter Berücksichtigung der [K^+], [Na^+] und [Cl^-] errechnet. Bei der Interpretation der ER-Spektren mittels des Ein-Schalen-Modells, unter Berücksichtigung der gemessenen Zellradien und -formen, konnten temperaturabhängige Parameter festgestellt werden. Es wurde Eine exponentielle Relation der zytoplasmatischen Leitfähigkeit zur Temperatur mit einem Koeffizienten von 0.059/°C gefunden. Unter physiologischen Standardbedingungen (37°C, 157 mM NaCl, σ_{37} = 1.50 S m^{-1}) war die Leitfähigkeit, σ_{37} = 1.519 ± 0.0451. Die Leitfähigkeit der HBRC steigt um einen Faktor von 1.985 ± 0.0226 für jede Temperaturerhöhung von 10°C. Damit ist der Q_{10}-Wert für die cytoplasmatische Leitfähigkeit $Q_{10} \approx 2$, ein typischer Wert für viele biologische Systeme. Die zytoplasmatische Permittivität ist mit einem Koeffizienten von -0.003/°C linear von der Temperatur abhängig.

Dieser deutliche Temperatureffekt muß vor allem in Experimenten berücksichtigt werden, bei denen die Zellen mittels elektrischer Felder bewegt werden, weil bei physiologischen Ionenkonzentrationen Joule'sche Wärme entsteht.

Abstract

Temperature effects on biological cells have many implications affecting the biochemical composition and physiological functions of the cell and perhaps of the whole organism.

It is the aim of this work to analyze the effects of temperature on dielectric parameters of Human Red Blood Cells (HRBCs).

The cells were suspended in external media with conductivities ranging from 0.02 to 3.00 S/m NaCl and observed at temperatures between 10 °C and 35 °C. An AC electric field with a frequency range from 10 kHz to 250 MHz was applied to a 4-electrode micro-chip chamber which was fabricated on glass chips by laser ablation of a platinum layer. The electrorotation (ER) spectra were first fitted using Lorentzian peak-fitting techniques.

The characteristic frequencies (f_{c1}, f_{c2},) and the rotation speeds (R_1, R_2) of ER peaks were found to increase with rising temperature. To obtain cell parameters at measuring temperature, the obtained f_{c1}, f_{c2}, R_1 and R_2 from the interpretation were fitted with the oblate single shell model for HRBC presented by Gimsa et al. (Biophys. J. (1999) 77:1316-1326). The starting value (at temperature 23°C) was also taken there from. Taking the standard temperature dependencies for all media parameters into account, the experimental points could only be fitted in a narrow conductivity range from around 0.20 S/m to 0.50 S/m at a temperature range from 20 °C to 25 C. For other observed solutions and temperatures, deviations of the experimental points from the theoretical curve were found. Effects on cell volume and cell radius according to changed external media and temperature were then taken into consideration. Increases in cell volume and cell water were observed at conductivities around 0.20 S/m to 0.50 S/m. At this conductivity range, the cells change shape, and an increase in cell radius was observed. For conductivities higher than 0.50 S/m, decreases in cell volume and cell water were found. Under these conditions, the cells turned into echinocytes and decreased in cell radius. With rising temperature, an increase in cell volume and cell radius was observed for all experimental solutions. The alterations of cell volume and cell water led to a change in the interior ionic concentration. Therefore, cytoplasmic conductivity of HRBCs was calculated using internal [K^+], [Na^+] and [Cl^-] and the Debye-Hückel-Onsager relation. Corrections using Walden's rule of viscosity were essential for valid estimates of conductivity. Cytoplasmic conductivity of HRBC is not a constant. An exponential relationship of the cytoplasmic conductivity to temperature with

a coefficient of 0.059/°C was found. Under standard physiological conditions (37°C, 157 mM NaCl, σ_{37} = 1.50 S m^{-1}) the conductivity was, σ_{37} = 1.519 ± 0.0451. HBRC conductivities increase by a factor of 1.985 ± 0.0226 for every increase in temperature of 10°C. This value of cytoplasmic conductivity, $Q_{10} \approx 2$, is a typical value found in many biological systems. The cytoplasmic permittivity is linearly related to temperature with a coefficient of -0.003/°C.

The strong temperature effect needs to be taken into account in experiments where cells are moved using electric fields because of Joule heating at physiological ion concentrations.

1 Introduction

1.1 The dielectric properties of biological materials

Investigation of dielectric properties of biological cells began more than 100 years ago. The scientists of those days assumed that biological cells behaved like an electrically conducting object. They were thought to consist of layers of materials with largely different dielectric properties. When they were suspended in a medium with different dielectric properties and exposed to an external electric field, these differences led to charge accumulation at their interfaces. Such behaviour is called electrical polarization, which is due to various effects, ranging from charge accumulation at the surfaces between materials with different electrical properties (interfacial polarization) to dipole orientation and other effects [1]. The interfacial polarization was first described by Maxwell [2], who modelled mixed dielectrics in terms of layers of materials. The next major advance was by Wagner [3] who modelled the dielectric properties of dilute suspensions of spheres immersed in a material with different dielectric properties. Interfacial polarizations are often called Maxwell–Wagner polarizations after the two major early contributors to the field.

The response of a biological cell to an applied electric field is characterized by two parameters i.e. the electrical conductivity (σ, in S/m) and the dielectric permittivity relative to free space (ε, in F/m). The conductivity is defined as the conductance, G of a unit volume of matter. It gives a measure of its ability to conduct electrons, i.e. let charge pass through it, whereas the dielectric permittivity is the capacitance, C of a unit volume of matter. It gives a measure of the polarizability of the material, i.e. its ability to store charge. Permittivity is often expressed as the relative permittivity (or dielectric constant, dimensionless), which is defined as the permittivity relative to that of vacuum (ε_0 =5.854 x 10^{-12} F/m): $\varepsilon_r = \varepsilon/\varepsilon_0$. Because the energy in the electric field is either stored by polarization of the material's components or lost by frictional motion of the constituent charge carriers and turned into heat (resistive loss), conductivity and permittivity are related. They are often expressed as the complex permittivity ε^* and conductivity σ^* to take advantage of this fact in theoretical calculations: $\varepsilon^* = \varepsilon - j\sigma/\omega$ or, equivalently: $\sigma^* = \sigma + j\omega\varepsilon$, where ω is the radial frequency (rad/s) of the applied electric field and $j = \sqrt{-1}$. For most substances, the permittivity and conductivity are only constant over a limited frequency range. The general tendency is for permittivity to fall, and conductivity to concomitantly increase, in a series of steps as frequency increases. These step changes are called dispersions, and each one reflects the loss of a particular polarization process at increasing frequencies. Biological materials can show quite large dispersions, especially at low frequencies. These are mainly caused by interfacial polarizations at the surfaces between the different materials of which a cell is composed. Reviews of the dielectric properties of cells and the different dispersions that occur have been given in the literature [1, 4–8].

1.2 General strategies for modelling the dielectric properties of biological cells

Cells have a heterogeneous structure, containing different materials with different dielectric properties. They have a similar structure consisting of cytoplasm surrounded by a membrane. The membrane surrounding the cell has a lipid bilayer structure. It is extremely thin (4–10 nm in thickness) and has incorporated into it large amounts of proteins. However, the effect of proteins and water on the membrane dielectric properties is unclear. As a result, the value of the membrane's relative permittivity has been given values ranging from about 2 to 10 [6, 9-10]. Transport of ions through the membrane is highly regulated by transmembrane channel proteins, and under normal circumstances, the membrane can be regarded as highly non-conducting. The cytoplasm is also highly complicated, particularly in eukaryotic cells. It contains not only large amounts of salts, proteins, nucleic acids, and smaller molecules but in many cases (e.g. eukaryotes) various membranous structures (e.g. nucleus, vacuoles, endoplasmic reticulum membranes) and membrane-bound organelles such as mitochondria and chloroplasts which can also affect the dielectric properties. The value of the inside relative permittivity has been attributed values ranging from about 50 to over 200 [4,-11-12] (compare pure water $\varepsilon_r = 79$). As a first approximation, however, the cytoplasm can be considered to be a highly conducting salt solution with a large concentration of dissolved organic material. For exploratory studies, human red blood cells were chosen as a simple model cell for experiments because insights gained on these very simple cells could be applied to more complex cells. It was found that the electrical properties of such cells greatly differed from those of simple electrolyte solutions. For example, Stewart [13] measured the resistance of red blood cells suspended in a conducting medium and found that at low frequencies erythrocytes behaved as non-conducting particles. The approach usually taken to model them is to replace the particle with a hypothetical particle of known size, shape, and distribution of charges and/or materials (for example in shells). Using this model, an overall 'equivalent homogeneous complex permittivity ε^* or conductivity σ^*' is calculated for the particle.

1.3 Dielectric techniques

As electrical technology improved, dielectric studies encompassed a steadily increasing range of frequencies and a variety of types of cells, and more attempts were undertaken to understand the underlying mechanisms. Studies of the dielectric properties of biological materials remain an interesting area of research. The determination of the parameters became easier which has encouraged increased efforts in this field. However, even though there are still many problems remaining to be solved, it was possible to measure electrical parameters of cells by observing their mechanical response to an applied electric field. It was also interesting to investigate their frequency-dependence responses to AC-fields, which leads to valuable information on the structure polarization effects which characterized by a variety of characteristic frequency-dependences known as dielectric dispersion. The interaction between the induced polarization and the external field produces various electro kinetic effects [14-16]. The dielectric polarization effects in a non-uniform electric field produces a dielectrophoretic (DEP) force. The force drives the particles away from regions of high electric field strength. A rotating field, in contrast, will induce the particle to spin, a phenomenon called electrorotation (ER). Experiments to analyze the frequency dependence of rotations of cells in a rotating electric field are experimentally easier to set up. Whereas, DEP measurement experiments have the disadvantage of requiring an asymmetric electric field, ER measurements are relatively easy to set up and it can be carried out on single cells exposed to a rotating electric field.

1.4 Electrorotation

ER has become a very powerful diagnostic technique for the measurement of certain critical dielectric properties of cells. It offers a means to study single cells *in vitro,* and allows investigation of the dielectric properties of single biological cells without irreversible damage. The technique of ER whereby a particle is induced to rotate in response to an applied rotating electric field has become widely utilized for characterizing the dielectric properties of suspended bioparticles [17–21]. Because of its intrinsic biochemical noninvasiveness, ER has been employed for characterizing live mammalian cells [12–15], yeast cells [4, 17, 18] and bacteria [19] as well as other bio-particles including liposomes [20] and protoplasts [21] without introducing any destructive interactions. Because of its single-cell resolution, ER allows the dielectric properties of selected particles or cells to be determined within heterogeneous mixtures and this represents a significant advance over more conventional bulk dielectric methods for biological determination because typical cell samples are intrinsically heterogeneous. The reason for the observable cell rotation is that the applied electric field induces a dipole moment of the cell. Cell rotation exhibits a threshold value of the electric field and occurs only if certain conditions concerning the electric properties of the cell and of the external medium are satisfied [22]. Lampa [23] was the first to set out the general conditions required for spontaneous rotation. Arnold and Zimmermann [24, 25] were the first to introduce a single cell into a rotating electric field using a four electrodes arrangement. In their experiments, the rotation speed of the cell was found to be frequency dependent and linearly dependent on the square of the field strength for any experimental frequency. In such experiments, cells at a very low concentration are suspended in electrolyte medium and exposed to a rotating electric field. The field induces a complex rotating dipole moment in the cell. It consists of a component that is in-phase to the external field (the real part) and a component out-of-phase to the external field (the imaginary part). For a given field frequency the dipole moment depends on the relative polarizability of the cell and external medium (the bulk electrolyte). The interaction of the out-of-phase part of the induced dipole moment with the external field leads to a torque, which can be observed microscopically as the rotation of individual cells. The measured parameter is the rotation speed, which is a function of the external field frequency, ordinarily with the electric field strength held constant. If the properties of the external medium and the cell geometry are known, the electric properties of the cell and its compartments, i.e. conductivities and permittivities can be inferred from the frequency dependence of the cell rotation speed and its direction [15, 17]. These pioneering works were followed by many theoretical or applied contributions. The experimental methods and data analysis used to characterise the rotation of single cells in a rotating field are well established [26-40].

1.5 Model interpretation of ER

A general model has been developed to investigate dielectric properties of cells using ER. The simplest model is to consider cells as a homogeneous spherical single shell covered by a homogeneous membrane. In this case, the radius of the cell and the membrane thickness as geometrical parameters are included in the corresponding equations, as well as the conductivities and the permittivities of the membrane, the cytoplasm, and the external medium. These model considerations indicated that the peak of the antifield rotation in its frequency position, and its amplitude, reflects the membrane properties of the cell. This first-characteristic-frequency is determined by the time constant of membrane charging. The maximum of the cofield rotation, i.e. the second-characteristic-frequency, indicates conductivity and permittivity of the cytoplasm in relation to that of the external milieu. Nevertheless, since most biological cells are not a simple homogeneous sphere, proper models for other cell geometries were then pursued. For example, the finite element model (FEM) developed by Gimsa and Wachner [34] for human red blood cells (HRBC) was used in the present study. The Gimsa and Wachner model [34] treats the HBRC as approximating an oblate spheroid in shape.

For a spherical cell of radius R, the rotation speed of a cell, is determined by the equilibrium of hydrodynamic friction T_{fric} and ER torque T_{ER}. Using Stoke's law, the friction for an oblate spheroid of axes ratio $a:b:c$ = 2:2:1, rotating around axis c at ω_c under laminar flow conditions is given by [41]:

$$T_{fric} = 5.64\,\pi\,\eta\,a^3\omega_c \tag{1.5.1}$$

Note however, that the axis ratio used in Equation 1.5.1 has been derived from the dielectric cell data [34]. It is an effective axes ratio that best fits the experimental data to the model. A more realistic ratio of $a:b:c$ = 3:3:1 (based on the actual geometry of human red blood cells) would result in a T_{fric} coefficient of 4.88. Nevertheless, Eq. 1.5.1 does not take the surface friction into account which will increase for more oblate shapes. The ER torque is proportional to the cell volume, the square of the electric field strength E, and Clausius-Mossotti factor K^* (for the definition of K^* please refer to [33]):

$$T_{ER} = \frac{4\pi a^2 c}{3}\varepsilon_0\,\varepsilon_e\,E^2\,\mathrm{Im}(K^*) \tag{1.5.2}$$

ε_0 and ε_e are the permittivity of vacuum and the relative permittivity of the external medium, respectively. The asterisk marks the complex Clausius-Mossotti factor. Usually, the external field strength in the centre of a four-electrode ER chamber is calculated from the applied voltage and the electrode tip distance. Nevertheless, the actual field strength is always lower than this. For our micro-chip design (Fig.3.2 see also Fig. 3.1), the field strength in the centre of the chamber is E = 0.806 V/x, with V and x standing for the electrode voltage and tip-to-tip distance, respectively [42]. Another correction must be introduced for the effect of the square topped measuring field on the induced torque. The higher harmonics result in a frequency dependent reduction of the torque in such fields [30]. The actual torque is reduced by a factor of 0.92 for well separated peaks. The rotation speed ω_c is derived for $T_{fric} = T_{ER}$:

$$\omega_c = \frac{T_{ER}/0.92}{5.64\pi\eta a^3} = 0.153\frac{\varepsilon_0\varepsilon_e c\,\mathrm{Im}(K^*)E^2}{a\eta} \qquad (1.5.3)$$

Along semi-axis a the Clausius-Mossotti factor is given by [34]:

$$K_a^* = \frac{a_{\mathrm{inf}}}{a_{\mathrm{inf}} - a}\left(1 - \frac{Z_a^i + Z^m}{Z_a^i + Z^m + Z_a^e}\frac{a_{\mathrm{inf}}}{a}\right) \qquad (1.5.4)$$

for a spheroidal cell with a thin membrane. The impedance components for the cytoplasm (Z^i), the membrane (Z^m) and the external medium (Z^e) are given by:

$$Z_a^i = a/(\sigma_i + j\omega\varepsilon_i\varepsilon_0) \qquad (1.5.5a)$$

$$Z^m = d/(\sigma + j\omega\varepsilon_m\varepsilon_0) \qquad (1.5.6b)$$

$$Z_a^e = (a_{\mathrm{inf}} - a)/(\sigma_e + j\omega\varepsilon_e\varepsilon_e) \qquad (1.5.7c)$$

with a, a_{inf}, d and j standing for the length of semi-axis a, the influential radius in a-direction, the membrane thickness, and $(-1)^{0.5}$, respectively [34]. In the present study, membrane conductance and membrane capacitance were calculated assuming a membrane thickness (d) of 8 nm [34]

For the human red cell we assumed the oblate cell model given by Gimsa and Wachner [34], with a long semi-axis of a = 3.3 µm. For an axis ratio of 1:2 an influential radius a_{inf}= 4.0 µm is obtained [33]. At 23 °C the relative external permittivity, membrane conductance, and membrane capacitance were taken to be 78.5, 480 S/m^2, and 9.97 mF/m^2, respectively [34]. For the conductivity and the relative permittivity of the cytoplasm at 23°C frequency values of 0.4 S/m and 212, respectively, have been published [33]. The cytoplasmic permittivity disperses around 15 MHz leading to a relative permittivity of 50 and a conductivity of 0.535 S/m at high frequencies (compare to parameters in Gimsa and Wachner [34]). All cell parameters were assumed to be temperature independent. In practical experiments, temperature effects during the experiment cannot be avoided.

1.6 Effect of temperature on ER investigation

Previous investigations of ER demonstrated that there were problems due to significant Joule's heating which produces a disruptive fluid convection. This effect can be avoided by suspending the cells in a very low ionic strength solution but the drawback to such an approach is that experimental results obtained under such conditions are of limited value in understanding the properties of red blood cells suspended in blood plasma under physiological conditions. In addition, the experiments are carried out at room temperature (25°C), not actual body temperature, and the assumption is made that the cell and medium parameters are temperature independent [28-37]. Recently, the development of better ER microelectrode chambers allows for the application of lower driving voltages and higher medium conductivities (electrolyte strengths closer to those found under physiological conditions). ER experiments can now be extended to the physiological range of ionic strengths [33] or even higher ionic strengths of the external medium [38]. Nevertheless, the currently used experimental techniques cannot completely avoid Joule's heating. Heat production is linearly related to the electric conductivity and the square of the applied voltage [43]. A temperature increase of ΔT affects the viscosity of the external medium (η), the permittivities (ε) and the conductivities (σ) of the system in the following ways:

$$\eta = \eta_{T_0} e^{-a\Delta T} \tag{1.6.1a}$$

$$\varepsilon = \varepsilon_{T_0}(1 - b\Delta T) \tag{1.6.1b}$$

$$\sigma = \sigma_{T_0}(1 + c\Delta T) \tag{1.6.1c}$$

where, η_{T_0}, ε_{T_0}, and σ_{T_0} refer respectively to viscosity, permittivity and conductivity at the starting reference temperature. Every 1 C° rise of temperature elevates the mobility of ions leading to an increase in the medium conductivity and decrease in medium viscosity and electrical permittivity. The temperature coefficients of conductivity (*c*, in Eq. 1.4.1c) and of viscosity (*a*, in Eq. 1.4.1a) have a value of about 2% per °C for normal aqueous solutions [44- 45]. The temperature coefficient of permittivity (*b*, in Eq. 1.4.1b) has been extrapolated from the temperature dependence of the water permittivity to be about

0.0046/°C [44]. Nevertheless, for the other media in the system, like the lipid-bilayer membrane and the cytoplasm, conductivity temperature coefficients were respectively reported to be 0.011 /°C and 0.015 /°C [45]. For the membrane capacitance, no temperature dependence has been addressed because any change of membrane capacitance would be very small compared to that of water [46]. Many authors have addressed temperature effects on the physiology of HRBCs (see for example [47-48]). Temperature alterations will not only affect the cell dielectric properties of all phases [49-51] but also other cell mechanisms such as membrane permeability [52-53], ion transport mechanisms [54-55], activation energy [55-56], cell volume and cell shape changes [57]. These disturbances, of course, alter ER spectra and consequently dielectric parameters [49]. The dielectric parameters of all phases of the cell, in general, cannot be independent of ionic transport processes across the membrane [51, 58-59]. For example, an increase in membrane conductivity and in interior ion concentrations will be obtained if membrane permeability is raised [60]. Thus, dielectric parameters changed by temperature lead also to an alteration of membrane transport and the ionic balance of cells.

1.7 Influence of temperature on membrane transport

It has been known that temperature adaptation of biological cells produces many side-problems affecting physiological functions and on biochemical parameters of the whole organism [51, 59 - 64]. These effects lead to changes in the properties and chemical composition of tissue membranes, and consequently alter ion transport processes across membranes. For example, cooling of mammalian erythrocytes cells to 0-5 °C results in a drastic fall in Na^+/K^+-ATPase activity and active transport of Na^+ and K^+ [53-55, 64]. It has also been shown that both Na^+/K^+ pumping and ionic leakage in red blood cells of hibernators are less affected by decreased temperature than those of the non-hibernating mammals [53, 56]. For the human red blood cell (HRBC), it was reported by several authors [49, 51, 64, 45] that temperature would not only affect the dielectric parameters of all phases, as described in the previous section, but also ion transport across membranes [52, 64]. As has already been addressed, a rise of temperature will enhance ionic mobilities and consequently increase membrane permeability [51, 59 - 60]. Increase in membrane permeability allows ions to move more freely through the membrane. The increase in the rate of ions crossing the cell membrane induce interior ion concentrations to change from the normal physiological state and cause an increase in membrane conductivity and ions transport across membrane [60]. The major membrane transport process occurring in HRBC is chloride exchange across the cell membrane and is mediated by the band-3 protein which has been identified as a chloride transporter. There are about 1.2 x 10^6 copies per cell and is the most abundant membrane protein. This protein is responsible for the fast anion exchange in HRBCs and was also assumed to contribute to the membrane dielectric properties [59]. If the protein's properties are altered, e.g. by inhibitors or a change of the temperature, the membrane properties will consequently be changed. Inhibition by the band 3 inhibitor 4, 4'-diisothiocynostilbene-2, 2'-disulphonate (DIDS), for example, results in an increase in the membrane capacitance from 4.63 mF/m^2 to 4.86 mF/m^2 and conductivity has been found to dramatically decrease from 250 Sm^{-2} to 20 Sm^{-2} [59, 64] confirming that the band 3 protein is responsible for the bulk of the total flux of ions across the cell membrane of the red blood cell.

In addition to inhibitor effects, some effects of temperature on ion transport across the cell membrane have already been addressed above. Human red blood cells behave differently above and below a critical temperature of about 15 ^oC. Temperatures below around 15 ^oC resulted in inhibition of both chloride transport rate and cation fluxes [52, 64]. These temperature effects were presumed to be caused by a change in the activation energy of the transport step [52]. Different explanations for this behaviour have also been proposed. There appear to be at least two possibilities: (a) the energy barrier for chloride transport decreases at a critical temperature (e.g. due to a phase transition of some membrane components, for example the well-known chilling injury found in plant cell membranes); or (b) chloride exchange is rate-limited by one step in the transport mechanism when the rate is slow in the low temperature range, whereas another step with somewhat lower activation energy becomes rate-limiting at higher temperatures. This critical change occurs at a constant temperature of around 15°C. The activation energy of membrane transport leads directly to ions translocation and diffusion across the membrane [63]. If it is altered by temperature, the dielectric parameters will be disturbed.

1.8 Influences of temperature on activation energy and ion diffusion across membrane

Ion diffusion across cell membranes in liquid solutions is totally different from those in gases. In liquids, molecules of ions are close together and within each others' sphere of mutual attraction. This is a critical difference between diffusion in a gas phase compared to that in a liquid phase. Hence, for any molecule to move, it must break away from its surrounding shell of molecules or drag them along with it. Diffusion in liquid consequently occurs in a discontinuous manner; a molecule is able to move only when it has acquired sufficient energy by collision to break away from its neighbors and push aside other molecules. Thus, the molecule diffuses in a series of jumps. For ions to transport across a membrane, a small solute molecule must detach itself from its surrounding solvent molecules and jump into the membrane phase; then it moves through the thickness of the membrane, perhaps by a series of small jumps; and detaches itself from the membrane environment and then jumps into the solvent phase again on the opposite side of the membrane. The molecule diffuses in a series of jumps requiring a certain critical activation energy. When the attractive forces between molecules are weak, diffusion is rapid. A small activation energy is required. Because of the activation energy required to make each jump possible, the Diffusion coefficient (*D*) of a substance in liquid is inversely proportional to the square root of its molecular weight times the temperature coefficient (often expressed as a Q_{10} value) raised to a power [66]. The relationship, derived from kinetic theory, demonstrates that the Q_{10} for diffusion of a substance in water depends on the activation energy necessary for a jump. If a large amount of energy is required, the membrane permeability is low. There are only a few molecules that have the necessary energy to diffuse at any moment; raising the temperature increases the number of molecules with the required energy and thereby has an appreciable effect on the net rate of diffusion. If a small amount of activation energy is required, the membrane permeability is high. For highly permeable species a greater fraction of the molecules possesses this minimal energy at any moment, and so raising the temperature has less of an effect on the net rate of the diffusion than in the case of relatively impermeable species. An elevation of temperature therefore generally increases the speed of the molecules and causes an increase in the rate of diffusion but the mobility of the species is also important. The time required for diffusion (t) of any ion varies directly with the square of the distance (λ) in a direction of the diffusing particles and inversely with D. The relation has been known as the Einstein's approximation equation defined as $\lambda = \sqrt{Dt}$ [66]. Thus, diffusion is extremely fast over short distances but exceedingly slow over long distances. If the distance of ions movement is constant like in cell membranes with a certain fixed thickness, increase in D according to temperature reduces the diffusion time. Ions can move through membrane with a higher diffusion rate. Physiologically, the diffusing ions are usually accompanied by water. The amount carried water is known as the hydration volume which can also be increased with increasing temperature [66, 67]. A large hydration volume carried by moving ions provides a large amount of water flowing through the membrane. A high diffusion rate of ions into the cell quickly causes it to swell. Thus, if this process occurs over the same duration but different temperatures, in the higher temperature case, the resultant increase in volume will certainly be larger than that at lower temperature. Clearly, change in temperature enhances the diffusion rate and causes red blood cells to swell. Changes in cell volume according to temperature will now be considered.

1.9 Influences of temperature on cell volume

As described in section 1.8, temperature affects the diffusion rate across cell membranes, and consequently induces the cell to swell or shrink. In this section, the temperature effects on water fluxes across cell membranes leading to alteration of cell volume will be further considered. In view of osmotic and hydrostatic pressures, an effect of temperature on a biological system cannot be avoided. It plays a major role in biological processes and it is known that small temperature changes may alter both, cell shape and cell volume [67, 68]. An altered osmotic balance of the external medium and the cytoplasm will generate water fluxes between the two phases. A net-influx causes the cell to swell. This will occur when the osmotic pressure of the outside medium is lower than of the inside. A net-efflux results in cell shrinkage which can be observed when the cells are suspended in a hypertonic media. Both of these behaviours can be found in most biological cells when adapting themselves to a new water potential environment. For example, after an initial passive swelling or shrinking, mammalian cells regulate their volume usually by returning to a near-normal volume. Several mechanisms are involved in this process such as the loss and gain of K^+ and Cl^- [88, 69].

To describe temperature dependence of water fluxes flowing through the cell, the Van't Hoff relation can be proposed as a viable physical model. The hydrostatic pressure is known to strongly depend on temperature. It will increase if the temperature is elevated. The increase in the external hydrostatic pressure will perturb the balance of the physiological osmotic pressure between two sides of the membrane. To re-balance the system, water moves down its chemical gradient and enters the cell. In this case, cell swelling will be observed. The amount of water flowing through a membrane is called water flux volume (J_v) and has the dimensions, volume per square metre of cell surface membrane per unit time (m^3 m^{-2} s^{-1} or m s^{-1}). The flux can be determined by the osmotic pressure difference ($\Delta\prod$) times a filtration coefficient (L_p), $J_v = -L_p.\Delta\prod$. L_p is a mechanical filtration capacity of the membrane. It is a mobility property and represents a velocity of fluid per unit pressure difference (hence its dimensions of m s^{-1} above). The negative L_p indicates the flux is from a region of low osmotic pressure to the region of high osmotic pressure. The L_p of any fluid is defined as [66]:

$$L_p = \frac{n\pi r^4}{8\eta\delta} \tag{1.9.1}$$

The filtration coefficient L_p is a function of membrane characteristics including the membrane thickness (δ), the viscosity of the fluid (η), the number of membrane pores per unit area (n) and the pore radius (r) [66]. The π in this equation is the mathematical constant equal to 3.14…and should not be confused with the symbol for the osmotic pressure ($\prod$). Theoretically, if the viscosity of the moving medium is decreased as a result of an increase in temperature, a bigger value of L_p will be generated. This is means more water will flow into the cell. Consequently, there will be an increase in the amount of water carried by ions as they cross the cell membrane because their hydrations shells of water molecules surrounding them will be larger. The amount of water carried by a coulomb of electricity through 1 cm^2 of membrane is so-called the electro-osmotic permeability (β). The parameter is defined as the coefficient relating to the flow of volume caused by an electric current under condition of zero pressure difference [70], and is expressed as:

$$\beta = \frac{f_1^0 r^2}{8\eta F} \tag{1.9.2}$$

where, F is Faraday's constant (9.6484 x 10^4 C eq^{-1}), f_1^0 is a frictional coefficient between a molecule of spherical shaped solute and an infinite amount of water, r is the pore radius and η is the viscosity. In a very loose membrane, the frictional coefficient approaches the value for a free solution which is related to the diffusion coefficient (D), expressed as $D = R{\cdot}T/\,f_1^0$ where R is the universal molar gas constant with a value of 8.3145 J mol^{-1} K^{-1} and T is the absolute temperature in Kelvin. In the case of K^+, for example, having a D value of 1.957 x 10^{-5} cm^2 s^{-1} [44], the calculated value for f_1^0 is 1.3x10^{10} N s mol^{-1} cm^{-1} [70]. Assuming that a membrane is characterized by a radius of r = 1 nm at a temperature at which the viscosity = 1 mPa s, a β of value of 1.7 x 10^{-3} cm^3 C^{-1} can be calculated. This value indicates that every coulomb of K^+ ions will exert a drag effect sufficient to carry 1.7 x 10^{-3} cm^3 of water through 1 cm^2 of the membrane. Assignment of δ to a constant membrane thickness provides a parameter so-called the permeability coefficient (*P*) [66]. The permeability coefficient is related directly to β and is expressed as:

$$P = u\frac{\beta}{\delta}\frac{RT}{F} \qquad (1.9.3)$$

where u is a mobility of ions in units of $m^2\ s^{-1}\ V^{-1}$. Theoretically, if β increases due to an elevation in temperature, the permeability coefficient should increase. The increase in the permeability coefficient should enhance ion fluxes and be accompanied by water flowing into the cell interior [52]. A swelling of the cell should be observed. In recent investigations of dielectric parameters by ER, all have assumed the cell volume to be constant [20-39, 49, 71-74]. This is probably not a justifiable or valid assumption because changes in cell volume will affect the determination of the polarization of the cells, and would strongly influence the induced dipoles moments of the cell [28-30]. In addition, a perturbation of cell volume will certainly induce changes in cell shape [75-77] and the internal ionic concentration will also change as described by Glaser et al. [78]. Thus it is necessary to take temperature, volume and ionic concentration changes into account in ER investigation.

1.10 Relation of cell volume and cell shape changes in Human Red Blood cells

Since HRBCs have no internal structure, their shape is determined solely by the membrane properties, which are essentially composed of two parts: the lipid bilayer and the cytoskeleton, a continuous network of proteins called spectrin. The normal shape of HRBCs in blood plasma is known as a discocyte. This shape can be transformed *in vitro* to so-called echinocytes or to stomatocytes (Fig. 1.10.1) by a plethora of exogenous conditions; for example, increase of the external electrolyte concentration [79-81], the increase of the pH of the medium [79-80] and a change in temperature [82-83]. Shape transformations resulting from the effects of both pH and temperature [80-83] were found to correlate with the transmembrane electrical potential ($\Delta U_{i,o}$) where (i) refers to the inside phase and (o) refers to the outside phase [81-83]. A positive electrical potential inside relative to the outside ($\Delta U_{i,o} > 0$) the HRBCs produces stomatocytes, and on the other hand a negative potential gives rise to echinocytes. There are a number of different viewpoints on the interpretation of this observed phenomenon and hypotheses about its underlying mechanism [75, 80, 83]. Some authors have established correlations between the stomatocyte-discocyte-echinocyte transitions and the effect of ion transport inhibitors (such as DIDS above) on the conformation of the Band 3 anion-exchange protein, resulting in an inhibition of the anion transport effectuated by this protein [83-87].

The most widely applicable quantitative theory of transition from a discocyte morphology to that of a stomatocyte or transformation into an echinocyte is provided by the bilayer-couple hypothesis [78]. Changes in shape are proposed to be due to an incorporation of molecules into the bilayer structure of the RBC membrane. Any factor, which leads to an expansion of the outer membrane leaflet relative to the inner one, produces a tendency to form convex structures, as the echinocytic spicule shape. Conversely, any expansion of the inner leaflet, relative to the outer one, favors the formation of cavities (stomatocytosis) accommodating the extra area. A wide range of experimental treatments were applied to HRBC to determine their effects on the HRBC's shape, its surface area, volume, and a mechanical characterization of the membrane. A change in cell volume accompanied by a change of shape occurs when the membrane surface area remains constant [88]. Under physiological conditions, HRBCs possess a cell surface area of 133 μm^2 [89]. However, using different methods, other values of 130 μm^2 [90] and of 138 μm^2 [78] have also been proposed. The volume enclosed by the membrane depends upon the amount and type of solutes in the cytoplasm and their concentrations in the suspending medium. Under physiological conditions, several values of average volume of HRBCs were found by different authors.

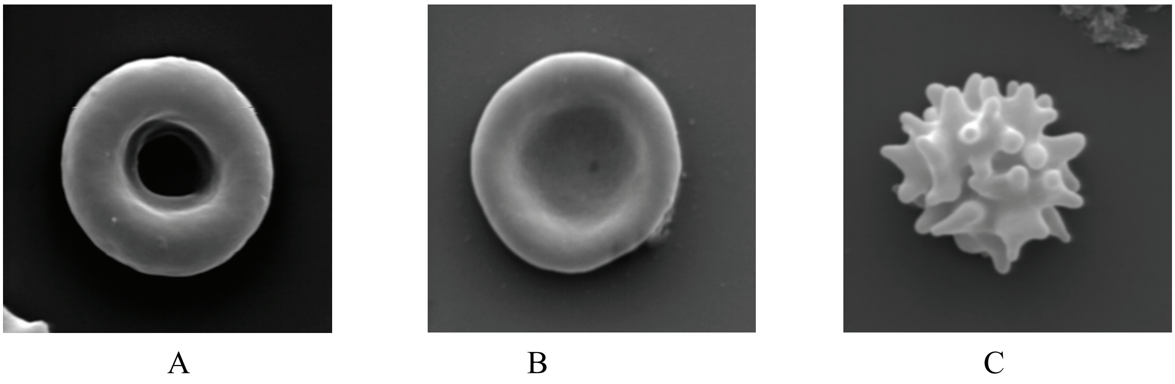

Fig. 1.10.1 Scanning electron microscopic picture of human erythrocyte shapes: (A) stomatocyte; (B) discocyte; (C) echinocyte.

With increase of the medium's ionic strength a red blood cell undergoes transformation in shape in the sequence of stomatocyte toward discocyte (normal condition) then toward echinocyte. Estimates of intracellular volumes of red blood cells under physiological conditions vary; estimates in one study range from 93 μm^3 to 88 μm^3 [90] but in another independent study a value of 90 μm^3 was reported [91]. Volume changes may occur concomitant to changes in shape. For example, increase in cell volume will be observed when an echinocyte is transforming to a stomatocyte [64, 83]. This behavior does not interfere with the formation of an echinocyte or stomatocyte, unless the volume increase is so large that the pressure difference between cytoplasm and medium rises and the membrane experiences isotropic tension. Physiologically, an increase in the cell volume leads to an increase in the cell radius and *vice versa*. In ER investigations, cell radius is an important parameter which affects a depolarizing factor of the cell (please see Eqs. 1.5.1-1.5.3) and consequently alters the characteristic point of the ER spectrum. Changes in the cell radius also disturb ionic concentrations in the cytoplasm.

1.11 Influence of cell volume on cytoplasmic conductivity

Generally, investigations of internal conductivity of HRBCs was experimentally obtained from cells which were under controlled and well-defined conditions. For example, the osmolality of the suspension medium was kept constant at a value of 300 mOsmol kg^{-1} [33, 38, 60, 64]. The cell volume was assumed to be constant [33, 103]. Most experiments were carried out at room temperature (usually 25 ^{o}C) [13-33, 38, 60, 64]. The influences of temperature were usually neglected [33, 64, 93] but an experimental temperature of 25°C is obviously quite different to the temperature experienced by red blood cells *in situ* (37 ^{o}C). Furthermore, it has been known that a small change in the surrounding medium, especially changes in the external conductivities [75-82] and temperature [83], will alter both cell shape and cell volume. Any volume change of the cells leads to an alteration of the concentration of all intracellular solutes, even if no net flux of them into or out of a cell has occurred. Under physiological conditions, a standard volume (V_0) *in vivo* situation of human red erythrocytes with a defined relative volume V_{std} = 100 % is characterized by a standard intracellular concentration of ions (c_{std} in mmol/l). All parameters of this standard condition are specified as: c_{std} (standard concentration) and V_{std}. This can be taken into account by introducing the dilution coefficient (δ) [78]:

$$\delta = \frac{qV}{V - (1-q)V_{std}} \tag{1.11.1}$$

where q is the relative water content and has a value of 0.71 in erythrocytes when $V = V_0$ [78]. Therefore, the concentration of non-exchangeable solutes in erythrocytes with an arbitrary volume V is equal to $\delta \cdot c_{std}$. Both arbitrary volume and water content can be obtained experimentally. The calculated δ provides the cytoplasmic concentration leading to the calculation of the cytoplasmic conductivity.

1.12 Influence of cytoplasmic concentrations on cytoplasmic conductivity

The conductivity of a salt solution (σ) can be calculated from the conductivity of individual ions species (i). Neglecting the ion-ion interactions, the σ can roughly be described by equivalent conductivity (Λ) and the concentration (c) as,

$$\sigma = \sum \sigma_i = \sum \Lambda_i c_i \tag{1.12.1}$$

The equivalent conductivity does vary significantly with the concentration of the ions; if the ionic concentration is increased, the equivalent conductivity decreases. The relation is known as Kohlrausch's law [64]:

$$\Lambda = \Lambda^0 - Ac^{\frac{1}{2}} \tag{1.12.2}$$

where, A is the slope of the plot between Λ against $c^{1/2}$, Λ^0 is the equivalent conductivity at infinite dilution, which is known as Kohlrausch's law of independent migration of ions given by:

$$\Lambda^0 = \lambda^0_{+i} + \lambda^0_{-j} = F(u_{+i} + u_{-j}) \tag{1.12.3}$$

The equivalent conductivity at infinite dilution of an electrolytic solution is the sum of the equivalent conductivity at finite solution of the ions constituting the electrolyte. Knowing the equivalent conductivity, a mobility (u) of the ion species can also be determined by multiplying by Faraday's constant (F = 96485 C/mol). However, the justification of Kohlrausch's law on theoretical grounds cannot be obtained within the framework of a macroscopic description of conductivity. It requires an intimate view of ions in motion and ion–ion interaction. Such interactions between positive and negative ions would determine to what extent they would influence each other when they move, and this would in turn bring about a decrease of conductivity. Briefly, the way in which ionic distribution affects the conductivity is in two ways. Firstly, if an electric potential is applied, a positive ion will move toward the negative electrode and must drag along with it an entourage of negative ions. The more concentrated the solution, the more the counter-ions provide a greater drag force between positive and negative ions. The ionic atmosphere around a moving ion is therefore not symmetrical; the charge density behind is greater than that in front, and this will result in a retardation in the motion of the ion. This influence on the speed of an ion is called the relaxation, or asymmetry, effect. A second factor, that retards the motion of an ion in solution, is the tendency of the applied potential to move the ionic atmosphere itself. This in turn will tend to drag along solvent molecules, because of the attractive forces between ions and solvent molecules. As a result, the ion at the centre of the ionic atmosphere is required to move upstream, and this is an additional retarding influence. This effect is known as the electrophoretic effect.

The interaction of ions moving in solvent was described in a interesting way by Bockris et al. [58]. "In the elementary treatment of the migration of ions, it was assumed that the drift velocity of an ion was determined solely by the electric force $\vec{F}$ arising from the externally applied field. When, however, the mutual interactions between an ion and its cloud were considered, it turned out that there were two other forces operating on an ion. These extra forces consisted of: (1) the relaxation force $\vec{F}_R$ resulting from the distortion of the cloud around a moving ion, and (2) the electrophoretic $\vec{F}_E$ arising from the fact that the ion share in the electrophoretic motion of its ion cloud. Thus, in a rigorous treatment of the migrational drift velocity of ions, one must consider a total force $\vec{F}_{total}$, which is the resultant of that due to the applied electric field with the relaxation and electrophoretic force."

$$\vec{F}_{total} = \vec{F} - \left(\vec{F}_E + \vec{F}_R\right) \tag{1.12.4}$$

The minus sign is used because both the electrophoretic and relaxation forces act in a direction opposite to that of the externally applied field. Since an ion is subject to a resultant, or net, force, its drift velocity, too, must be a net drift velocity resolvable into components. Furthermore, since each component force should produce a component of the overall drift velocity, $\vec{v}_d$, there must be three components of the net drift velocity. The first component which shall be designated, $\vec{v}_o$, is the direct result of the externally applied field only and excludes the influence of interactions between the ion and the ionic cloud; the second is the electrophoretic component, $\vec{v}_E$ and arises from the participation of the ion in the electrophoretic motion of its cloud; and, finally, the third component is the relaxation field component, $\vec{v}_R$ originating from the relaxation force which retards movement in an opposite sense to the applied field. Since the electrophoretic and relaxation forces act in an opposite sense to the externally applied field, it follows that the electrophoretic and relaxation components must diminish the overall drift velocity:

$$\vec{v}_d = \vec{v}_o - \left(\vec{v}_E + \vec{v}_R\right) \tag{1.12.5}$$

At appreciable concentrations, the ions can be regarded as coupled or interacting with each other i.e. in an ionic-atmosphere. This results in the drift of positive ions toward the negative electrode, which hinders the drift of negative ions toward the positive electrode, i.e. the interionic interaction results in the positive ions equivalent conductivity reducing the magnitude of the negative ions equivalent conductivity to below the infinite dilution value, and vice versa. To make quantitative estimate of these effects, however, one must make a calculation of the influence of ionic- cloud effect on the phenomenon of conduction.

This task was done 1923 by the Dutch physical chemistry Peter Debye and German physicist Erich Hückel [93]. Their work described the decrease in equivalent conductivity (σ) of a strong electrolyte that was attributed to the mutual interference of the ions, which becomes more pronounced as the concentration increases. The expression obtained on this basis for the equivalent conductivity of an electrolyte solution of concentration (c) is known as Debye - Hückel – Onsager equation given by:

$$\Lambda = \Lambda^0 - (P + Q\Lambda^0)\sqrt{c} \tag{1.12.6}$$

where, P and Q can be expressed in term of various constant and properties of the system. For the particular case of a symmetrical electrolyte i.e. one for which the two ions have equal and opposite sign ($z_+ = -z_- = z$), P and Q are given by,

$$P = \frac{zeF}{3\pi\eta}\left(\frac{2z^2e^2L}{\varepsilon_0\varepsilon k_BT}\right)^{\frac{1}{2}} \tag{1.12.7}$$

and

$$Q = \frac{z^2e^2w}{24\pi\varepsilon_0\varepsilon k_BT}\left(\frac{2z^2e^2L}{\pi\varepsilon_0\varepsilon k_BT}\right)^{\frac{1}{2}} \tag{1.12.8}$$

where, z is the valence of the ion, e_0 is electronic charge = 1.602 x 10^{-19} C, L is Avogadro's number = 6.022 x 10^{23} mol^{-1}, k_B is Boltzmann's constant = 1.38 x 10^{-23} J K^{-1}, T is absolute temperature, ε_0 is dielectric permittivity of vacuum = 8.85 x 10^{-12} C V^{-1} m^{-1}, ε is the dielectric constant and w is a number whose magnitude depends on the type of electrolyte: for a uni-univalent electrolyte, $w = 2 - \sqrt{2} = 0.586$.

The cytoplasm of the human red blood cell is not an ideal solution. It contains a haemoglobin solution whose Newtonian viscosity (η) is about 5.91 mPa s at 37°C [91]. The viscosity generates a drag force hindering the movement of ions in the cell. To calculate the mobility of ions hindered by the viscosity, Walden's law can be applied:

$$\Lambda\eta = \frac{ze_0F}{6\pi r} \qquad (1.12.9)$$

where, η is the relative viscosity, r is an effective radius of ions having a constant value for any solvent solution at a given temperature. The calculated mobilities reduce the magnitude of equivalent conductivity to below the infinite dilution value. The magnitudes of several quantities of ions at infinite dilution are altered.

1.13 Effect of the solvent on ion mobility at infinite dilution

Since the solvents in biological systems are not pure water, switching of the ions from water to non-aqueous solution (biological solvents), their general parameters change considerably. The quantities that will be most obviously affected are the viscosity, the dielectric constant of the medium, the distance of the closest approach of the solvated ions, and the radii of the solvated ions. Changes in these parameters result in changes in the mobility and the equivalent conductivity of the ions at infinite dilution as well as the concentration of free ions to change, and cause the conductance behavior of an a biological electrolyte (blood plasma and cytoplasm) to vary considerably from that of a simple electrolyte solution. To understand more about these phenomena, the relationships between viscosity, ionic mobility and conductivities described by Walden's law (Eq.1.12.9) have been taken into consideration. It is obviously seen that an increase in the viscosity of the medium leads to a decrease in the infinite dilution mobility, and vice versa. And this can be the reason for the decrease of ionic mobility described by Pauly and Schwan [96]. If the ionic mobility is reduced by the viscosity, the conductivity should be affected in a similar way. The Walden's relation gives the explanation of why the conductivity of ion moving in water and those moving in a complex non-aqueous solution are different. However, a parameter that one should be careful in using in Walden's equation is the radii of the moving ions. The rule was previously presented in the form where $\Lambda\eta = \text{constant}$, assuming the radii of the moving ions are independent of the solvent. In fact, the radius of the kinetic entity may be changed by going from one type of solvent to another, essentially because of changes in the structure of the solvation sheath around the ion. In some cases, changes in radii of the solvated ions are mainly due to the changes in the sizes of the solvent molecules in the solvation sheath. Therefore, Waldens' rule should be used in the form shown in Eq. (1.12.9) where r is the radius of the ionic entity concerned in a given solvent.

1.14 Proposal

The investigations of dielectric parameters of biological cells by ER have become a field of intensive research that is increasingly leading to practical and technological applications and can now be accessed in media similar to those found under physiological conditions and even at higher ionic strengths of the external medium. Nevertheless, ER experiment has still been carried out under conditions which are often not close to actual physiological conditions and assumptions used in the models might not be valid under physiological conditions. Experimental problems due to the methodology of ER measurement also cannot be completely avoided. For example, the investigation of ER at physiological values of electrolytes in the external medium or at higher conductivities meet a problem due to Joule's heating. Increased temperature effects are found in all observed dielectric parameters, including the viscosity of the external medium, the conductivity of the bathing electrolyte and within the cytoplasm and also induced cell volume and cell shape changes. Such changes will certainly disturb the observed dielectric parameters which may also affect some of the assumptions inherent in the models used to interpret the data.

Therefore, investigation of temperature effects on ER behavior of HRBCs developed into a major aim of this work. The RC model of Gimsa and Wachner [34] was used as a basic model. Temperature dependent dielectric parameters were taken into account to determine the conductivities and permittivities for all phases at the experimental temperature. Cell volume and cell shape changes due to both the composition of the external media and temperature were also introduced into the model. However, the standard RBC model cannot be used for all experimental conditions, for example, it cannot be used for echinocyte cells. The cytoplasmic conductivity was determined using the Debye - Hückel –

Onsager relation. The relationship between cytoplasmic conductivity and temperature will be investigated. The temperature coefficient of the conductivity will be calculated.

In this investigation, the experiment was divided into five steps:

The first step was to investigate whether the dielectric parameters of cytoplasm depended on the external media. ER spectra influenced by external conductivities will be measured experimentally.

The second step of the study was to observe of how temperature affected ER spectra. ER spectra under a range of experimental temperatures were investigated. The data derived from the spectra for all observing temperatures will be used to calculate a set of dielectric parameters and their dependency upon temperature will be determined.

The third step of the study was to observe cell volume changes in a range of temperatures and external medium. Changes in cell volume leads to an alteration of the cytoplasmic conductivity and its dependence upon temperature will be determined.

The fourth investigation was an investigation of changes in cell shape as a function of temperature and external media. In this part of the project, temperature dependencies of cell radii were measured.

The last step of the work was to determine the temperature dependence of conductivities and permittivities of both the cytoplasm and the cell membrane.

2 Theory

Theoretical calculations of the temperature dependence of ER spectrum

To interpret temperature dependence of ER, the simplified equations created by Gimsa and Wachner [34] were modified. The general temperature dependent dielectric parameters presented in Eq. 1.3.6b and c were taken into account for any aqueous medium. The modified equations of temperature dependence of first (f_{c1t}), and second (f_{c2t}) characteristic-frequencies as well as of first (R_1), and second (R_2) rotation peaks can be presented in the following forms:

$$f_{c1t} = \frac{1}{2\pi rC}\left(\frac{\sigma_{et}\sigma_{it}}{\sigma_{et}+\xi\sigma_{it}} + rg_t\right) \qquad (2.1.1)$$

$$f_{c2t} = \frac{1}{2\pi\varepsilon_0}\left(\frac{\sigma_{et}+\xi\sigma_{it}}{\sigma_{et}+\xi\varepsilon_{it}}\right) \qquad (2.1.2)$$

$$R_{1t} = \frac{-(\zeta+1)^2\sigma_{it}^2\sigma_{et}}{2(\sigma_{et}+\xi\sigma_{it})(rg_t(\sigma_{et}+\xi\sigma_{it})+\sigma_{et}\sigma_{it})} \qquad (2.1.3)$$

$$R_{2t} = \frac{(\zeta+1)^2(\sigma_{it}\varepsilon_{et}-\varepsilon_{it}\sigma_{et})}{2(\sigma_{et}+\xi\sigma_{it})(\varepsilon_{et}+\xi\varepsilon_{it})} \qquad (2.1.4)$$

where, C and g_t are called area specific capacitance and conductance expressed as $C = \varepsilon_0\varepsilon_m / d$ and $g_t = \sigma_{mt} / d$, C is assumed to be temperature independent since it has very low temperature coefficients for the permittivities of fatty acid-chain-like compounds [44]. The parameters $\sigma_{et}, \sigma_{it}, \varepsilon_{et}, \varepsilon_{it}, \sigma_{mt}$ have been defined as:

$$\sigma_{et} = \sigma_e(1+0.02\Delta T) \qquad (2.1.5)$$

$$\sigma_{it} = \sigma_i(1+0.015\Delta T) \qquad (2.1.6)$$

$$\sigma_{mt} = \sigma_m(1+0.011\Delta T) \qquad (2.1.7)$$

$$\varepsilon_{et} = \varepsilon_e(1-0.0046\Delta T) \qquad (2.1.8)$$

$$\varepsilon_{it} = \varepsilon_i(1-0.003\Delta T) \qquad (2.1.9)$$

when σ_e, σ_i, ε_e, ε_i and σ_m are starting values. The coefficient parameters presented in Eqs. 2.1.5 and 2.1.8 were taken from [44]. For the coefficients appearing in Eqs. 2.1.6, 2.1.7 and 2.1.9 please see [50]. The theoretical calculation curves of f_{c1t} f_{c2t} R_{1t} and R_{2t} according to the above equations for all observed external conductivities are illustrated in Figs. 2.1 and 2.2.

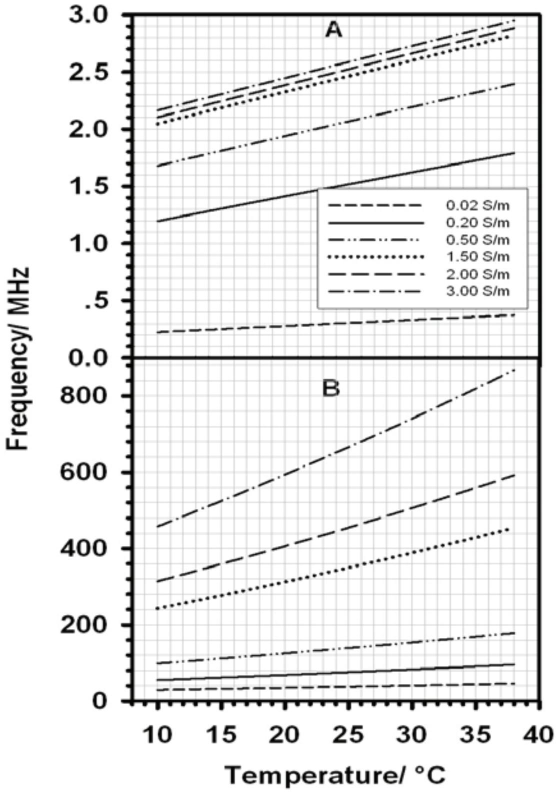

Fig. 2.1 Theoretical calculation of temperature dependence of f_{c1} (A) and f_{c2} (B) at six difference external conductivities

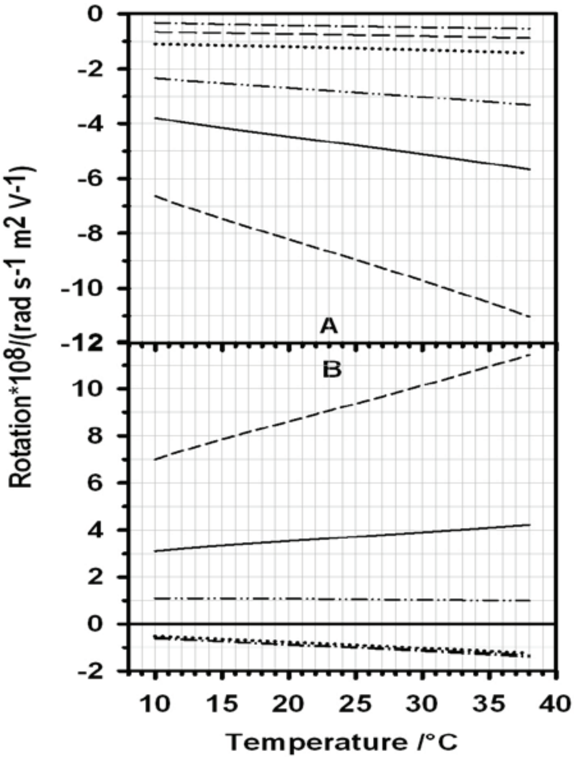

Fig. 2.2 Theoretical calculation of temperature dependence of R_1 (A) and R_2 (B) at six difference external conductivities (see line types in Fig. 2.4)

To obtain the ER spectrum, Eqs. 2.1.5-2.1.9 were introduced into the Lorentz equation, defined as:

$$R = \frac{2R_1 f / f_{c1}}{1 + (f / f_{c1})^2} + \frac{2R_2 f / f_{c2}}{1 + (f / f_{c2})^2} \qquad (2.1.10)$$

where R, f and f_c stand for the peak rotation speed, field frequency, and characteristic frequency, respectively. The ER peaks obtained from the Lorentzian peaks were compared with those obtained from the interpretation of the model [34]. Qualitatively, the difference between the two comparative peaks was very small. The maximum difference in values of about 15 % was obtained at external conductivity of 0.02 S/m (Fig. 2.3). The difference decreased at higher conductivities (please see Figs.2.3 and also 2.4). The results show that the simplified equations from [34] can be successfully used for interpretation of temperature dependence of ER spectra. The relation of rotational peaks to external conductivities and temperature were summarized and are shown in Fig. 2.5.

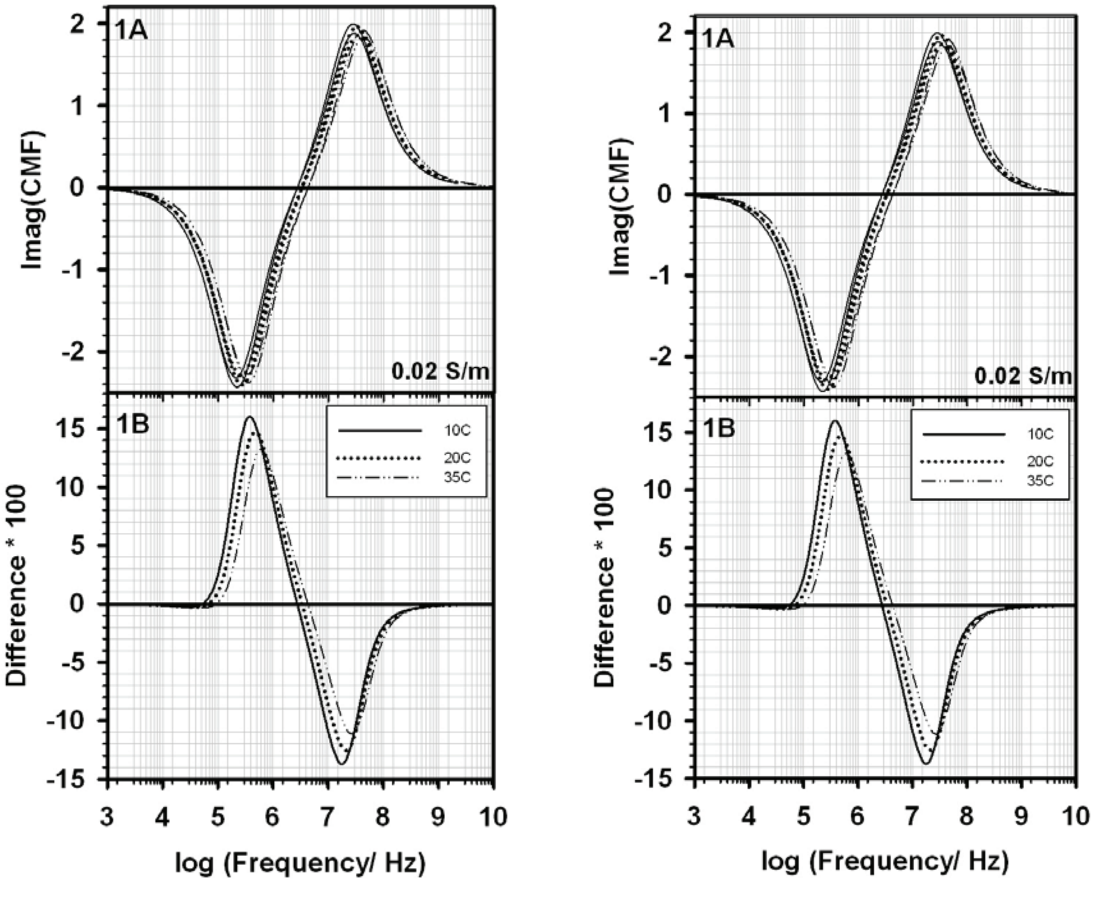

Fig. 2.3 (A) comparisons of ER spectra obtained using two models at 3 selected temperatures for the external conductivities of 0.02 S/m and of 0.50 S/m. (B) Their difference values for comparison of the two models.

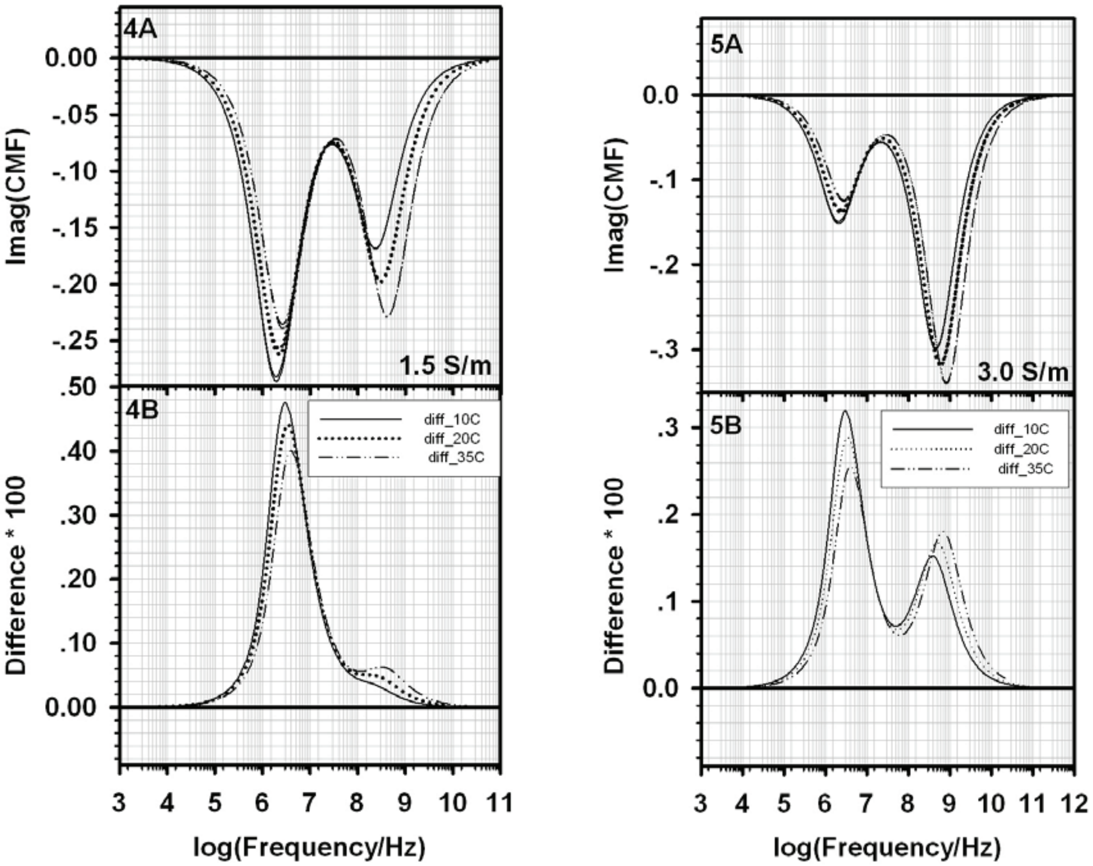

Fig. 2.4 (A) comparisons of ER spectra obtained using two models at 3 selected temperatures for the external conductivities of 1.50 S/m and of 3.00 S/m. (B). Their difference values for comparison of the two models.

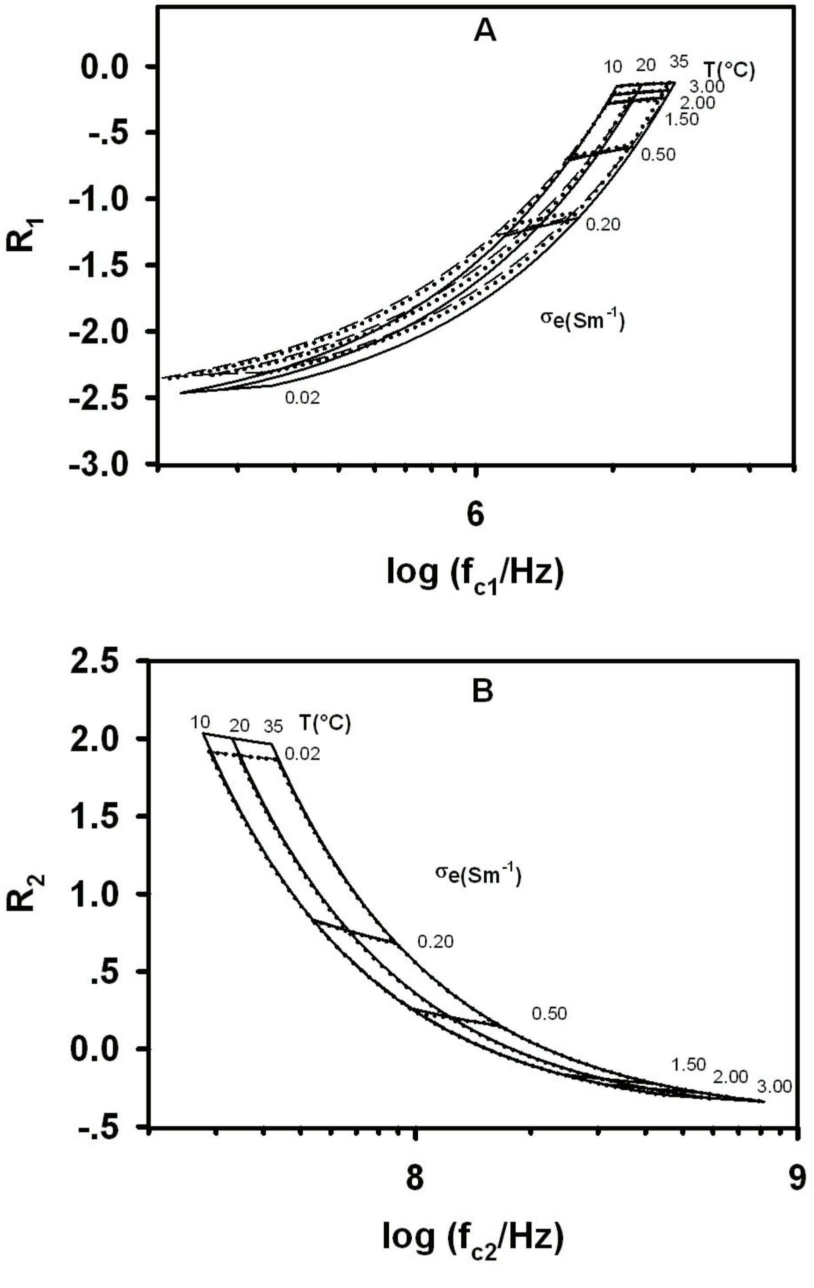

Fig. 2.5 Dependence of R_1 (A) and of R_2 (B) on the field frequencies, the external conductivity and the temperature

3 Materials and methods

3.1 Preparation of solutions

3.1.1 Phosphate Buffer (PB) solutions

PB buffer was prepared from 58 mM of

(1)	$NaH_2PO_4 \cdot H_20$	(M = 137.99 g/mol)	8.0034 g/L
(2)	$Na_2HPO_4 \cdot 12H_20$	(M = 358.14 g/mol)	20.7721 g/L

pH of both solutions were measured with a Hanna pH meter (pH 211-instrument Microprocessor, Italy). To adjust to a pH of 6, about 2 ml of solution (2) with pH of about 8.73 was added into 20 ml of solution (1) with pH of about 4.6.

3.1.2 Measuring solutions

Two 300 mOsm kg^{-1} solutions of NaCl and a solution of sucrose each containing of 1 mM of PB buffer were mixed to adjust the conductivities. The details tabulated in Table 3.1 were used to prepare the solutions. The approximate amount of NaCl and sucrose solutions for all measuring solutions were tabulate in Table 3.2. The conductivity of the solution was measured in the temperature compensation mode (20 °C) with an InoLab-conductometer (WTW, Weilheim, Germany). Conductivities below 0.1 S/m were measured with a LF 39 (Sensortechnik Meinsberg GmbH, Meinsberg, Germany). The conductivities for other temperatures were extrapolated according to Eq. (1.3.6c). The data were presented in Tab. 3.3. The amount of NaCl dissolved in each solution was determined and is shown in Table 3.4. The measured concentrations of NaCl were used to calculate the ionic strength (*I*) of the solutions using the relation:

$$I = \frac{1}{2} \sum_i c_i z_i^2 \qquad (3.1.1)$$

where, c_i is the molar concentration of the ions of type i which have the valence of z_i. For a uni-univalent electrolyte such as NaCl, which behaves very closely to that of an ideal solute, the ionic strength is equal to the molar concentration. The viscosities of all measuring solutions were determined by a falling-ball viscosimeter MLW (VEB MLW Prüfgerätewerk Medingen, Freital, GDR). The measured data were tabulated in Tab. 3.5.

Solutions	Molecular weight (g/mol)	Concentration (M)	Mass (g/l)	Phosphate Buffer (ml/l)	Osmotic coefficient	Conductivity before/after adding of PB (S/m)
300 mOsm.kg^{-1} of NaCl	58.44	157.00	9.1751	17.24	0.93	~ 1.5/ ~ 1.5
300 mOsm.kg^{-1} of sucrose	342.30	263.00	90.0789	17.24	1.14	~0.0018/ ~0.0080

Tab. 3.1 Chemical properties of 300 mOsm.kg^{-1} of NaCl and sucrose solutions containing 1mM of PB buffer

Conductivity of solutions (S/m)	Amount of sucrose solution (ml)	Amount of NaCl solution (ml)
0.02	100	1
0.20	100	17
0.40	90	38
0.50	80	48
1.50	-	100
2.00	-	100 +0.381 g NaCl
3.00	-	100 +1.1334 g NaCl

Tab. 3.2 The approximate amount of 300 mOsm.kg^{-1} of NaCl and sucrose in different measuring solutions

Starting conductivity (S/m)	Temperature °C				
(20°C)	10	15	25	30	35
0.020	0.016	0.018	0.022	0.024	0.026
0.200	0.160	0.180	0.220	0.240	0.260
0.400	0.320	0.360	0.440	0.480	0.520
0.500	0.400	0.450	0.550	0.600	0.650
1.000	0.800	0.900	1.100	1.200	1.300
1.500	1.200	1.350	1.650	1.800	1.950
2.000	1.600	1.800	2.200	2.400	2.600
3.000	2.400	2.700	3.300	3.600	3.900

Tab. 3.3 Eight observed conductivities were calculated at six different temperatures with the temperature compensation mode (20°C). The starting conductivities refer to the values measured at 20 °C.

σ_s Sm^{-1}	[NaCl] mol L^{-1}	Ionic strength mol L^{-1}
0.0220	0.0016±0.0000	0.0016±0.0000
0.2200	0.0227±0.0006	0.0227±0.0006
0.4400	0.0468±0.0007	0.0468±0.0007
0.5500	0.0584±0.0015	0.0584±0.0015
0.1200	0.1154±0.0045	0.1154±0.0045
1.6100	0.1570±0.0000	0.1570±0.0000
2.2100	0.2238±0.0044	0.2238±0.0044
3.3100	0.3427±0.0061	0.3427±0.0061

Tab. 3.4 Ionic concentrations and ionic strengths of NaCl for eight measured solutions measured at 25 °C (Standard laboratory experimental temperature). Values are means ± SE (n = 5)

Conductivity S/m at 20°C	Viscosity mPa.s					
	10 °C	15 °C	20 °C	25 °C	30 °C	35 °C
0.020	1.767 ± 0.009	1.539 ± 0.003	1.357 ± 0.008	1.197 ± 0.007	1.062 ± 0.007	0.957 ± 0.002
0.200	1.714 ± 0.006	1.489 ± 0.002	1.308 ± 0.009	1.137 ± 0.004	1.020 ± 0.004	0.921 ± 0.003
0.400	1.646 ± 0.001	1.436 ± 0.004	1.255 ± 0.001	1.119 ± 0.004	0.981 ± 0.007	0.892 ± 0.010
0.500	1619 ± 0.002	1.399 ± 0.005	1.247 ± 0.004	1.103 ± 0.005	0.981 ± 0.005	0.879 ± 0.002
1.000	1475 ± 0.010	1.277 ± 0.003	1.127 ± 0.006	1.004 ± 0.004	0.901 ± 0.005	0.825 ± 0.007
1.500	1389 ± 0.001	1.205 ± 0.103	1.082 ± 0.007	0.960 ± 0.006	0.861 ± 0.003	0.784 ± 0.002
2.000	1396 ± 0.000	1.225 ± 0.003	1.059 ± 0.006	0.959 ± 0.007	0.851 ± 0.001	0.773 ± 0.005
3.000	1415 ± 0.005	1.225 ± 0.000	1.086 ± 0.002	0.960 ± 0.012	0.864 ± 0.007	0.788 ± 0.005

Tab. 3.5 The measured viscosities for eight experimental solutions at 8 different conductivities over a temperature range of 10 °C to 35 °C. Values are means ± SE (n = 5)

3.1.3 DIDS solution

4,4'- diisothiocyanostilbene-2,2' disulphonate, DIDS (M = 552.5 g/mol, Sigma, Steinheim, Germany,) a known Cl$^-$ transport inhibiter at 6 mM dissolved in H_2O was prepared as a stock solution. For 1 ml of the solution, 3.315 mg of DIDS was used.

3.2 Preparations of red blood cells

Human blood cells obtained from the local blood bank (Abteilung für Transfusionsmedizin Blutspende, Universität Rostock) stored for no longer than 3 days at 4°C were used. For electrorotation experiments fresh blood was suspended into the measuring solution at a volume concentration (hematocrit, Hct) of 0.02%. For volume experiments, the red blood cells were first separated from blood plasma by centrifugation at 2000 g for 8 min. The supernatant plasma (and buffy coat) were removed with a syringe and the sediment was used for the volume experiments.

3.3 Preparation of the cell suspension for ER measurement

10 ml of the desired solution were equilibrated to the experimental temperature in a thermostat bath prior to the suspension of fresh blood at a volume concentration of 0.02% for each experiment. 5 µl of this suspension was transferred to the measuring chamber.

3.4 Microscopic observation and measurement of cell radii

To observe the cells, a microscope (Carl Zeiss, Jena) with an objective of magnification 50x was used. The source of illumination was a halogen lamp, 6V 15 W. A video camera was mounted to observe and record the microscopic images. The cell's radii were measured on a monitor. The scales on the monitor were calibrated using an objective micrometer. For the measuring of the cell radius of echinocytes with asymmetrical spikes, an average of the outer (top of spikes) and the inner (base of spikes) radii was used as a provisional estimate of their size.

3.5 ER measurements

The measuring chamber, illustrated in Fig 3.1, is based on a rectangular glass micro-chip with 4 platinum electrodes. The chip is shown in Fig. 3.2. Rotating electric fields in the range from 50 kHz to 250 MHz were generated by application of four progressively 90°-phase shifted signals of a peak-to-peak voltage of $5V_{P-P}$ from a radio-frequency generator HP 8131A (Hewlett Packard, USA). The experimental scheme is illustrated in Fig. 3.3. ER spectra of 4-6 different cells were recorded via a video system at each experimental conductivity. At conductivities above 2.00 S/m and above 25 °C no complete spectra could be recorded on a single cell due to thermal convections in the suspending medium due to Joule's heating. Therefore, a new cell suspension was transferred to the chamber for every measuring point. Measurements did not take longer than 30 s. All measurements were finished within 5 min after inserting the cell suspension into the experimental setup.

The temperature of the chamber was controlled by a small thermistor. The conductivity of the suspension was measured in the temperature compensation mode (20°C) of the conductometer. To avoid cell damage by the temperature increase during the measurements care was taken to avoid temperatures above 42 C°.

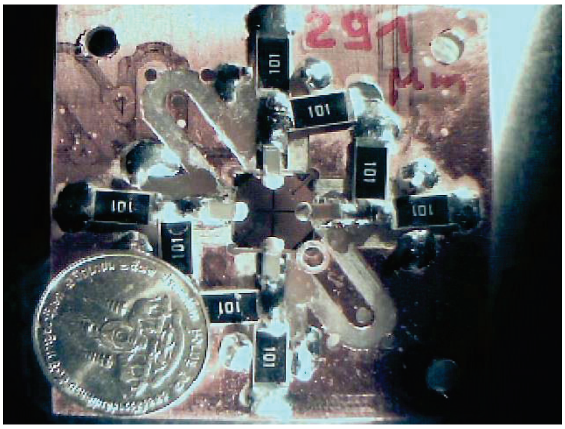

Fig. 3.1 The measuring chamber

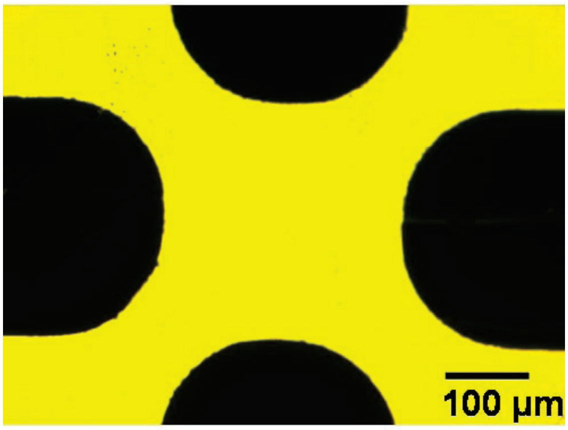

Fig. 3.2 Photomicrograph of microchip electrode chamber with an electrode tip-to-tip distance of about 300 µm.

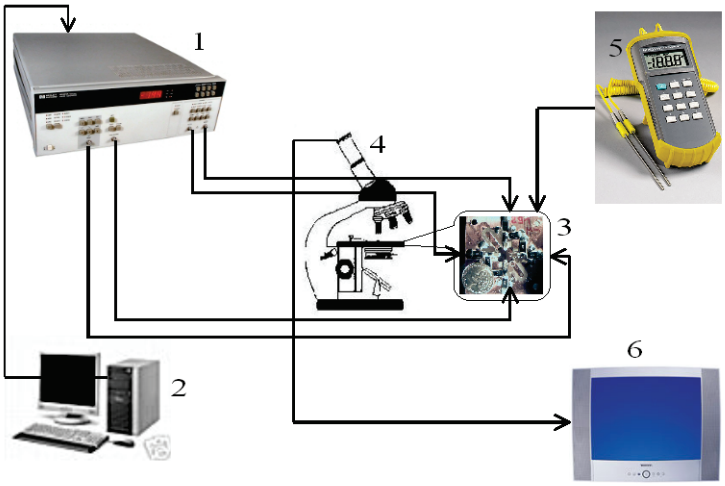

Fig. 3.3 Experimental equipment scheme. A rotating electric field was generated by a radio-frequency generator (1) with signals of a peak-to-peak voltage of 5V$_{PP}$. The generator was controlled by a computer program (2). The frequency range from 50 kHz to 250 MHz were generated by application of four progressively 90°-phase shifted were exposed to the measuring chamber (3) which was placed on the stage of the microscope (4). The chamber was thermostated to control the experimental temperature using a small thermistor (5). Measurements were carried out in the chamber under the microscope. The rotations of the cells were recorded by a video camera and were measured via a monitor (6).

3.6 Interpretation of ER spectra

ER spectrum is formed by a rotation of a cell at varied frequencies. The rotation can be obtained from the rotational speed of cell defined as:

$$R = \frac{2\pi}{T}\left(\frac{d^2}{V^2}\right) \tag{3.6.1}$$

where T is the rotational time, d is the electrode distance and V is the voltage applied to the electrodes. To access the cell parameters, the obtained spectra were first fitted to a function consisting of two Lorentzian peaks, corresponding to the two major ER peaks [32]:

$$R = \frac{2R_1 f / f_{c1}}{1+(f/f_{c1})^2} + \frac{2R_2 f / f_{c2}}{1+(f/f_{c2})^2} \tag{3.6.2}$$

The obtained characteristic points (f_{c1}, f_{c2}, R_1, R_2) were compared with the theoretical predictions calculated from model of Gimsa and Wachner [34]. The cell parameters at varied temperatures could be determined by taking into account standard cell parameters presented in [34] using temperature dependent parameters as in the Eqs. (1.6.6 a-c).

3.7 DIDS treatment

For experiments with DIDS treatment, DIDS at a concentration of 20 µM was used based on the optimal concentration found by Georgiewa et al. [65]. 3.3 µl of DIDS from a stock solution were added into 10 ml of the suspension of fresh blood at a volume concentration of 0.02%.

3.8 Volume measurements

The whole blood was centrifuged at 2000 g for 8 min in an Eppendorf tube (1.5 ml). The supernatant and the buffy coat were discarded and the Hct of the red-cell sediment was determined in hematocrit-capillaries by centrifugation at 10,000 g for 8 min (Sigma-centrifuge, Fisher Bioblock Scientific 1-15, Osterode, Germany). From the Hct the amount of measuring solution was calculated that was needed for the dilution of 50 µl of the sediment to a cell concentration of 10%. The cells were incubated in the measuring solution for 5 min and the Hct was determined by hematocrit-centrifugation at 10,000 g for 8 min.

3.9 Hematocrit

After centrifugation, the Hct was determined by measuring both the total height of blood and plasma and the height of the blood cell column (ignoring the white buffy coat layer). The hematocrit volume was calculated by,

$$Hct\ (\%) = [\text{height of packed red cells (mm)} \times 100] / [\text{height of packed red cells and plasma(mm)}] \qquad (3.9.1)$$

There is a small but consistent error in all microhematocrit determinations of about 3 %, due to some plasma being trapped between red cells after the blood has been centrifuged (Gedde et al. [80]). The International Council for Standardization in Hematology (ICSH) [94] has recommended that in routine clinical practice no correction should be applied.

3.10 Red cell count

The cell number was microscopically determined in a cell-counting chamber by hemocytometry (chamber, Fein-Optik Bad Blankenburg, GDR). The chamber had a graduation of 1/400 mm^2 and a depth of 0.1 mm in 400 counting fields. The volume of the fluid in the chamber is 0.1 mm^3. The number of cells counts was calculated by:

$$cell\ count = N \cdot (D/A) \qquad (3.10.1)$$

where, N is the total number of cells counted, D is a dilution of blood and A is the total counting area (in mm^2).

The mean cell volume (MCV) was determined by dividing of Hct by the cell count (number of cell per liter) [94]. A constant correction for the trapped water volume of 3% has been assumed in all *Hct* calculations (Gedde et al.) [80]. Thus, for the purposes of the present study, the 3% correction factor was applied unlike in typical clinical practice where Hct is used for other purposes.

3.11 Determination of cell water

Cells in the Eppendorf tube were spun down after 5 min of suspension. 300 µl of the packed cell volume (PVC) were pipetted into a tarred test tube. In parallel, the Hct was determined. The tube was weighed before and after drying at 80°C for 24 hours. The cell water determination was carried out as follows [52]:

$$\%\ \text{water in RBC} = \frac{\text{wet weigth - dry weight}}{\text{wet weight}} * 100 - (100 - Hct) * \frac{100}{Hct} \qquad (3.11.1)$$

4 Results

4.1 Measuring solutions

4.1.1 Conductivity of solutions

The conductivities of the experimental solutions were measured in the temperature compensation mode (20°C). The conductivity was found to linearly increase with temperature. The value at constant temperature is correlated with that obtained from theoretical extrapolation according to Eq. (1.6.1c). The extrapolated data for all temperature measurements are tabulated in Tab. 4.1. The temperature dependent conductivities of the solutions obtained from measurements and from calculations are illustrated in Fig. 4.1. The results obtained experimentally are very close to those obtained from theoretical calculations. In this study therefore, the conductivity values of all solutions were taken from the extrapolation curve.

Starting conductivity (S/m)	Temperature °C				
(20°C)	10	15	25	30	35
0.020	0.016	0.018	0.022	0.024	0.026
0.200	0.160	0.180	0.220	0.240	0.260
0.400	0.320	0.360	0.440	0.480	0.520
0.500	0.400	0.450	0.550	0.600	0.650
1.000	0.800	0.900	1.100	1.200	1.300
1.500	1.200	1.350	1.650	1.800	1.950
2.000	1.600	1.800	2.200	2.400	2.600
3.000	2.400	2.700	3.300	3.600	3.900

Tab. 4.1 Temperature dependence conductivity for eight measuring solutions at 20°C. The data were extrapolated to six different temperatures using data measured in the temperature compensation mode of the conductivity meter. The starting conductivities refer to the values measured at 20 °C which is taken as the standard condition for the conductivity determinations. The standard experimental temperature in the present study was 25°C and so the results are shown in bold type.

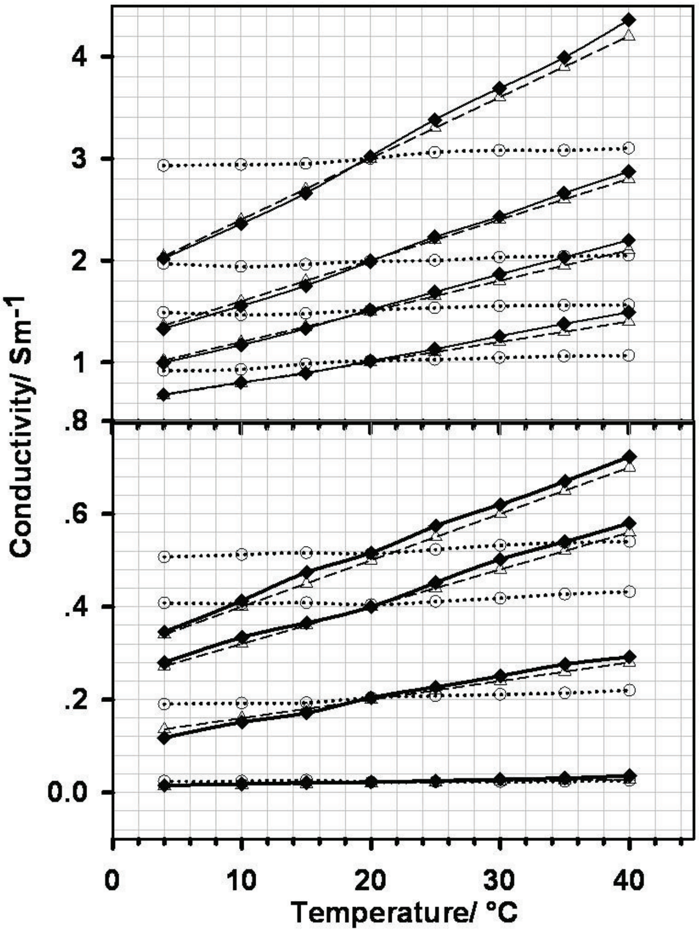

Fig. 4.1 Conductivities of eight experimental solutions were plotted as a function of temperature. The data obtained from the measurement (diamonds) and from the theoretical extrapolation (triangles up) tabulated in Tab. 4.1 are compared. The experimental measurements were carried out using a conductometer in temperature compensation mode (20 °C).

4.1.2 Ionic strength of the solutions

The amount of NaCl dissolving in each solution was measured and is shown in Tab. 4.2. The measured concentrations of NaCl were used to calculate the ionic strength of the solutions The plot of the concentration of NaCl over the range of ionic strengths used is shown in Fig. 4.2. The ionic strength of the solutions increased proportionally to its concentration.

σ_s Sm^{-1}	[NaCl] $molL^{-1}$	Ionic strength $molL^{-1}$
0.022	0.0016±0.0000	0.0016±0.0000
0.220	0.0227±0.0006	0.0227±0.0006
0.440	0.0468±0.0007	0.0468±0.0007
0.550	0.0584±0.0015	0.0584±0.0015
1.200	0.1154±0.0045	0.1154±0.0045
1.610	0.1570±0.0000	0.1570±0.0000
2.210	0.2238±0.0044	0.2238±0.0044
3.310	0.3427±0.0061	0.3427±0.0061

Tab. 4.2 Ionic concentrations and ionic strengths of NaCl for eight solutions measured at the standard experimental laboratory temperature of 25 °C (σ_s). Values are means ± SE (n = 5)

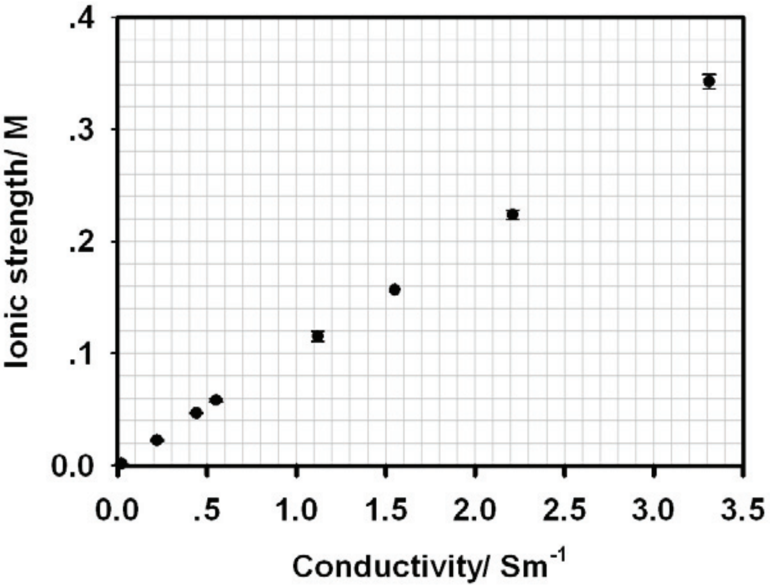

Fig. 4.2 Ionic strengths of the measuring solutions vs. their conductivities

4.1.3 Equivalent conductivity of solutions

Molar conductivity of any solution is proportional to its molar concentration. Normalizing the molar conductivity by the number of the ionic charges, an equivalent conductivity can be calculated for a given concentration using Eq. (1.12.1). For a uni-univalent electrolyte like NaCl, equivalent conductivity is equal to the molar conductivity. The equivalent conductivity varies significantly with the concentration of ions. It decreases as the ionic concentration increases. Tab. 4.3 shows that the molar conductivities of NaCl dissolved in water at 25 °C decreases with increasing concentrations [95]. For equivalent conductivities of all measuring solutions, please see Tab. 4.5.

Compound	Infinite Dilution, Λ^0	Concentration (M)						
		0.0005	0.001	0.005	0.01	0.02	0.05	0.1
NaCl	126.39	124.44	123.68	120.59	118.45	138.25	133.22	128.64

Tab. 4.3 The molar conductivity for NaCl at different concentrations dissolved in water at 25 °C calculated according to the Debye-Hückel - Onsager’s relation [93].

4.1.4 Viscosity of solutions

The viscosities of the measuring solutions at six different temperatures were determined by a falling-ball viscosimeter MLW (VEB MLW Prüfgerätewerk Medingen, Freital, GDR). The measured data are tabulated in Tab. 4.4. The data were plotted over temperature and are shown in Fig. 4.3. The viscosities for all solutions decreased with increasing temperature. To fit a curve to the data, Eq. (1.6.1a) was used. The fit for all solutions gave an estimated temperature coefficient of about 0.02/°C which agrees very well with theory. The change in viscosity is not affected only by temperature; it also depends on the ionic concentration and the properties of the solvent. From Fig. 4.4, we can see that the viscosities of the solutions containing sucrose (conductivities of 0.02 S/m to 1.00 S/m) decreased with decreasing concentrations of sucrose. Inversely, in the solutions of pure NaCl (conductivities of higher than 1.00 S/m), the viscosities increased with increasing concentrations.

Conductivity S/m at 20 °C	Viscosity mPa.s					
	10 °C	15 °C	20 °C	25 °C	30 °C	35 °C
0.020	1.767 ± 0.009	1.539 ± 0.003	1.357 ± 0.008	1.197 ± 0.007	1.062 ± 0.007	0.957 ± 0.002
0.200	1.714 ± 0.006	1.489 ± 0.002	1.308 ± 0.009	1.137 ± 0.004	1.020 ± 0.004	0.921 ± 0.003
0.400	1.646 ± 0.001	1.436 ± 0.004	1.255 ± 0.001	1.119 ± 0.004	0.981 ± 0.007	0.892 ± 0.010
0.500	1619 ± 0.002	1.399 ± 0.005	1.247 ± 0.004	1.103 ± 0.005	0.981 ± 0.005	0.879 ± 0.002
1.000	1475 ± 0.010	1.277 ± 0.003	1.127 ± 0.006	1.004 ± 0.004	0.901 ± 0.005	0.825 ± 0.007
1.500	1389 ± 0.001	1.205 ± 0.103	1.082 ± 0.007	0.960 ± 0.006	0.861 ± 0.003	0.784 ± 0.002
2.000	1396 ± 0.000	1.225 ± 0.003	1.059 ± 0.006	0.959 ± 0.007	0.851 ± 0.001	0.773 ± 0.005
3.000	1415 ± 0.005	1.225 ± 0.000	1.086 ± 0.002	0.960 ± 0.012	0.864 ± 0.007	0.788 ± 0.005

Tab. 4.4 Measured viscosities of the experimental solutions at 8 different conductivities over a temperature range of 10 °C to 35 °C. Values are means ± SE (n = 5)

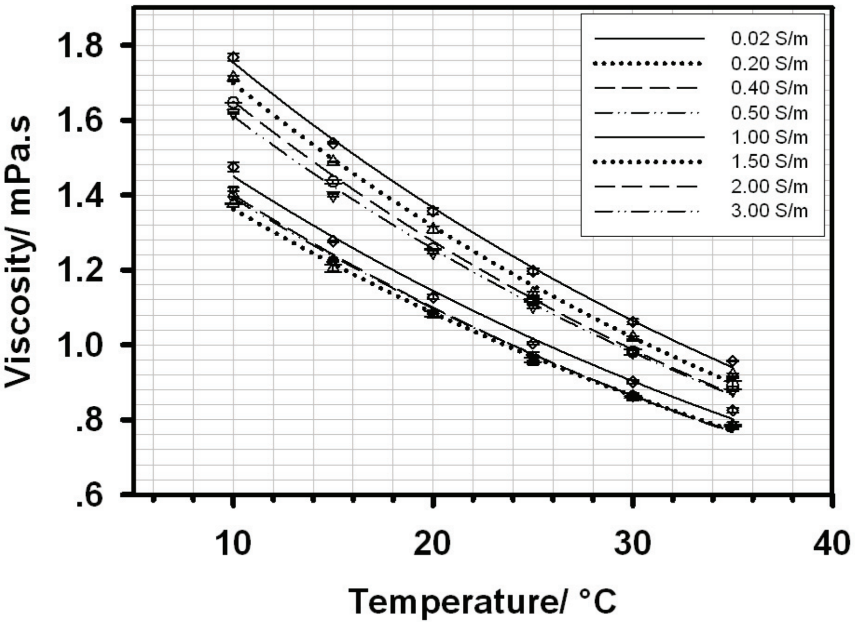

Fig. 4.3 Plot of viscosity of the experimental solutions at 8 different conductivities over a range of temperatures. The Eq. (1.6.1a) was used to fit the experimental points. The temperature coefficient of 0.02/ °C was obtained experimentally from the fit for all conductivities. Error bars are ±SE, based on five replicates.

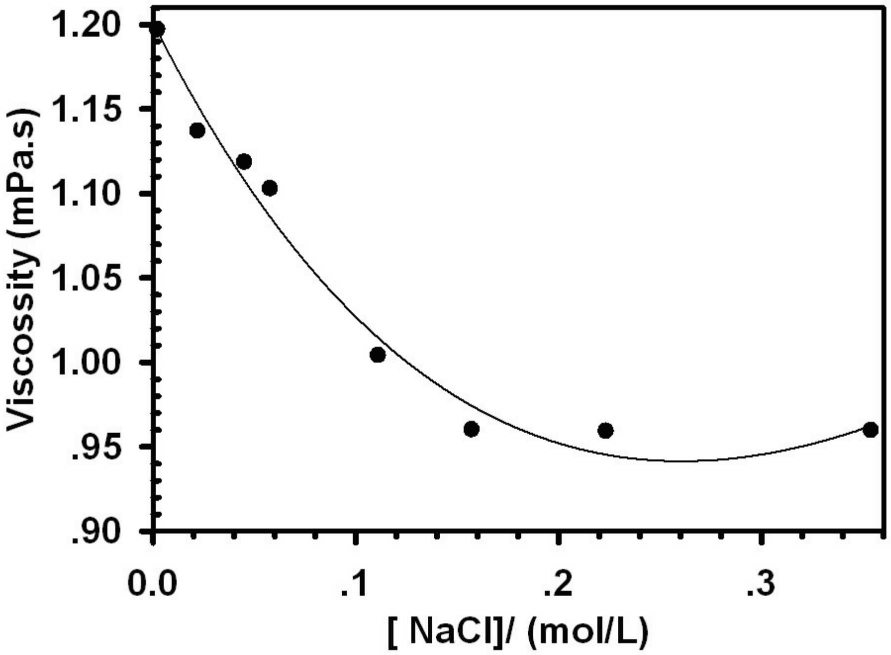

Fig. 4.4 Viscosities of the observed solutions at 25 °C over a range of concentrations of NaCl. Those solutions below 0.15 M NaCl were isotonically adjusted with sucrose, hence their increasing viscosity as the [NaCl] was decreased. Error bars are ±SE, based on five replicates.

4.1.5 A relation of molar conductivity to viscosity

In the case of pure water, change in viscosity is caused by only temperature. Nevertheless, in the case of any solution, the viscosity can be changed by alteration of both the concentration of solutes, as previously presented, and their molar conductivity expressed in Eq. 1.12.9. In Tab. 4.5, the viscosities, as well as the molar concentrations, of eight experimental solutions, measured at 25 °C, are presented.

Conductivity Sm^{-1}	**Viscosity** mPa.s	**[NaCl]** $molL^{-1}$	**Equiv. Conductivity** $Scm^{2}mol^{-1}$	**Equiv. Conductivity*Viscosity** $Scm^{2}mol^{-1}.mPa.s$
0.022	1.197 ± 0.007	0.002±0.000	142.803±1.527	170.964±2.180
0.220	1.137 ± 0.004	0.023±0.002	96.185±0.615	109.374±1.011
0.440	1.120 ± 0.003	0.047±0.007	94.587±1.315	105.819±1.774
0.550	1.104 ± 0.005	0.059±0.002	93.505±0.476	103.136±0.902
1.200	1.005 ± 0.003	0.117±0.003	103.76±0.305	103.20±0.311
1.610	0.963 ± 0.026	0.157±0.000	102.548±0.000	98.472±0.630
2.210	0.961 ± 0.004	0.220±0.004	100.324±1.700	96.250±1.820
3.310	0.967 ± 0.065	0.345±0.003	96.104±1.252	92.250±1.450

Tab. 4.5 Viscosities, ionic concentrations, equivalent conductivities and the product of the equivalent conductivities and the viscosities of eight experimental solutions measured at 25 °C. Values are means ± SE (n = 5)

The equivalent conductivities of the solutions were obtained by dividing the conductivity by the molar concentration. The product of the equivalent conductivities and the viscosities are shown the column five. The plot of equivalent conductivities of experimental solutions, before and after taking the viscosities of the solution into account after normalizing to that of water at 25 °C, are presented over the concentrations of NaCl used in the present study in Fig. 4.5. The data were first corrected for the viscosity of the solution, and then fitted to the Debye-Hückel-Onsager's equation (Eq. 1.12.7) [93]. Without correction for viscosity, no experimental points could be fitted with the theory. When Debye, Hückel and Onsager [93] first published their equation they pointed out that experimental results only conformed to theory at concentrations smaller than 0.001 M. At higher concentrations, the effect of viscosity as predicted by Walden' rule had to be taken into account. After correction for viscosity, the points could be closely fitted to the theory. In the present study, an agreement of the experimental points with the theory could be observed only in the concentration range of 0.01 – 0.1 M NaCl. At concentrations below 0.0015 M and higher than 0.1 M, dramatic deviations of the experimental points from the theoretical curve were found (Fig. 4.5).

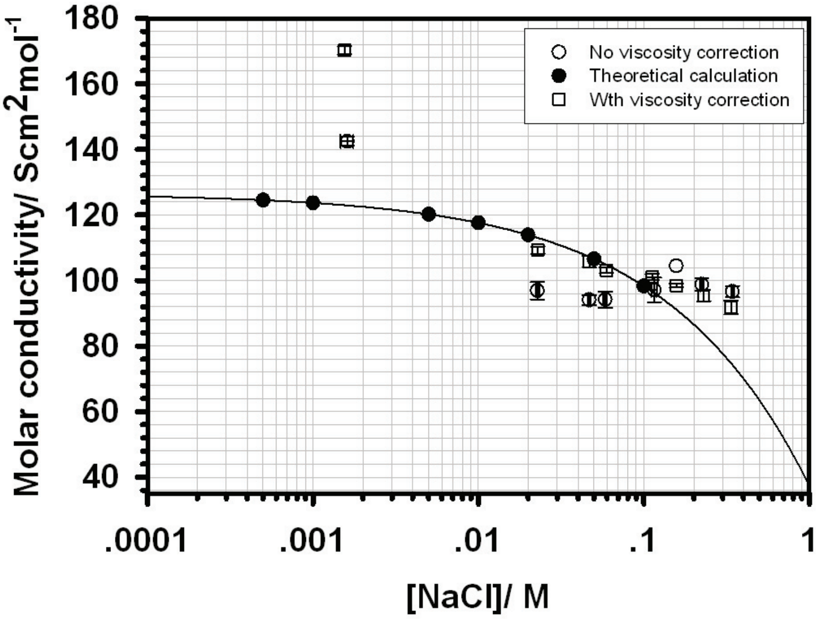

Fig. 4.5 The molar conductivities of experimental solutions at 25 °C containing 1 mM Phosphate buffer with and without corrections for the viscosity, compared with those obtained from theoretical calculations [93]. Error bars are ±SE, based on five replicates.

4.2 ER measurement

4.2.1 Effect of external conductivities on the ER spectrum

Complete ER spectra were measured as described under Materials and Methods. Fig. 4.6 shows ER spectra for eight selected external conductivities. For determination of the ER peaks, a non-linear least error-square fit procedure was used to fit a Lorentzian function to the measuring points. Co- and anti-field rotation peaks are clearly visible at low (Figs.4.6A and B) and medium (Figs.4.6C and D) conductivities, respectively. At high conductivities (Figs.4.6E-H) only negative peaks were observed. With increasing conductivity all peaks are shifted towards higher frequencies (see also Fig.4.7). Around 1 S/m the second peak changes its sign. Please note that the frequency of a rotation peak is only equivalent to the characteristic frequency of an underlying process if peaks are well separated. Thus, the superposition of different peaks may mimic peak frequencies different from the actual characteristic frequencies. In Fig.4.7 two characteristic frequencies (Figs.4.7A and B) and in Fig.4.8 the respective peak heights (Figs.4.8A and B) obtained from the fits have been plotted against the external conductivity. For comparison, my own new data has been plotted together with those already published in [17, 29]. The theoretical curves in Fig.4.7 have been calculated assuming an oblate cell model [18] with a long half-axis, axis ratio, relative external permittivity, membrane conductivity and membrane capacitance to be 3.6 μm, 1:2, 78, 1 μS/m, and $0.997*10^{-2}$ F/m^2, respectively.

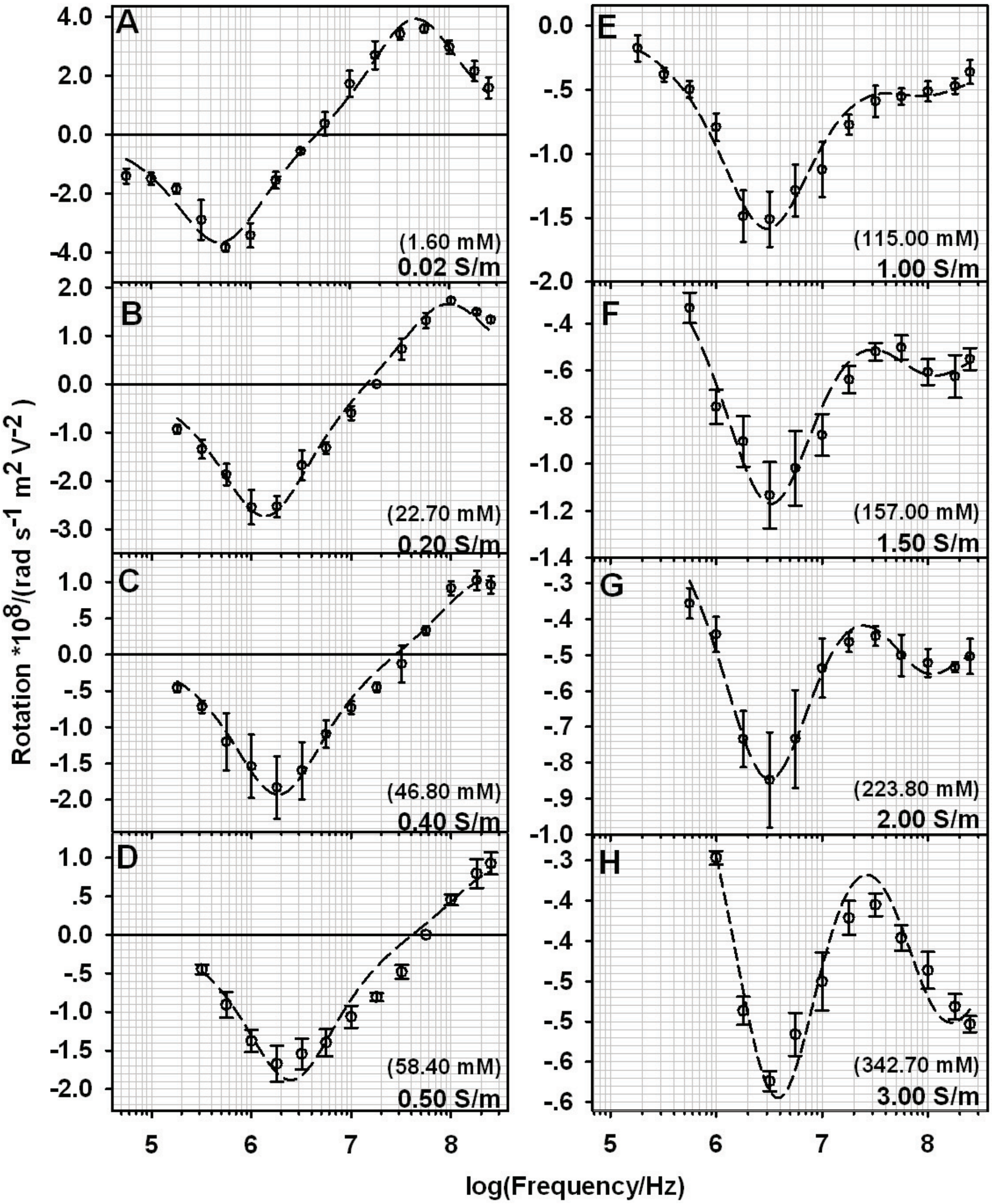

Fig. 4.6 ER spectra of HRBCs at different external conductivities. Two superimposed Lorentzian peaks were fitted to the measuring points. Error bars are ±SE, based on five replicates.

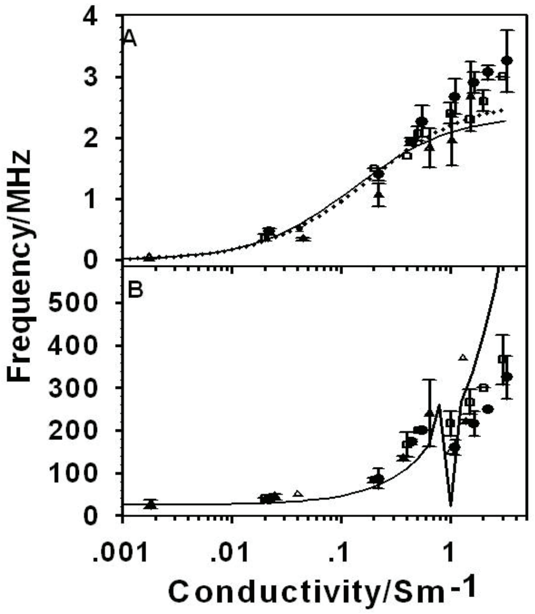

Fig. 4.7 Characteristic frequency of the first peak, fc_1 (A) and second peak, fc_2 (B) of experimental points (circles) over a range of external conductivity. Triangle down and square are representing published in [33] and [60], respectively. For curves see text.

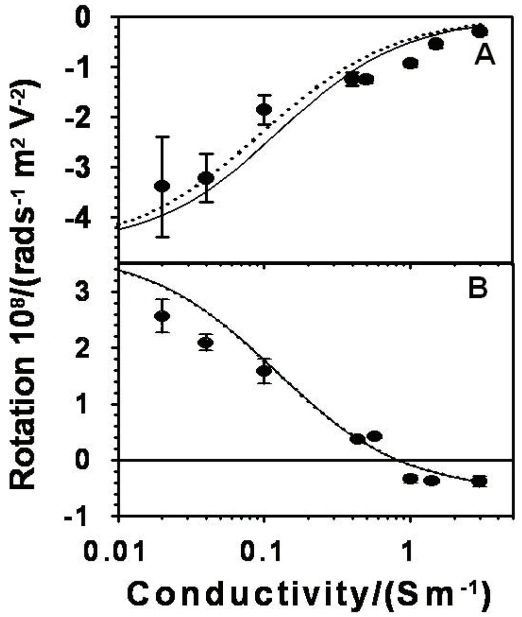

Fig. 4.8 Normalized rotation speed at the first peak (A) and second peak (B)

The solid line shows values calculated assuming cytoplasmic conductivity and relative permittivity frequency independent values of 0.535 S/m and 50, respectively. The dotted line represents frequency dependent parameters with a conductivity of 0.4 S/m and a relative permittivity of 212 at low frequencies, dispersing around 15 MHz to become 0.535 S/m and 50 at high frequencies, respectively (compare to values in [33]). Rotation speeds at the first and second ER peaks are presented in Fig.4.3A and B, respectively. For conductivities lower than 0.5 S/m the second peak was positive, switching to negative at conductivities higher than 1.0 S/m (Fig.4.8B). This switching led to the discontinuity in the f_{c2}-curve shown in Fig.4.7B. At high conductivity values the rotation speed was very low (Figs.4.8A and B).

4.2.2 Effect of temperature on ER spectrum

Fig. 4.9 shows ER spectra for six different experimental temperatures, measured in eight selected solutions, with conductivities ranging from 0.02 S/m to 3.00 S/m. A linear temperature dependence was found for all solutions (cp. to Eq. 1.6.1c). At low and medium conductivities (0.02 S/m to 0.50 S/m), co- and anti-field rotation peaks were clearly visible. Starting at conductivities of 1.00 S/m, and higher, the second peak changed from positive to negative. A strong shift of f_{c1} towards higher frequencies was observed for conductivities higher than 2.00 S/m at 30 °C and 35 °C. Nevertheless, changes in temperature did not alter the overall shape of the ER spectra ([50], see also Fig. 4.9)

In Tab. 4.6 presents the temperature dependent parameters used to derive the theoretical curves in Figs. 4.10 and 4.11. Frequency independence, as well as cell parameters for a dispersive cytoplasm, have been taken from [33]. Temperature dependencies according to Eq. 1.6.1b-c have been used to calculate the permittivities and conductivities for temperatures deviating from 23 °C. No temperature dependence has been assumed for the membrane permittivity since the temperature coefficients for the permittivities of fatty acid-chain-like compounds are known to be very low [44]. The frequency dependent transitions of the cytoplasmic permittivity and conductivity have been described according to the dispersion relation by the following phenomenological equations [33]:

$$\varepsilon_i = \varepsilon_i^{\infty} + \Delta\varepsilon \frac{1}{1+(\omega\tau)^{2(1-\alpha)}} \qquad \text{and} \quad \sigma_i = \sigma_i^{0} + \Delta\sigma \frac{(\omega\tau)^{2(1-\alpha)}}{1+(\omega\tau)^{2(1-\alpha)}} \qquad (4.2.1)$$

where, ω and τ are the circular frequency of the field and the time constant of the cytoplasmic dispersion, respectively. ε_i^{∞}, $\Delta\varepsilon$, σ_i^0 and $\Delta\sigma$ are the relative permittivity at infinitely high frequency, the dielectric decrement as well as the cytoplasmic conductivity at low frequency, and the conductivity increase resulting from the dispersion, respectively (see Tab. 4.1). Two different values for the dispersion width (α) have been considered, $\alpha = 0$ and $\alpha = 0.5$.

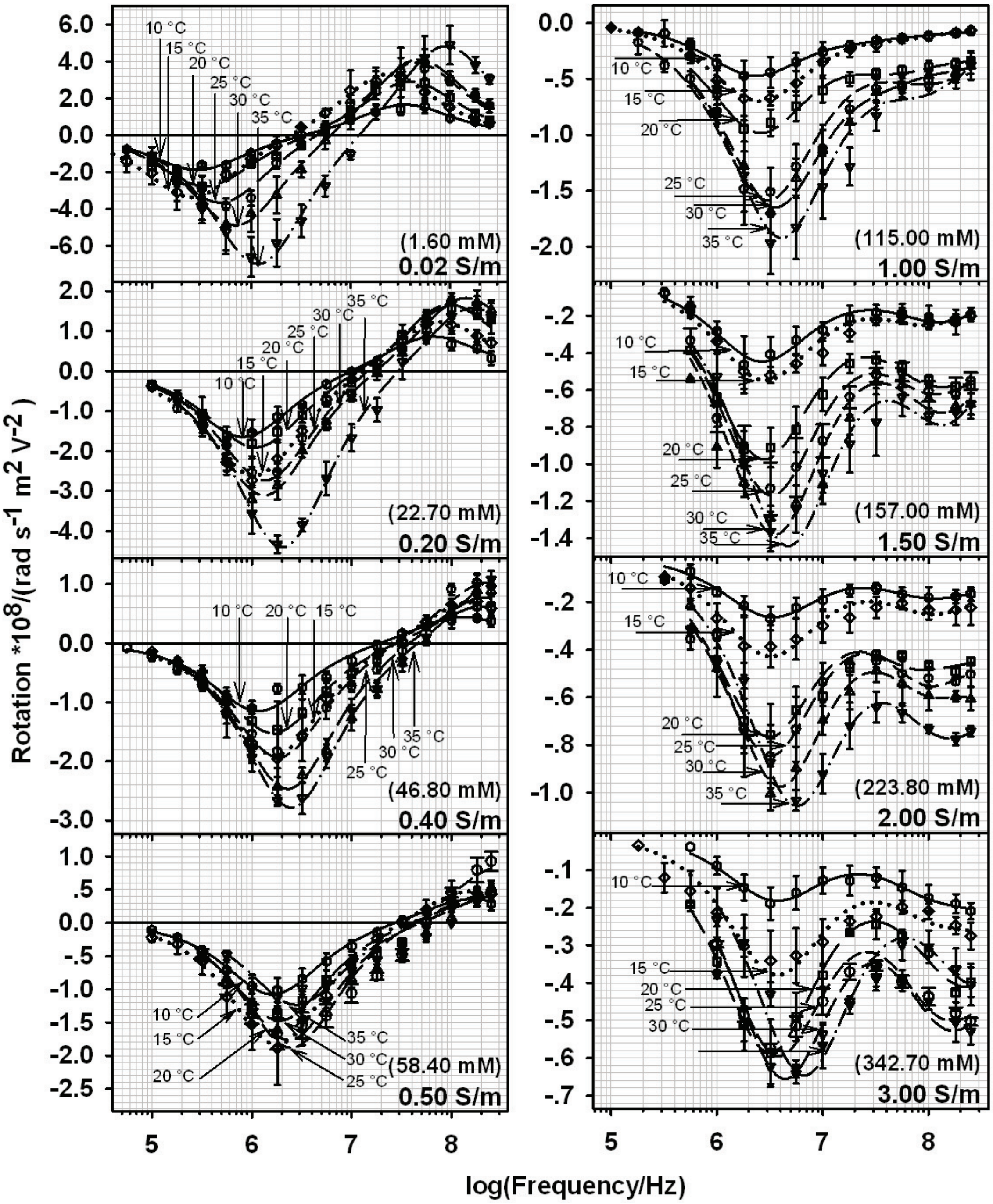

Fig. 4.9 ER spectra for various different external conductivities at six different temperatures, 10 °C (hexagons, solid lines), 15 °C (diamonds, dotted lines), 20 °C (squares, long dash lines), 25 °C (circles, medium dash lines), 30 °C (triangles up, short dash lines), and 35 °C (triangles down, dash-dot lines). The conductivities given in the figures refer to the conductivities measured at 20 °C. The data in parentheses are the corresponding ionic strengths of the solutions. The spectra were measured in square-topped fields. Two superimposed Lorentzian peaks of the general form 2R f f_c / (f^2 + f_c^2) were fitted to the measuring points. R, f and f_c stand for peak rotation speed, field frequency, and characteristic frequency, respectively. Error bars are ±SE, based on five replicates.

Parameter	10 °C	15 °C	20 °C	23 °C [33]	25 °C	30 °C	35 °C
External permittivity	83.8	82.0	80.2	***78.5***	78.5	76.6	74.8
Membrane permittivity	9.04	9.04	9.04	***9.04***	9.04	9.04	9.04
Internal permittivity before and after dispersion (or no dispersion)	224.5 53.0	219.7 51.8	214.9 50.7	***212.0*** ***50.0***	210.1 49.5	205.2 48.4	200.3 47.2
Dielectric decrement	171.5	167.9	164.2	***162.0***	160.6	156.8	153.1
Range of the external conductivity (S/m)	0.018 – 2.400	0.016 - 2.700	0.020 - 3.000	***0.001 - 1.390***	0.022 - 3.400	0.024 - 3.600	0.026 - 3.900
Membrane conductance (μS/m^2)	355.2	403.2	451.2	***480.0***	499.2	547.2	595.2
Internal conductivity before and after dispersion (or no dispersion) (S/m)	0.301 0.409	0.342 0.457	0.376 0.506	***0.400*** ***0.535***	0.416 0.554	0.456 0.603	0.496 0.652

Tab. 4.6 Electric cell parameters for 23 °C (*bold italics*) obtained from [33] were extrapolated according to Eq.1.6.1 b-c. Starting and end values of the relative permittivity and conductivity of the dispersive cytoplasm (Eq. 4.2.1) were assumed to depend on temperature. In the model, these values were assumed not to depend upon on the dispersion width. The "no dispersion" data were also used in a model with frequency independent parameters (compare to Figs. 4.10 and 4.11). These parameters largely coincide with those given for around 100 MHz in [33].

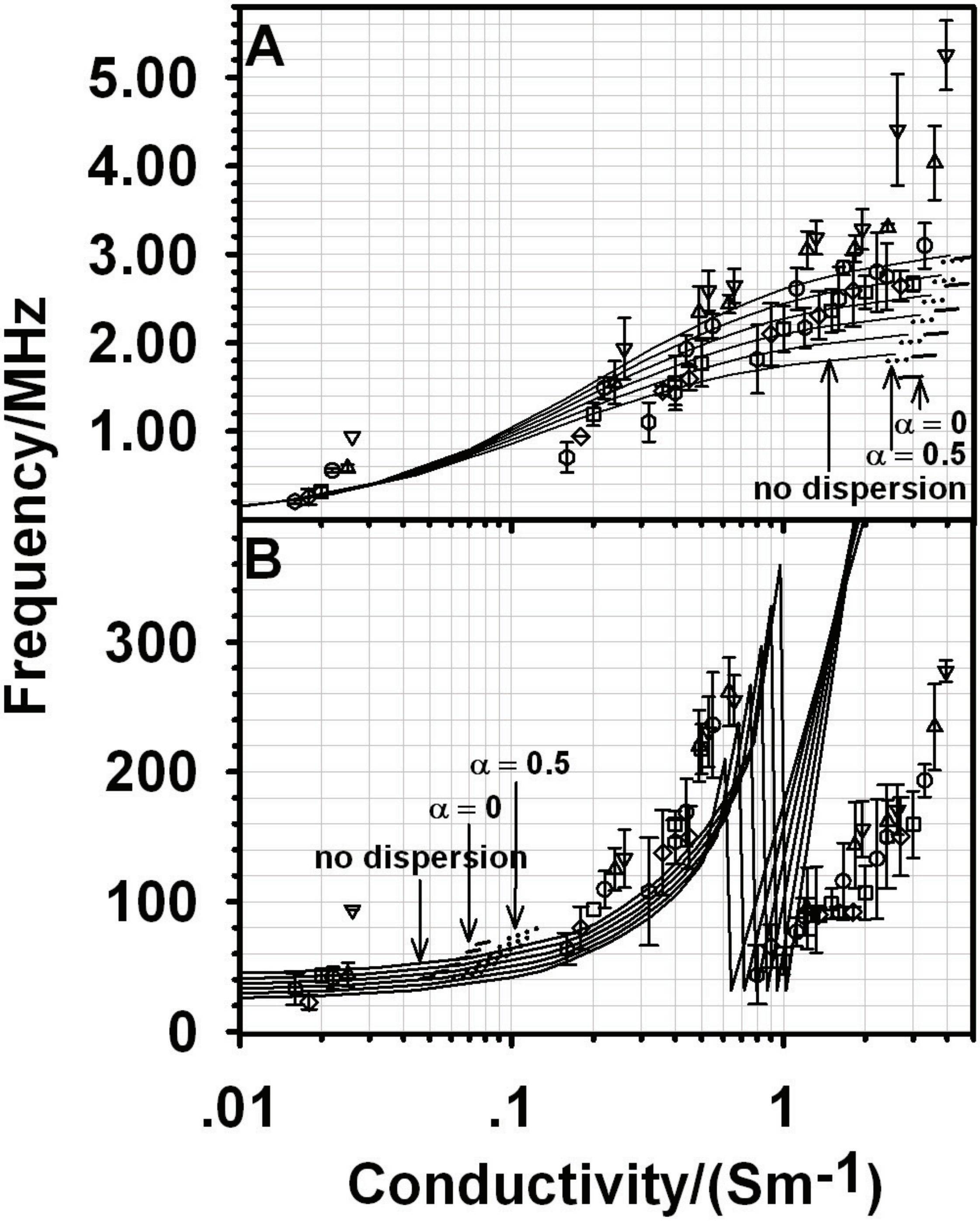

Fig. 4.10 First (A) and second (B) characteristic frequencies of Fig. 4.9 plotted against external conductivity for a range of different temperatures (for symbols see Fig. 4.9). Please note that all frequencies were divided by a factor of 1.066 to correct for the square wave measuring field (for details see [31]). The theoretical curves were calculated according to the temperature dependent parameters given in Tab. 4.6. *Frequency independent* parameters were assumed for the full curves. For comparison, the position of the curves with *frequency dependent* parameters are marked by short continuous and dotted lines. The dispersion-width α is marked in the figure (see Eq. 4.2.1). Error bars are ±SE, based on five replicates.

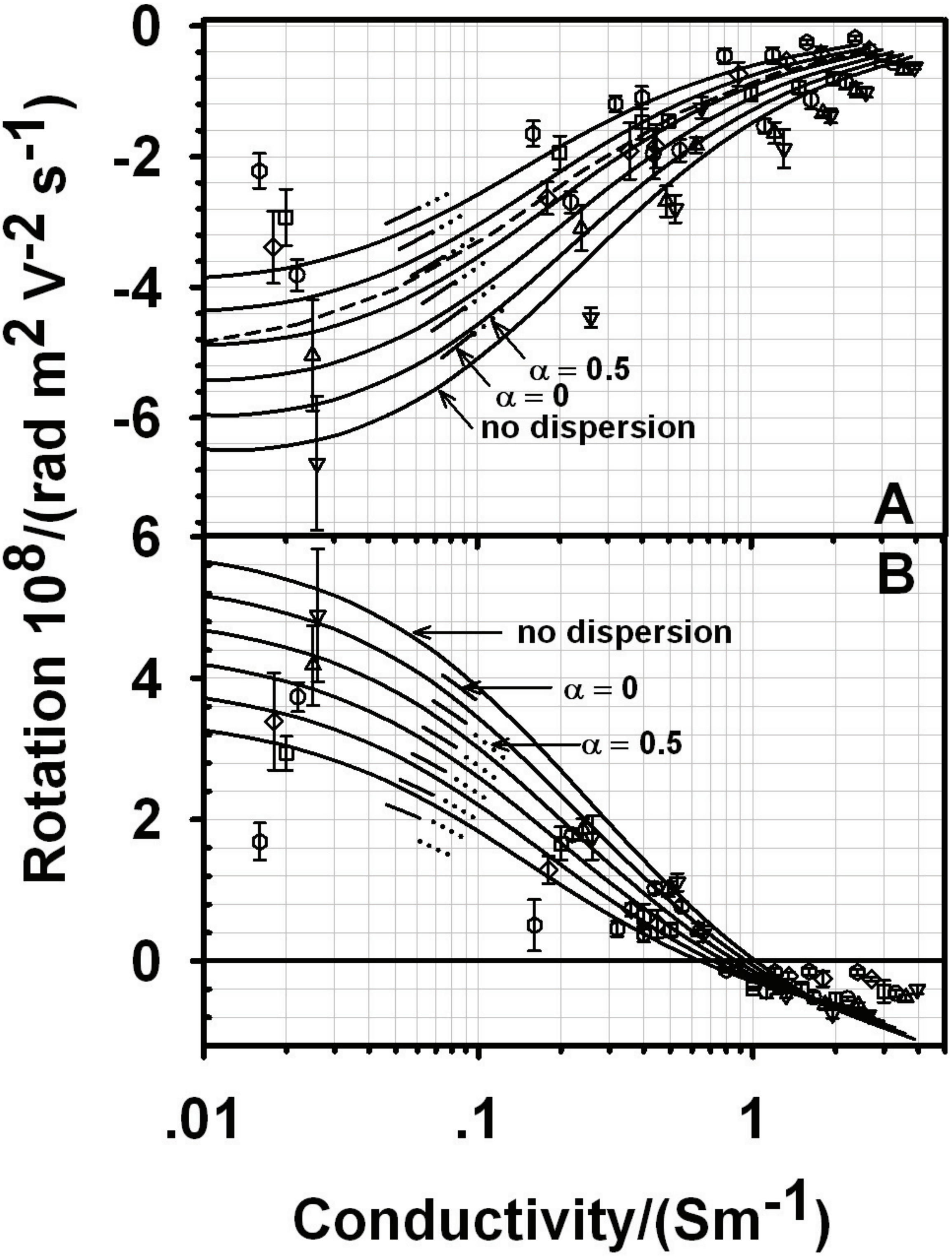

Fig. 4.11 Rotation peak amplitudes of the first (A) and second (B) peak obtained from the spectra fits of Fig. 4.9. For symbols and line types please see Fig. 4.10. An additional curve (dashed line) is given for the first peak at 15 °C assuming a reduced membrane conductance of 20 S/m^2 (see discussion). Error bars are ±SE, based on five replicates.

4.2.3 The anomalous rotation speed at 15 °C

An anomalous increase in the rotation speed was observed for low and medium conductivities at 15 °C (see Fig 4.11A). The ER spectra of control HRBCs and cells treated with DIDS were compared to test whether this behavior is related to an alteration in the anion transport, mediated by the anion exchange protein known as the band 3 protein (capnophorin). DIDS treatment led to an increase in the rotation speed (magnitude of R_1, Fig. 4.12) at all experimental temperatures except at 15 °C where no increase was observed.

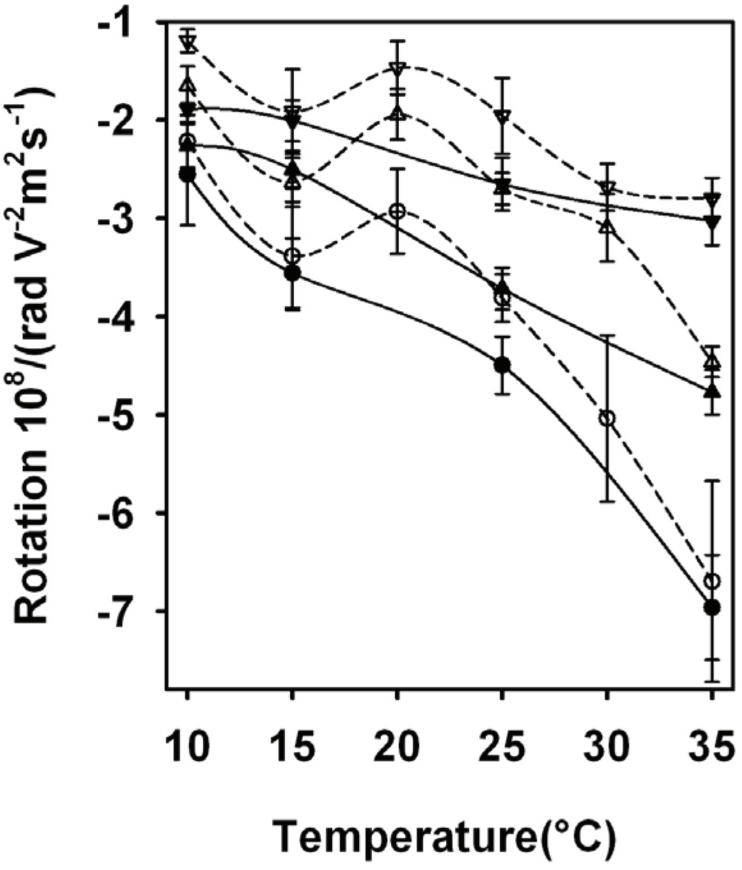

Fig. 4.12 First rotation peak at different selected temperatures for control (open symbols, dashed lines) and DIDS treated (filled symbols, solid lines) cells. The circles, upward triangles and the downward triangles represent external conductivities of 0.02 S/m, 0.20 S/m and 0.40 S/m, respectively. Error bars are ±SE, based on five replicates

4.3 Cell volume and cell water of HRBCs

4.3.1 Effect of external media on cell volume and cell water

Using the hematocrit-capillary method described under Materials and Methods, I found a cell volume of about 94.5 μm^3 with a relative water content of 0.71 for physiological conditions (cells from full blood, blood plasma conductivity around 1.48 S/m). When the cells were transferred to isotonic measuring solutions of different ionic strength a rapid volume change could be observed within 5 min (Fig. 4.13).

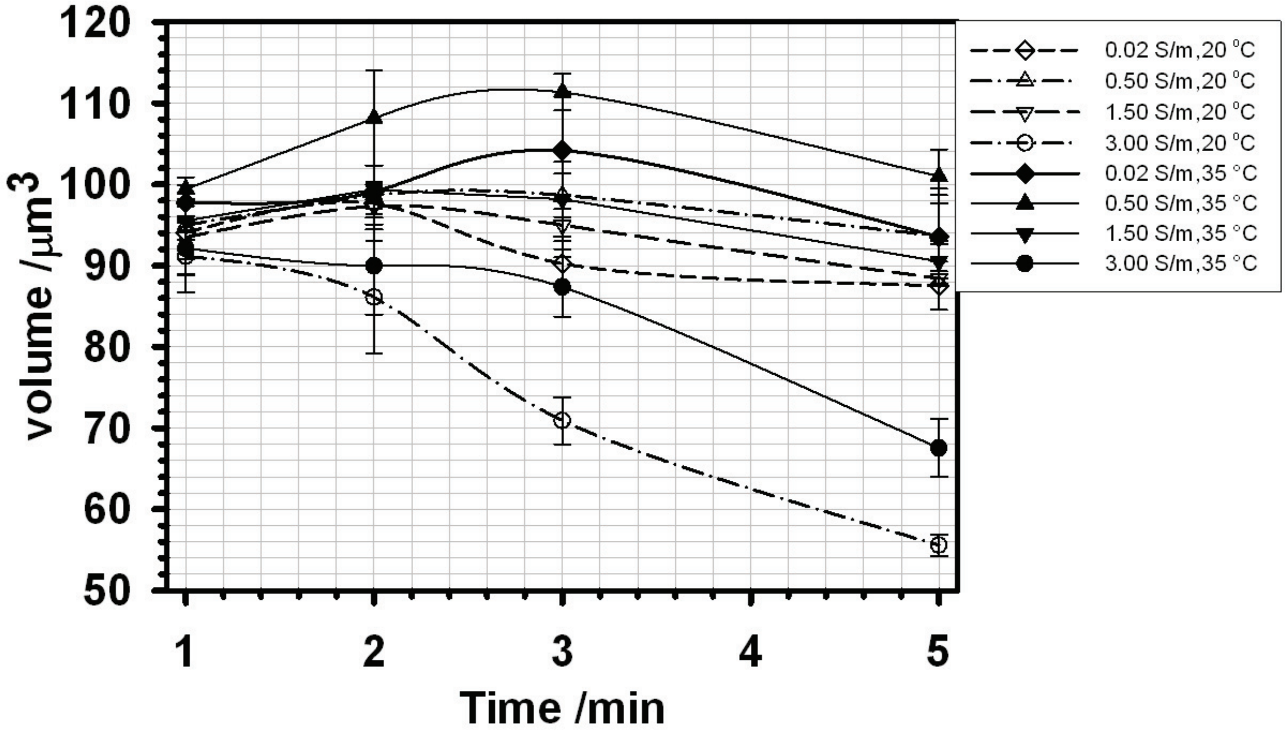

Fig. 4.13 Time dependent volume changes of HRBCs suspended in external conductivities of 0.02 S/m to 3.00 S/m. Error bars are ±SE, based on five replicates

This change depended on the temperature of the medium. At 1.5 S/m (isotonic NaCl, no sugar added) the cell volume was almost constant at temperatures of 20 °C and 35 °C. The volume decreased in the 3 S/m NaCl solution which is a non-physiologically high ionic concentration. Curiously, an increase in cell volume beyond the physiological value of 100% was observed at lower conductivities and higher temperatures even though the solutions were isotonic (see discussion). As can be seen from the volume measurements, the process of volume adjustment did not come to an end after 5 min. However, 5 min was the longest suspension time of the cells for ER-experiments. Using suspensions times of 5 min or less the cell volumes did strongly depend on the measuring conditions (Fig. 4.14A).

The figure compares experimental data for 20 °C and 35°C. Using 5 min incubation times, a relative volume beyond 100% could be observed in the medium ionic strength range at higher temperatures. This behaviour is reflected in the cell water content (Fig. 4.14B). At lower conductivities of 0.02 S/m to 0.50 S/m the cell volume increases with increasing NaCl concentrations. However, a cell volume decrease with increasing external NaCl concentrations was found at conductivities higher than 1.5 S/m. The dilution coefficient (δ), which is related to cell volume and cell water, can be calculated using Eq. 1.11.1.

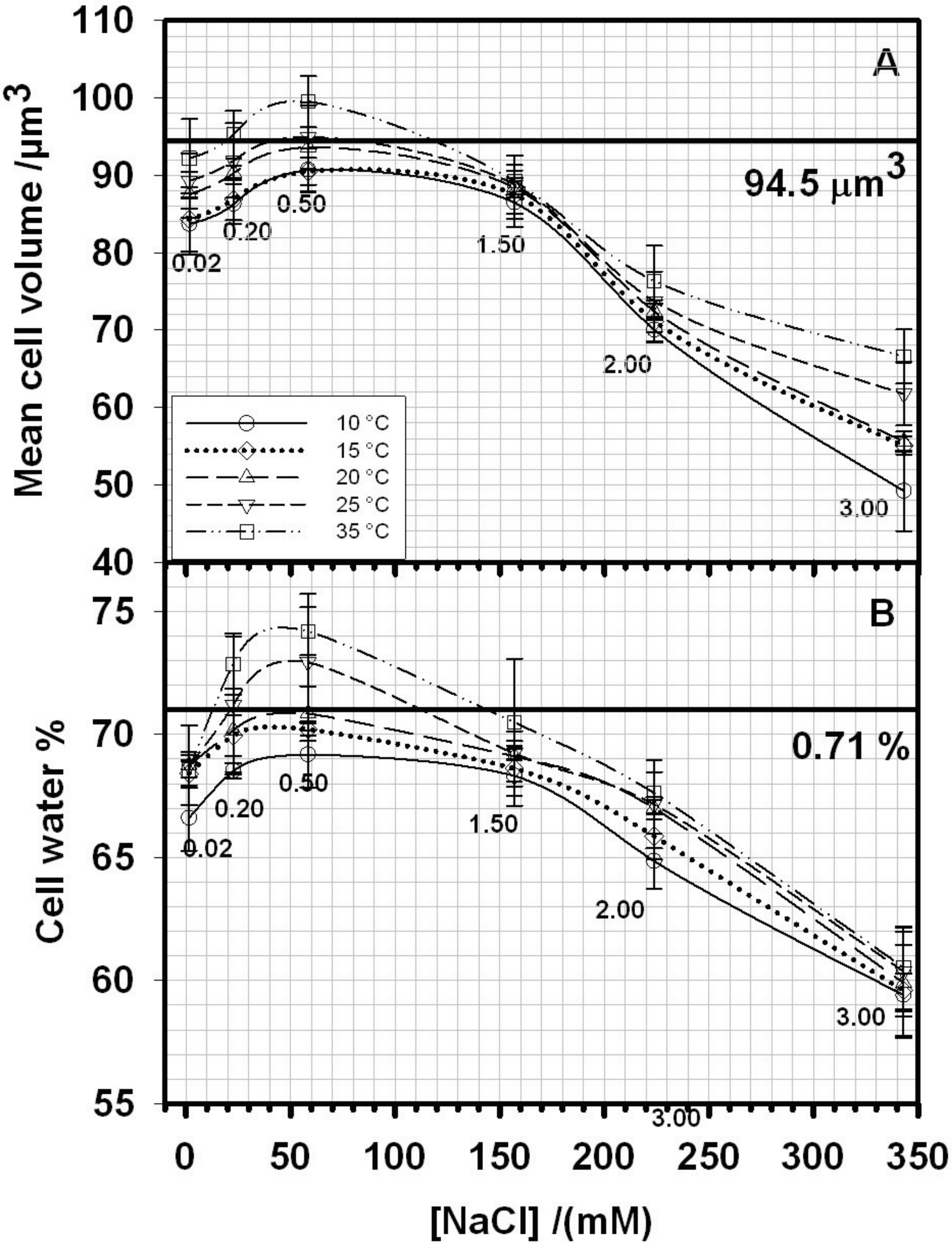

Fig. 4.14 Mean cell volume (A) and relative cell water content (B) of red cells at different external concentrations of NaCl compared to the measured physiological value (the reference lines on the graphs). The experimental temperature was adjusted from 10°C to 35 °C. The numbers appearing on the graphs refer to the external conductivities in S/m. Error bars are ±SE, based on five replicates

Fig. 4.15 shows a plot of the δ value vs. conductivity. At low conductivity to medium conductivities (0.02 S/m to 0.50 S/m) and conductivity at physiological state (1.50 S/m), δ stays almost constant but then rapidly increases at higher conductivities where cell water and cell volume fall and there are also changes in cell shape.

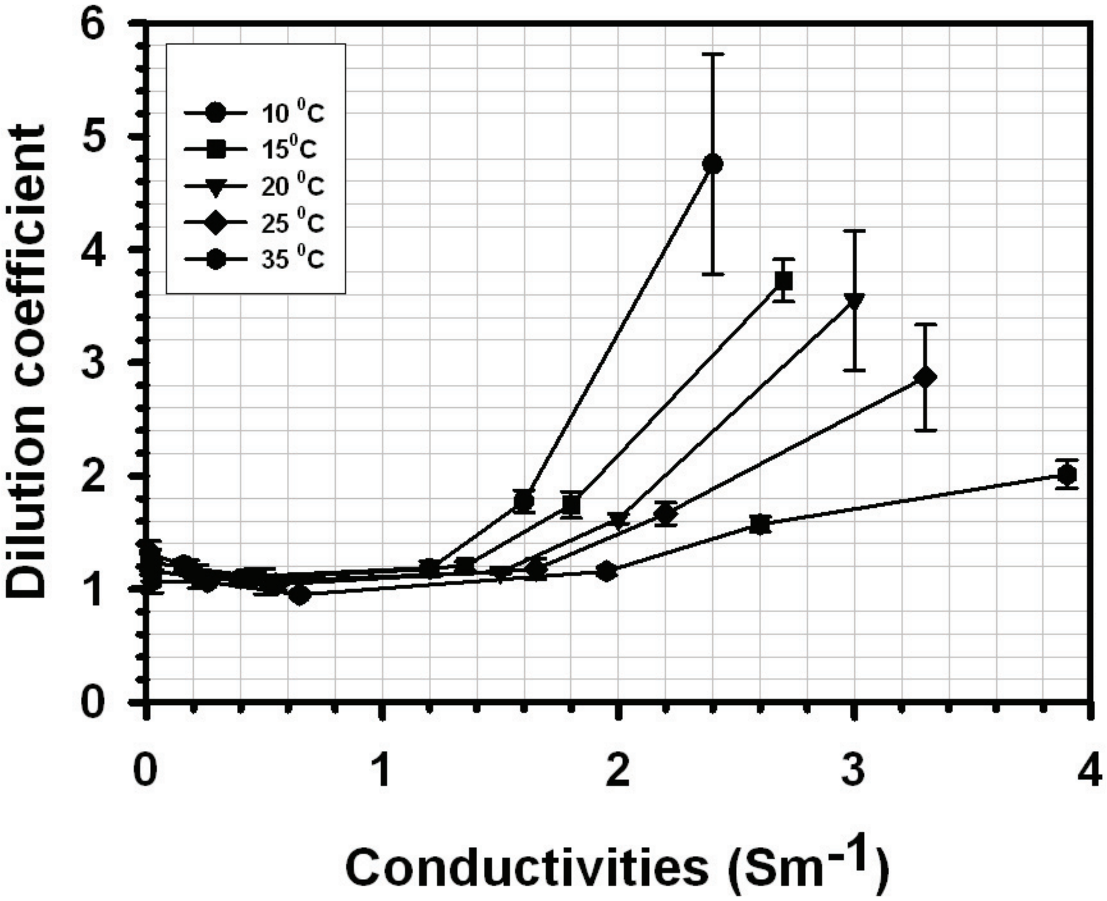

Fig. 4.15 Dilution coefficient at experimental conductivities for 5 experimental temperatures. Error bars are ±SE, based on five replicates

4.3.2 Effect of temperature on cell volume and cell water

To further characterize the nature of the volume changes depending on temperature, the data on cell volume change when they were suspended for 5 mins in different experimental solutions were plotted over a range of experimental temperatures (Fig. 4.16). The experimental points were fitted with the Arrhenius-relation [97] defined as:

$$K_R = Ae^{-\frac{E_A}{RT}} \qquad (4.2.2)$$

This equation describes the temperature dependence of a chemical reaction and reaction rate of physiochemical processes, such as diffusion, membrane transport, respiration rate of cold-blooded animals such as fish and reptiles, kinetics of phase transition etc. To evaluate the experimental data, the logarithmic form is used:

$$\ln K_R = \ln A - \frac{E_A}{RT} \tag{4.2.3}$$

where, K_R is the rate constant; E_A is activation energy; A is an empirical factor, and R is the universal molar gas constant with a value of 8.31 J/mol.K. Applying this kind of evaluation, y = ln K_R , in this case means the rate of volume changes influenced by temperature was plotted against x = 1/T. The graph is shown in Fig. 4.17.

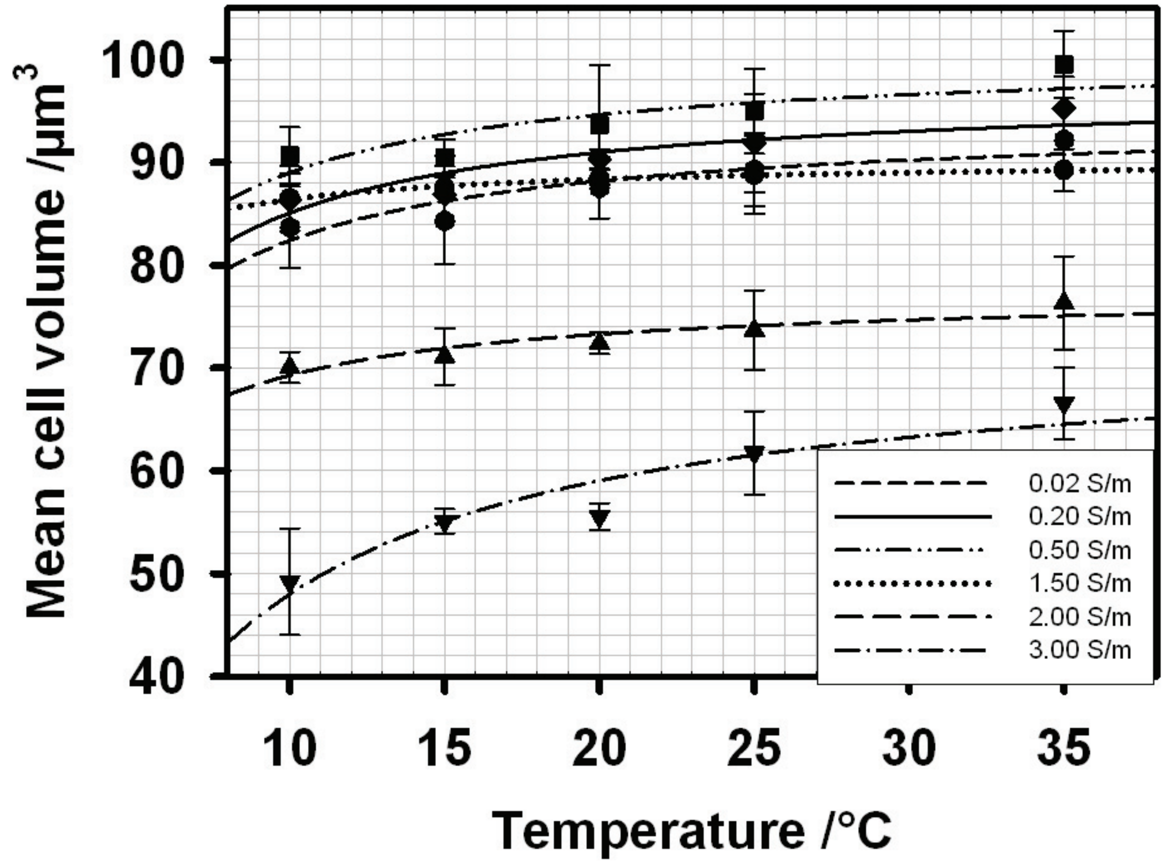

Fig. 4.16 Volume changes over temperature of HRBCs suspended in six different external conductivities. The Arrhenius relation was used to fit the curves to the experimental data points. Error bars are ±SE, based on five replicates

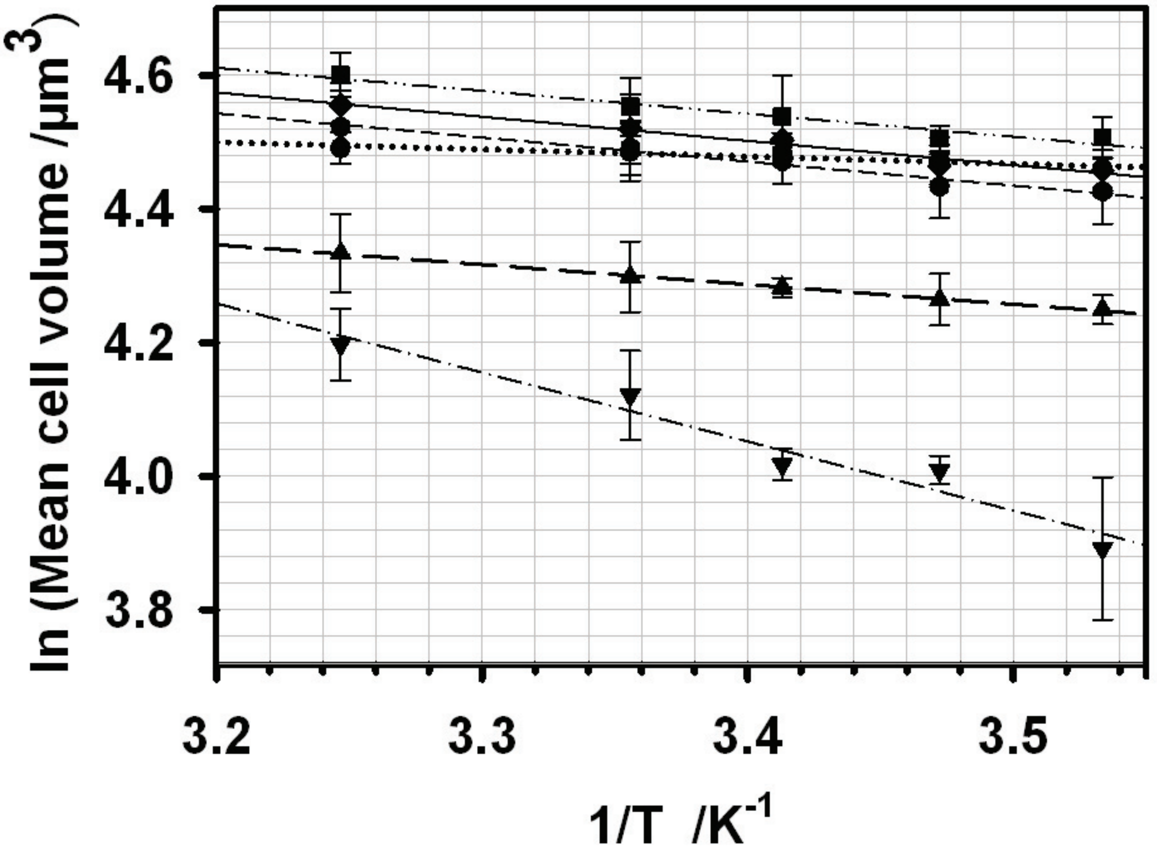

Fig. 4.17 Arrhenius plot of Fig. 4.16

The slope of the straight line is E_A/R. The value of ln A can be read from the crossing point with the abscissa giving the volume at the start of the experiment, where there is no temperature difference. From the plot of Fig. 4.17, the slope of the graph gives a measure of the activation energy, whereas the crossing point with the abscissa gives the rate constant in terms of the logarithm value of the volume change, i.e. exchange fluxes of ions and small osmolytes across the membrane, as well as their recruitment in the cytoplasm, e.g. by a pH-dependent ion dissociation from hemoglobin. The activation energies obtained from the fit are shown in Fig. 4.18 and indicate the electrical energy required to provide a driving force for net movements of ions across the membrane plotted over the ionic concentrations of the suspending solution.

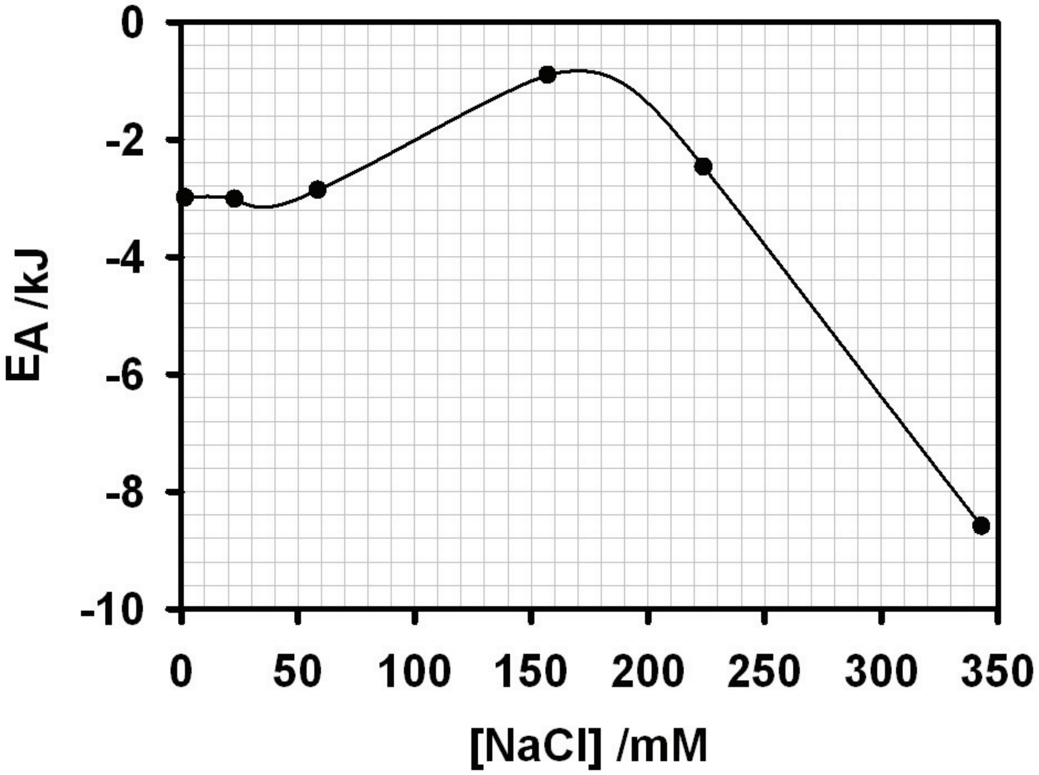

Fig. 4.18Activation energy obtained from the Arrhenius plots of Fig. 4.17

Highly negative activation energy means there is a high ionic concentration difference across the membrane at low and high external conductivity. At the NaCl concentration around the physiological value (150 mM NaCl or at conductivity of about 1.50 S/m), the lowest of activation energy of about -0.8 kJ/mol was obtained. This means that in 1.50 S/m NaCl there was little or no ionic concentration difference across the membrane and hence no volume change.

4.4 Influence of cell volume on cytoplasmic conductivity

The internal conductivity of red blood cells is largely due to its ion content composed primarily of K^+, Na^+, Mg^{++}, $C1^-$, and some large ions, predominantly dissociated hemoglobin molecules. In an ideal electrolytic solution, mobility and limiting ionic conductance values for K^+, Na^+, Mg^{++}, and HCO_3^- are known and are tabulated (Tab. 4.7).

	(1)	(2)	(3)	(4)	(5)	(6)
Ion	Intracellular Concentration mol l^{-1}	Limiting Ionic Conductances S m^2 mol^{-1} x 10^{-4}	Conductivity Contribution S m^{-1}	Molar Conductivity Influenced by Viscosity S m^2 mol^{-1} x 10^{-4}	Effective Conductivity Influenced by Viscosity S m^{-1}	Effective Conductivity Influenced by Cell Water S m^{-1}
Na^+	0.0186	49.86	0.09	31.44	0.06	0.03
K^+	0.095	72.97	0.69	46.02	0.44	0.26
½ Mg^{++}	0.0051	52.97	0.03	33.41	0.02	0.01
Cl^-	0.055	75.88	0.42	47.85	0.26	0.15
HCO_3^-	0.015	44.27	0.07	27.92	0.04	0.02
X^-	0.01	35.61	0.04	22.46	0.02	0.01
HbO_2^-	0.042	26.63	0.11	16.79	0.07	0.04
Total	0.2407	358.19	1.44	225.90	0.91	0.53

Tab. 4.7 Calculation of the internal conductivity of HRBC under physiological conditions using known concentrations of different ionic species and limiting ionic conductance values at 25 °C [98]. The internal viscosity of 5.91 mPa.s at 37 °C [91] was introduced into Walden's law. The calculated cytoplasmic conductivities are presented in the fifth column in S m^{-1}. The effective conductivities (Sm^{-1}) in column six were obtained from the difference of conductivity at finite dilution (column four) and of cytoplasmic conductivity influenced by viscosity (column five). The volume effect of haemoglobin was not considered because it could be neglected.

The first and second columns of Tab. 4.7 give the ionic balance in the human red blood cell [93, 95 - 96]. The third column gives limiting ionic conductances for all ions of interest at 25 °C. The fourth column shows the corresponding contribution of the several ions to the "ideal specific internal conductivity" of the cell interior (calculated using Eq.1.12.1). The addition of the individual contributions results in an ideal specific internal conductivity of 14.4 S/m was obtained. The contribution of the "HbO-" amounts to 7.6% due to the net charge of 6.4 electron charges per molecule. The cytoplasm is not pure water. It also contains other macromolecules with a total viscosity of 5.91 mPa s at 37 °C [91]. By introducing the viscosity into the Walden's law, the molar conductivities decrease and consequently reduce the additive effects of individual ions to give an effective cytoplasmic conductivity of about 0.92 S/m. To reach the actual conductivity, the experimental finding that the water content in the cell (effectively the osmotic volume of the cell) under physiological conditions is about 71% [78] needs to be taken in account. Taking this 71% value into account the actual cytoplasm conductivity can be estimated to be 0.53 S/m. The value agrees very well with those reported in the literature [17, 29, 33]. For other experimental solutions, the cytoplasmic conductivity under each condition was calculated using the same procedure. The ionic concentrations in the cytoplasm (first column) are strongly dependent on the dilution coefficient delta (δ) which is related to cell volume and cell water (Eq. 1.11.1). (for more details, please see section 1.11). The limiting ionic conductances (second column) vary with ionic concentration (Eq. 1.12.2). Under physiological conditions, a standard volume (V_0) *in vivo* situations of human red erythrocytes, with a defined relative volume V_0 = 100 % (cell volume of 98 μm^3) is characterized by the external ionic concentration (in mmol/l). All parameters of this standard condition are specified as: c_0 (standard concentration tabulated in the second column of Tab. 4.7) and V_0. Variation in cell volume can be taken into account by introducing the dilution coefficient term delta (δ) [78]. Therefore, the concentration of non-exchangeable solutes in erythrocytes with an arbitrary volume V is equal to $\delta \cdot c_0$. Both arbitrary volume and water content can be measured experimentally and are shown in Fig. 4.14. The calculation was done in the following way: First a constant hemoglobin volume per cell of V_{Hb} = 28.4 μm^3 was calculated assuming a cell volume of 98 μm^3 and haemoglobin occupying 29 % of the total volume [78 and references cited therein]. This volume is assumed to be "electrically inert". Since the equilibration of water and pH are both very fast [97] the cells will be in osmotic equilibrium for all volume measurements.

Under these assumptions, volume changes will be governed by the adaptation of the osmotic value of ions and small acolytes (sugar, ATP, metabolites) in the cell water to the constant external osmotic pressure. For the physiological 100% volume of V_0 = 94.5 μm^3 (my own experimentally determined value) a cell water volume of $V_{W0} = V_0 - V_{Hb} = (94.5\text{-}27.4)\ \mu m^3$ = 67.1 μm^3 is obtained. The cell water volume, V_W, was assumed to be variable, i.e. changes in the overall cell volume are solely due to a change in V_W at a constant ion concentration, c_W, in the cell water (in other words V_{hb} is taken as a constant). The physiological ionic concentration in the cytoplasm would be $c_W * V_{W0}/V_0$. For a different cell volume (V) the concentration in the cytoplasm becomes $c_c = c_W * V_W/V$. Neglecting the conductivity contributions of the small osmolytes, the cytoplasmic conductivity at any different cell volume was calculated by multiplying the cytoplasmic concentration of all ionic species corrected by δ with their molar conductivities (Λ_i) as described by Pauly and Schwan [96]

(Eq. 1.12.1). A plot of calculated cytoplasmic conductivities over the experimental range of external media conductivities is shown in Fig. 4.19. The calculated intracellular conductivities over a range of temperatures in different experimental solutions are tabulated in Tab. 4.8. A plot of cytoplasmic conductivities over temperatures is presented in Fig. 4.20A. For all experimental solutions, the increase in temperature every 10°C (Q_{10}) as well as the temperature coefficients obtained from the fit are tabulated in Tab 4.9.

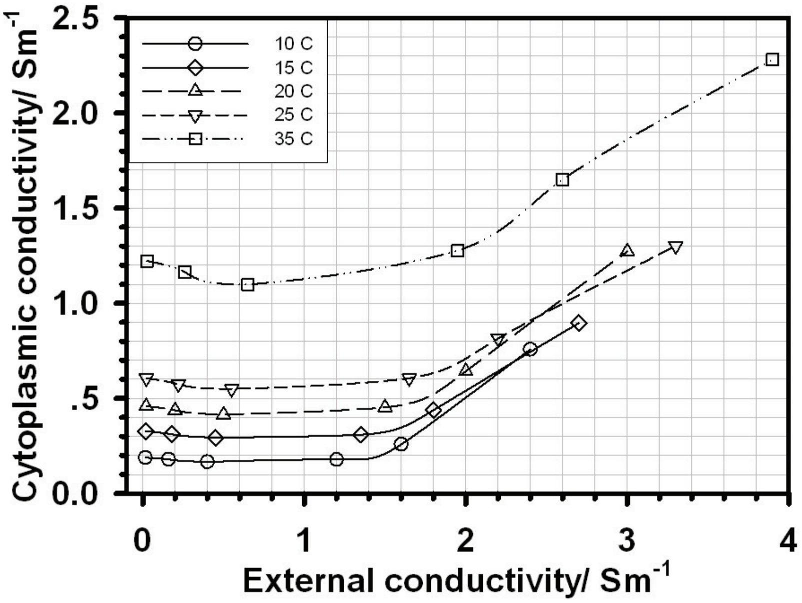

Fig. 4.19 Calculated cytoplasmic conductivities of HBBCs plotted against the conductivity of the external medium at five experimental temperatures

Conductivity (S m^{-1}) at 20°C	Cytoplasmic conductivity (S m^{-1})					Temperature Coefficient
	10 °C	15 °C	20 °C	25 °C	35 °C	°C^{-1}
0.02	0.198±0.001	0.330±0.016	0.450±0.007	0.600±0.076	1.180±0.010	0.0664±0.0033
0.20	0.180±0.013	0.320±0.007	0.440±0.002	0.590±0.073	1.200±0.017	0.0690±0.0068
0.50	0.164±0.052	0.300±0.013	0.420±0.053	0.550±0.023	1.080±0.028	0.0669±0.0081
1.50	**0.180±0.003**	**0.310±0.047**	**0.460±0.007**	**0.630±0.015**	**1.310±0.063**	**0.0731±0.0033**
2.00	0.270±0.009	0.460±0.047	0.640±0.020	0.888±0.054	1.780±0.105	0.0699±0.0037
3.00	0.710±0.192	0.990±0.055	1.120±0.141	1.390±0.014	2.250±0.184	0.0447±0.0050

Tab.4.8 The calculated cytoplasmic conductivities for all suspending solutions at five experimental temperatures. The calculation is the same procedure as that for physiological in Tab. 4.7. The volume effect of haemoglobin has been considered by the introduction of the delta term (δ) into ionic concentrations presented in column 2 of Tab. 4.7. The conductivity of normal blood has a conductivity of about 1.5 S m^{-1} and so these results are shown in bold type. Values are means ± SE (n = 5).

For all experimental solutions (except in 3.0 S/m NaCl), the temperature coefficient has a value of about 0.068 S/m which is 3 times higher than that of water. The temperature coefficient was significantly lower (0.045 S/m) at 3.00 S/m, but this solution is well outside not actual physiological concentrations of NaCl. The conductivities could be plotted as an Arrhenius relationship (Fig. 4.20B). The activation energy for all experimental solutions obtained from the fit are shown in Tab. 4.9. The activation energy value obtained (-53 kJ/mol) is 3 times higher than that of water. The temperature coefficient of the cytoplasm was determined according to Kohlrausch's law [93]. The calculated conductivities of cytoplasm for all suspending solutions were divided by their concentration and plotted against the square root of their concentrations as in Eq. 1.12.2 (Fig. 4.21). The Λ^0, which is obtained from the y-axis intercepts in Fig. 4.21 were plotted against temperatures. The temperature coefficient at finite dilution of cytoplasm was then is determined and is shown in Fig. 4.22

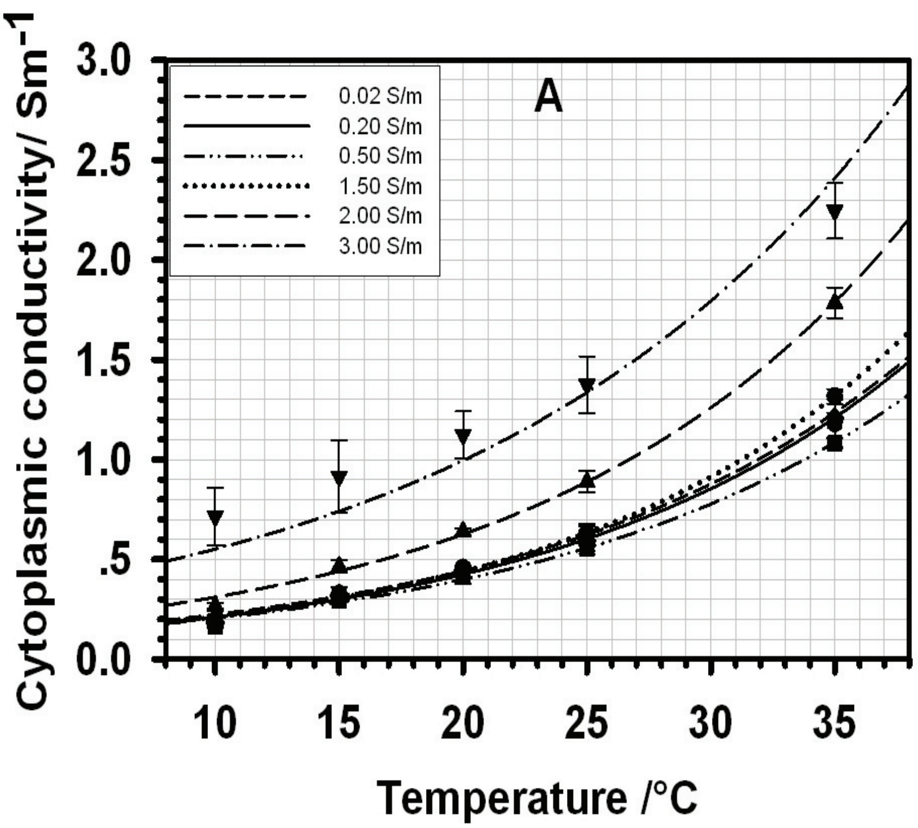

Fig. 4.20A Temperature dependent cytoplasmic conductivities of red cells at five suspending experimental external conductivities as well as at physiological control conditions (long dash line pointed by the arrow) were compared. To fit the experimental points, the relation of temperature dependence of viscosity, $A = a * \exp(B * T)$, was used. Data points are means ± SE (n = 5).

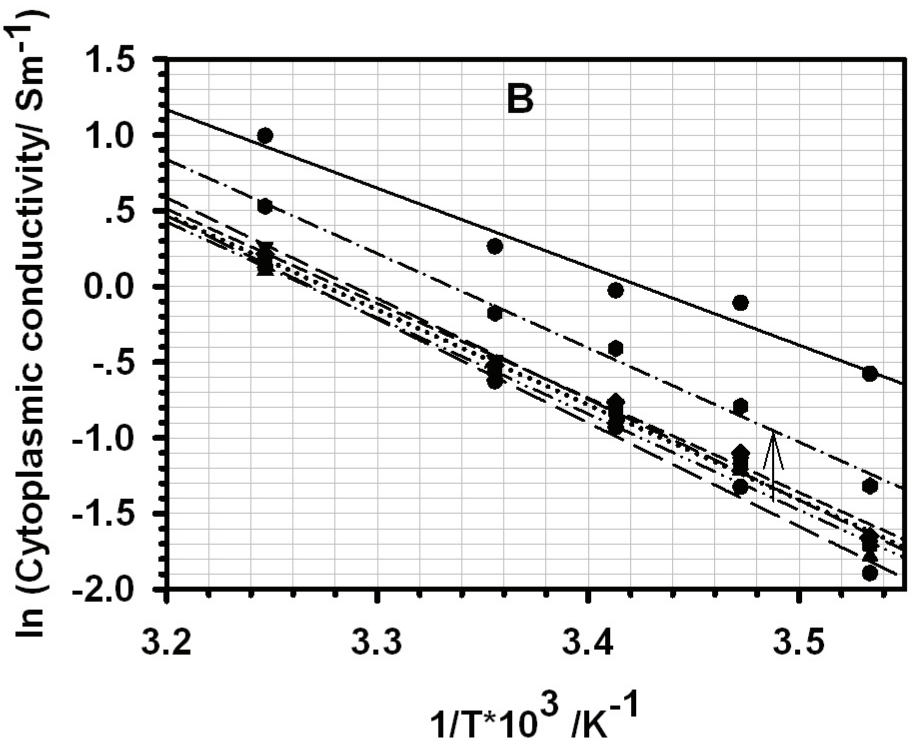

Fig. 4.20B Arrhenius plots of the data shown in Fig. 4.19A.

Sulotion	water	*in vivo*	0.02 S/m	0.20 S/m	0.50 S/m	1.50 S/m	2.00 S/m	3.00 S/m
E_A (kJ)	14.483	56.880	51.871	52.117	52.694	55.335	51.720	43.071
Effective E_A	1.000	*3.927*	*3.582*	*3.599*	*3.638*	*3.821*	*3.571*	*2.974*
Temperature coefficient conductivity (% /K)	0.020	0.074	0.069	0.068	0.068	0.069	0.068	0.059
Effective Temperature coefficient	1.000	*3.708*	*3.447*	*3.422*	*3.412*	*3.447*	*3.378*	*2.950*

Tab 4.9 Activation energies (E_A) of the HRBC cytoplasm obtained from the slopes of Fig. 4.20B using temperature coefficients obtained from Fig. 4.16. The effective E_A as well as the effective temperature coefficient of water which was determined from the Arrhenius plot of viscosity of water is included for comparison.

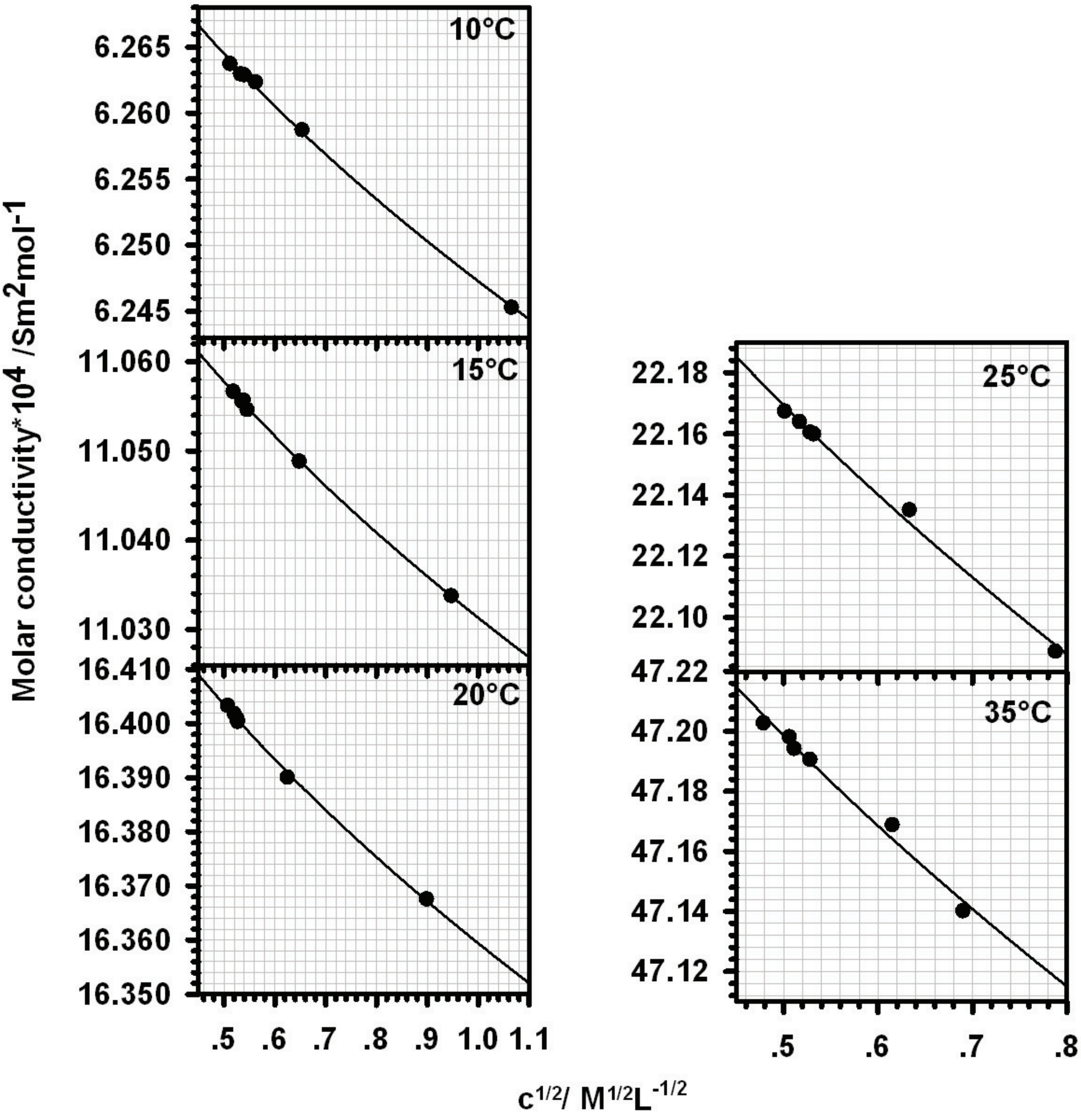

Fig. 4.21 Molar conductivities of HRBCs at five experimental temperatures were plotted against the square root of the external concentrations. The points were fitted to Kohlrausch's law (Eq.1.12.2). The fit provides the linear regression of 1. The intercept at the y-axis refers to the value of the limiting molar conductivity.

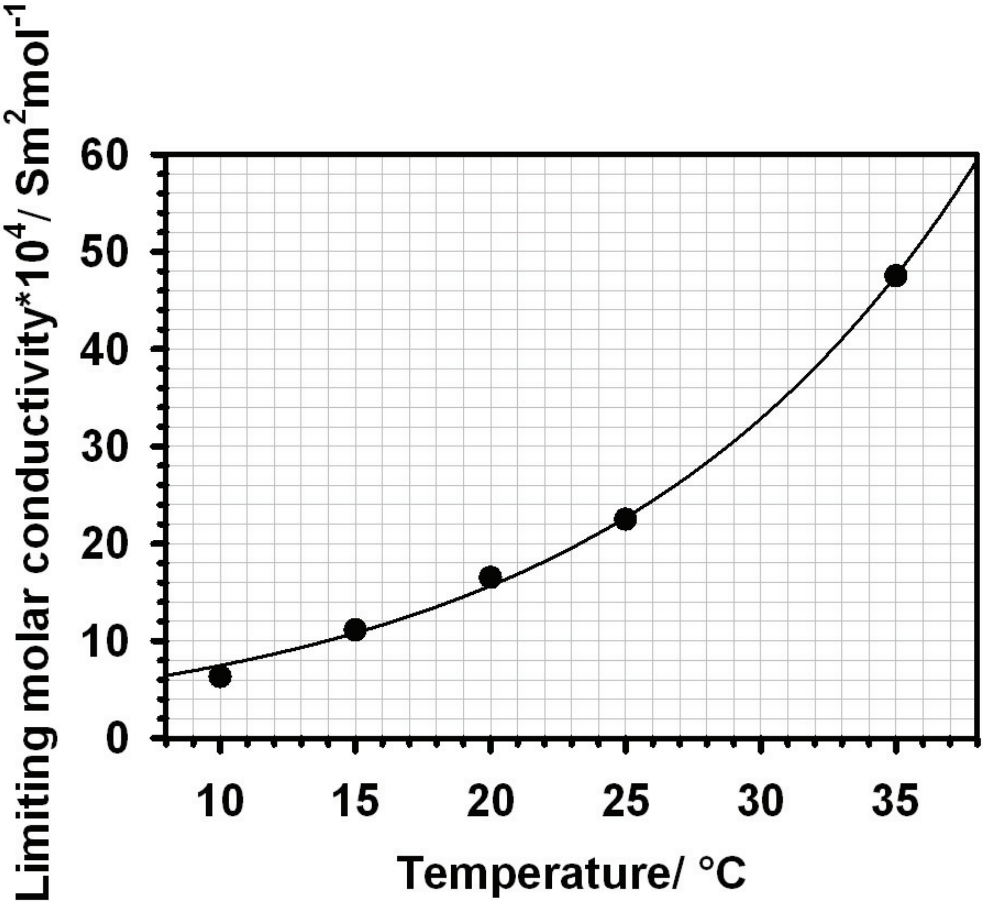

Fig. 4.22 Limiting molar conductivity of cytoplasm of HRBCs obtained from the interception of the fit in Fig. 4.21. The points were fitted to the equation $A = a * \exp(B * T)$. The fit provides the linear regression of 1. A temperature coefficient of about 0.067/°C was obtained.

4.5 Influence of external media and temperatures on cell shape

Since the shape of HRBCs can be changed drastically either by external media [47, 69, 75-78, 80, 100-103] and/or temperature [82-83], the shapes of the cells were microscopically observed while they were suspended in a range of experimental solutions at different temperatures. Selected electronmicrographs showing various shapes are presented in Fig. 4.23. For isotonic solutions, with conductivities of 0.02 S/m at a temperature of 25 °C, the cells remain normal erythrocytes (discocytes). With rising of temperatures, stomatocytes become dominant. However, when external solutions are changed to hypertonic conditions and temperatures reduced to below 20 °C, echinocytes were obtained. As erythrocytes undergo cell volume changes while the surface area of the membrane remains constant [41, 103], any change of cell shape disturbs the cell volume [57, 68, 83-87].

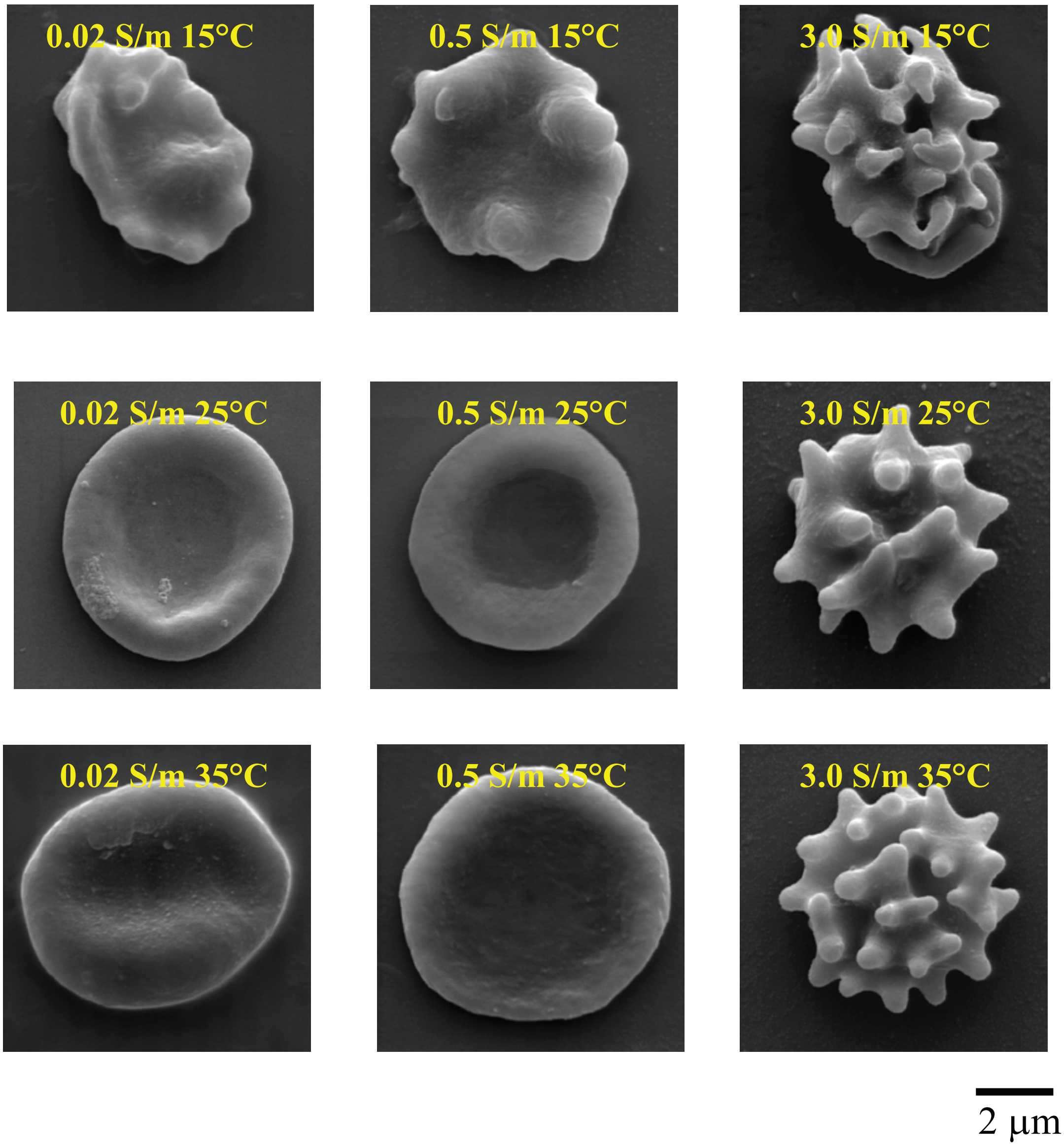

Fig. 4.23 Electronmicrographs of HRBCs shapes at 3 selected temperatures suspended in isotonic solutions (0.02 and 0.50 S/m) and hypertonic solution (3.00 S/m).

It was observed using a light microscope, that changes in cell shape from echinocyte to stomatocyte increases the major (*a*) axes of cell radius. The measured value for all suspending solutions, at 5 experimental temperatures, were microscopically measured via a video camera and tabulated in Tab. 4.10. Changes of *a* over the range of experimental solutions are shown in Fig. 4.24. Temperature dependencies of *a* for all experimental solutions are presented in Fig. 4.25. The minor axis (*c*), calculated from the measured cell volume, and *a* axes are tabulated in column three of Tab. 4.10. Changes in cell geometry lead to the alteration of the interpretation of ER because the models used incorrectly assume that cell volume and cell radius were constant [30-41]. Cell geometry changes as a function of both the composition of the external solution and the temperature. To take into account the actual cell geometry and to access the real cell parameters of HRBCs, the Finite Element Model (FEM) modeled by Gimsa and Wachner (1999) [34] was used to interpret the ER measurements. All characteristic points on the ER spectrum (f_{c1}, f_{c2}, R_1, R_2) depend on the cell geometry called the normalized influential radius (ξ) defined as:

$$\xi = \frac{a_{\inf l}}{a} - 1 \qquad (4.5.1)$$

where,

$$a_{\inf l} = \left(\frac{1}{1-n}\right)a \qquad (4.5.2)$$

n is a depolarizing factor for oblate spheroids given by,

$$n = \frac{1}{2}\left[1 - \frac{1+e^2}{e^3}\left(e - \arctan e\right)\right] \quad with \quad e = \sqrt{\left(\frac{a}{c}\right)^2 - 1} \qquad (4.5.3)$$

and for prolate spheroids given by,

$$n = \frac{1}{2}\left[1 - \frac{1-e^2}{2e^3}\left(\ln\frac{1+e}{1-e} - 2e\right)\right] \quad with \quad e = \sqrt{1 - \left(\frac{a}{c}\right)^2} \qquad (4.5.4)$$

In Fig. 4.26, the temperature dependence of ξ is presented.

Conductivity Sm^{-1}	a-axis mm	c-axis mm	n	$a_{infl.}/a$	x	$a_{infl.}$ mm
(1)	(2)	(3)	(4)	(5)	(6)	(7)
0.02						
10°C	3.08±0.18	2.34± 0.25	0.30±0.02	1.42±0.05	0.42±0.05	4.37±0.01
15°C	3.17±0.00	2.34±0.01	0.29±0.01	1.41±0.01	0.41±0.01	4.46±0.02
20°C	3.47±0.18	2.42±0.04	0.28±0.03	1.40±0.06	0.40±0.06	4.78±0.04
25°C	3.50±0.00	2.25±0.26	0.27±0.02	1.37±0.03	0.37±0.03	4.80±0.11
35°C	3.96±0.50	1.58±0.37	0.20±0.04	1.26±0.08	0.26±0.08	4.97±0.38
0.20						
10°C	3.37±0.18	2.26±0.30	0.28±0.03	1.38±0.05	0.38±0.05	4.67±0.08
15°C	3.50±0.00	2.30±0.02	0.27±0.01	1.38±0.02	0.38±0.02	4.83±0.07
20°C	3.58±1.77	2.13±0.16	0.26±0.17	1.35±0.03	0.35±0.03	4.85±0.14
25°C	3.75±0.00	1.90±0.01	0.24±0.01	1.31±0.02	0.31±0.02	4.92±0.01
35°C	4.25±0.00	1.42±0.01	0.18±0.01	1.22±0.01	0.22±0.01	5.20±0.01
0.50						
10°C	3.54±0.18	2.11±0.32	0.26±0.03	1.35±0.05	0.35±0.05	4.79±0.01
15°C	3.67±0.00	2.09±0.08	0.25±0.01	1.34±0.01	0.34±0.01	4.92±0.04
20°C	3.75±0.18	1.89±0.09	0.24±0.01	1.31±0.01	0.31±0.01	4.91±0.15
25°C	3.83±0.18	1.74±0.13	0.22±0.01	1.29±0.03	0.29±0.03	4.93±0.01
35°C	4.46±0.18	1.30±0.19	0.17±0.02	1.20±0.03	0.20±0.03	5.34±0.06
1.50						
10°C	3.37±0.00	1.99±0.25	0.26±0.00	1.35±0.05	0.35±0.00	4.56±0.00
15°C	3.42±0.18	2.02±0.03	0.26±0.01	1.35±0.01	0.35±0.01	4.61±0.20
20°C	3.50±0.36	1.78±0.33	0.24±0.01	1.31±0.01	0.31±0.01	4.59±0.01
25°C	3.60±0.18	1.68±0.01	0.23±0.01	1.30±0.02	0.29±0.02	4.65±0.02
35°C	3.67±0.00	1.84±0.12	0.24±0.01	1.31±0.16	0.31±0.16	4.80±0.05
3.00						
10°C	3.04±0.18	1.47±0.10	0.23±0.01	1.30±0.01	0.30±0.30	3.96±0.19
15°C	3.12±0.00	1.45±0.03	0.23±0.01	1.29±0.01	0.29±0.01	4.04±0.01
20°C	3.21±0.00	1.47±0.15	0.22±0.25	1.29±0.01	0.29±0.01	4.13±0.07
25°C	3.29±0.18	1.52±0.01	0.22±0.01	1.29±0.02	0.29±0.02	4.25±0.16
35°C	3.50±0.00	1.52±0.10	0.22±0.08	1.28±0.14	0.28±0.01	4.46±0.05

Tab 4.10 Length of the major (a-axis) and minor (c-axis) axes, a depolarizing factor (n), a ratio of influential to major axes ($a_{infl.}/a$), a normalized influential ratio (ξ) and influential radius ($a_{infl.}$) of HRBCs suspended in media with five different external conductivities at five different experimental temperatures. Values are means ± SE (n = 5)

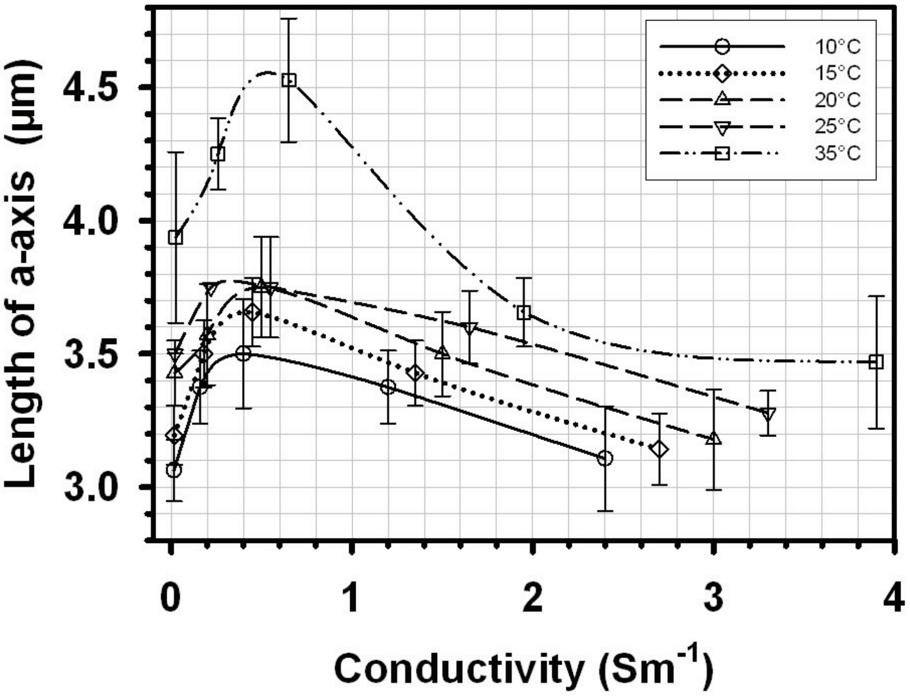

Fig. 4.24 Lengths of *a*-axes of HRBCs at various external conductivities for five different experimental temperatures. Error bars are ±SE, based on five replicates

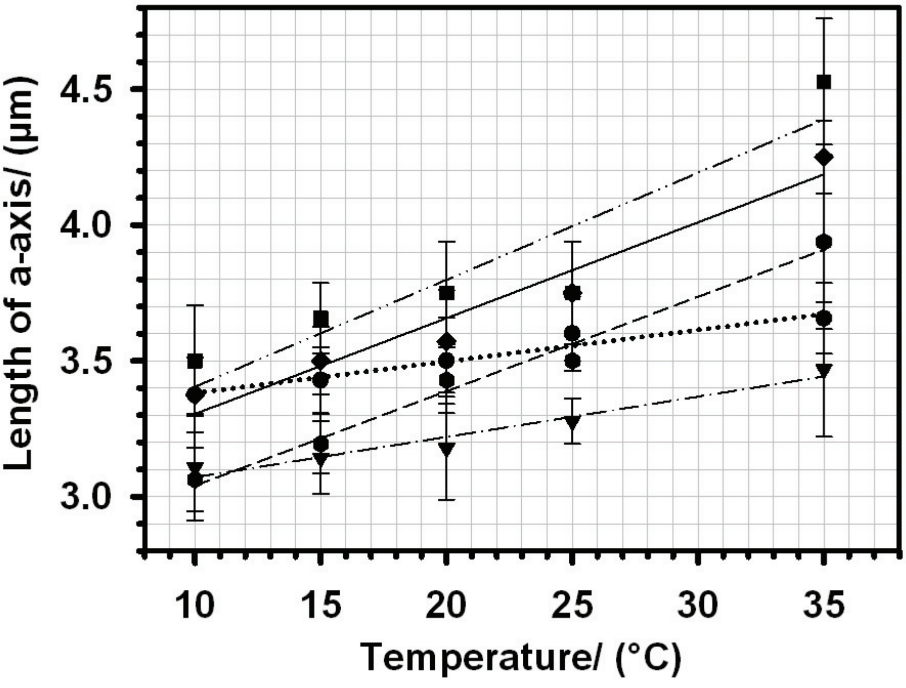

Fig. 4.25 Lengths of *a*-axes of HRBCs at various temperatures for five experimental external conductivities. Error bars are ±SE, based on five replicates

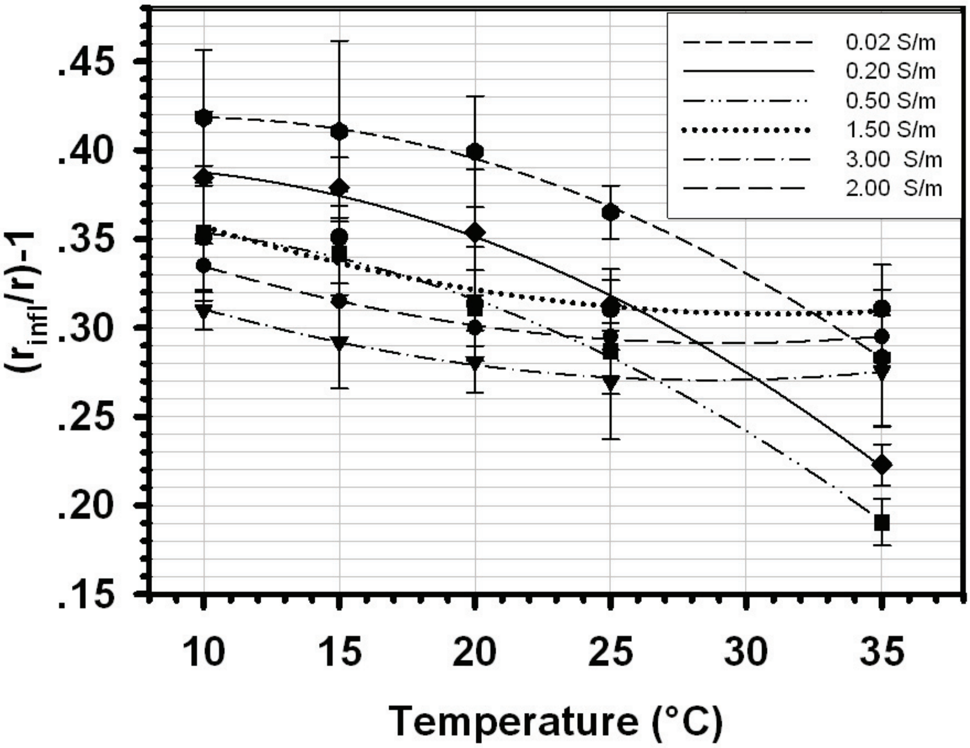

Fig. 4.26 Normalized axes ratio of HRBCs at various temperatures for six different experimental conductivities. Error bars are ±SE, based on five replicates

4.6 Cell parameters of HRBCs obtained from the interpretation of the FEM

In section 4.2.2, an increase in frequency peaks and rotation peaks with increasing temperature was hypothesized to be caused by changes in the cell properties. Assuming linearly temperature dependent parameters and introducing the data into the model of Gimsa and Wachner [34], under an assumption of no change in cell volume and cell radius, the experimental data could only be fitted to the model under conditions where the cell shape remains spheroid, that is for an external conductivity range of 0.2 S/m to 0.4 S/m at a temperature range of 20 °C to 25 °C. The first and the second rotation peaks obtained experimentally were faster than those expected from the theoretical calculations. Shifts of the characteristic points f_{c1}, f_{c2}, R_1 and R_2 that could not be interpreted within the basic tenents of the model were hypothesized as being due to other effects which have been omitted or some parameters of the model have incorrectly been assumed to be constant. For example, cell volume and cell radius have been assumed to not change for all experimental conditions [26-39]. Cytoplasmic conductivity was assumed to be independent from the conductivity of the external electrolyte, even though it has been known that it can easily be altered by changes of the environment of the red blood cell, such as the external ionic strengths and temperature [51-56, 69, 74].

To calculate the cell parameters under actual experimental conditions, the ER spectra were directly fitted by the FEM. The measured cell radius and the actual ξ presented in Tab. 4.9 were introduced into the model. The experimental solutions were not pure water and so the ER spectra observed depended on the amount of NaCl dissolved in the water [89]. The real permittivities of all external solutions presented in Tab. 4.11 were introduced into the model. Table 4.11 shows that the calculated relative permittivities of the experimental solutions were linearly related to temperature over the experimental range of temperatures and conductivities. The permittivity decreased by 0.350 ± 0.001 %/°C. The cytoplasmic conductivities presented in Fig. 4.27 obtained from the fit were found to be exponentially temperature dependent. The temperature coefficient of about 0.055/°C was obtained based upon all the experimental solutions used. The relative cytoplasmic permittivity (relative to the permittivity of vacuum), obtained from the fit for all external solutions presented in Fig. 4.28, on the other hand was linearly temperature dependent with a coefficient of **-0.30 ± 0.004 %/°C**. This temperature coefficient is less than one half that found for the external solution: a relative permittivity of about 51 (compared the the permittivity of vacuum) was calculated at 20 °C, about 50 at 25°C and about 48 at normal body temperature (37 °C) for the NaCl solution most similar to blood plasma (0.15 S/m).

Conductivity	Calculated Relative Permittivity (Vacuum 100%)						
S m^{-1} at 20°C	10°C	15°C	20°C	**25°C**	30°C	35°C	slope/°C
0.02	81.81	80.05	78.29	**76.53**	74.77	73.01	-0.35
0.20	81.85	80.09	78.33	**76.57**	74.80	73.04	-0.35
0.50	81.91	80.15	78.39	**76.63**	74.86	73.10	-0.35
1.50	82.11	80.35	78.58	**76.81**	75.05	73.28	-0.35
2.00	81.33	79.58	77.83	**76.08**	74.33	72.58	-0.35
3.00	79.93	78.21	76.49	**74.77**	73.05	71.33	-0.34

Tab 4.11 Calculated permittivities (% relative to vacuum) of six different solutions for six different temperatures. The starting value at 25°C for the conductivities of lower than 1.50 S/m were obtained from [89]. For the conductivities higher than 1.50 S/m, the effect of NaCl was taken into account according to [89, 99]. The relative permittivity decreases linearly with temperature, over the experimental range, approximately -0.350 ± 0.001 %/°C.

Conductivity (Sm^{-1}) at 20°C	Cytoplasmic Conductivity (Sm^{-1})					Temperature
	10 °C	15 °C	20 °C	25 °C	35 °C	Coefficient /°C
0.02	0.249±0.000	0.291±0.037	0.480±0.057	0.630±0.047	0.833±0.178	0.056±0.0050
0.20	0.283±0.038	0.410±0.057	0.604±0.042	0.907±0.059	0.930±0.070	0.051±0.0013
0.50	0.382±0.052	0.379±0.025	0.423±0.038	0.699±0.044	1.196±0.130	0.050±0.0006
1.50	**0.353±0.021**	**0.412±0.034**	**0.421±0.010**	**0.554±0.011**	**0.851±0.045**	**0.050±0.0012**
2.00	0.536±0.043	0.593±0.024	0.721±0.012	0.772±0.039	1.781±0.059	0.051±0.0092
3.00	0.721±0.021	0.848±0.023	0.849±0.021	0.897±0.036	2.186±0.038	0.051±0.000

Tab.4.12 The obtained cytoplasmic conductivities from the fit of FEM for all suspending solutions at five experimental temperatures. The conductivity of normal blood has a conductivity of about 1.5 S m^{-1} and so these results are shown in bold type. Values are means ± SE (n = 5).

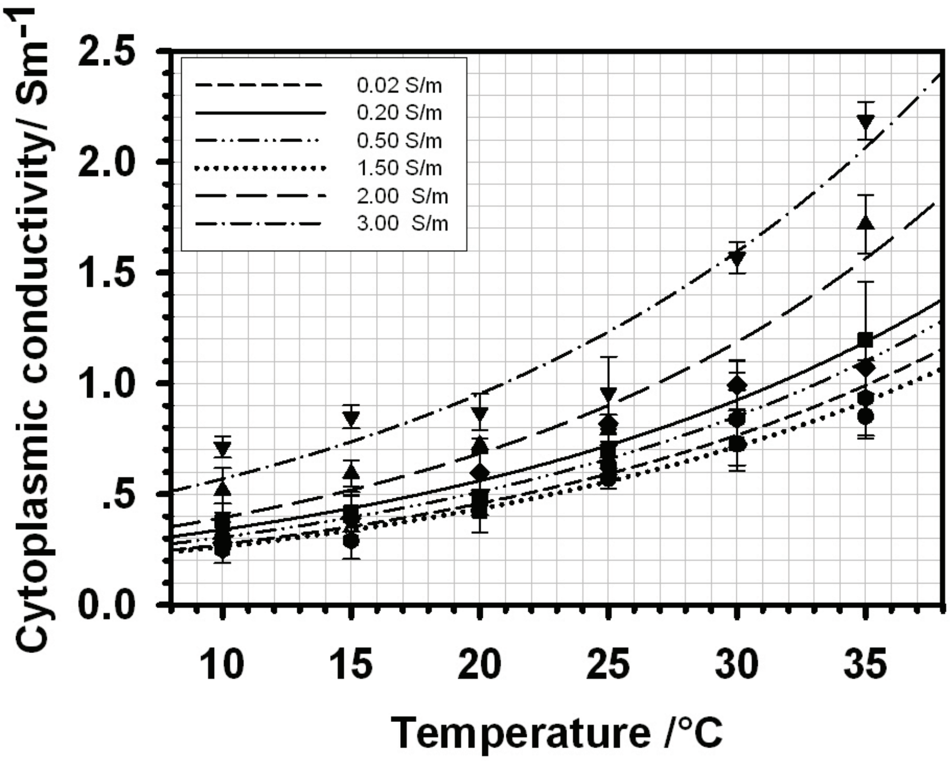

Fig. 4.27 Cytoplasmic conductivity of red blood cells for six external conductivities at six temperatures. The data were obtained from the fit of ER spectra. To fit the experimental points, the equation for temperature dependent viscosity, $A = a * \exp(B * T)$, was used. The temperature coefficient of about 0.051/°C could be calculated based on all the experimental solutions. Error bars are ±SE, based on five replicates.

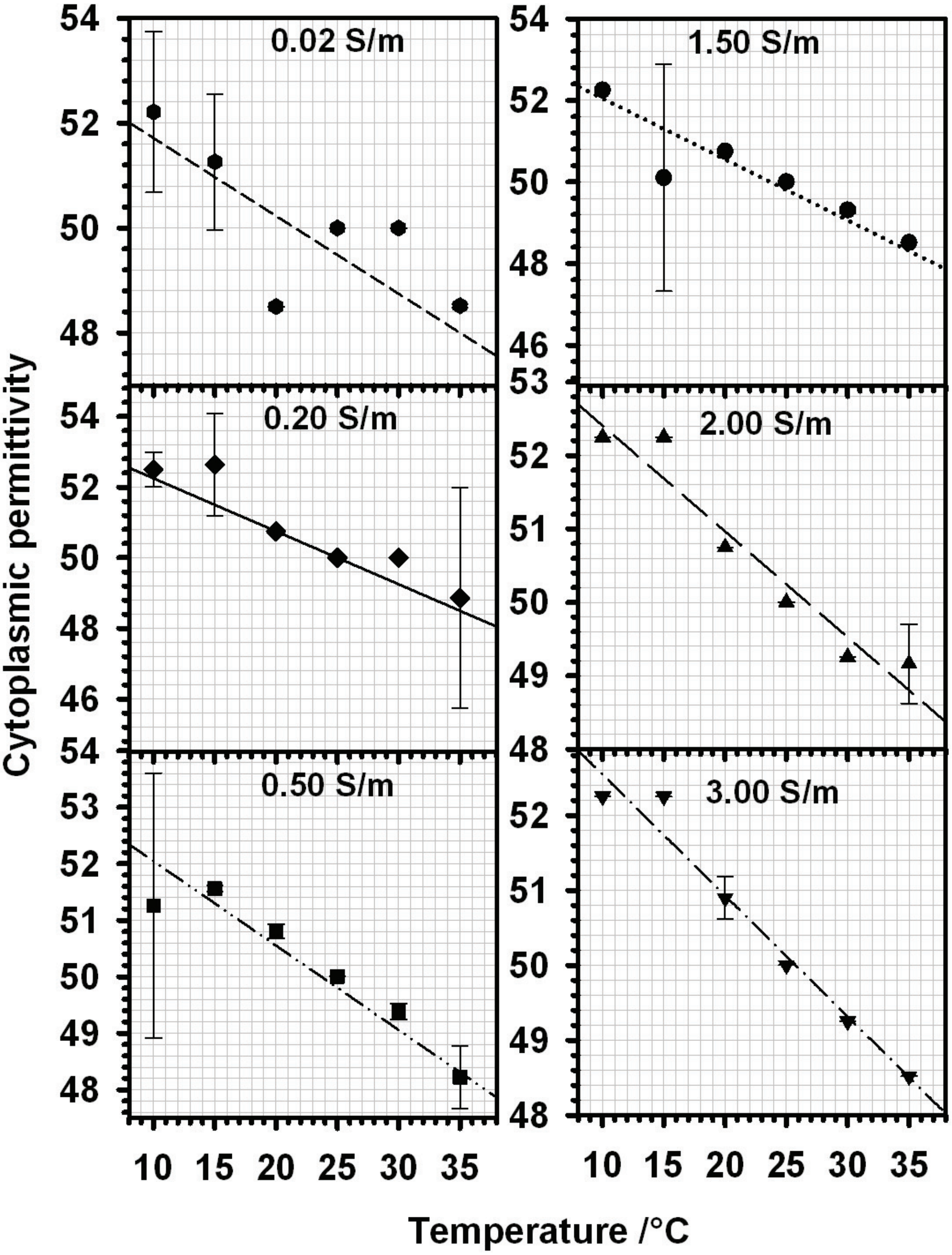

Fig. 4.28 Plots of cytoplasmic relative permittivity (% relative to permittivity of a vacuum) of HRBCs for six external conductivities at six temperatures. The data obtained were from the fit of ER spectra. To fit the points, Eq. (1.6.1b) was used. Relative cytoplasmic permittivities decreased linearly with temperature with an average slope of -0.3 ± 0.004 %/C. This slope is much lower that found for the external solution (Table 4.11). Error bars are ±SE, based on five replicates.

5 Discussion

5.1 Solutions

5.1.1 Conductivity of solutions

The conductivities of the experimental solutions were measured in the temperature compensation mode (20°C). The conductivities increased with increasing temperature. The values obtained from the experimentally were very close to those calculated from theory (Eq. 1.6.1c see also Fig. 4.1). The increase in conductivity of about 2 percent per ^{o}C is due to an effect of temperature on Λ^0 [44]. Increase in Λ^0 leads directly to Λ (Eq. 1.12.2) and consequently to conductivity of that solution (Eq. 1.12.1).

5.1.2 Ionic strength of the solutions

Ionic strength of any electrolyte solution is proportional to its concentration (Eq. 4.1.1) times the ionic valencies of the constituent ions. For an uni-univalent electrolyte like NaCl with ionic valency equal to 1, the ionic strength is equal to the molar concentration (Tab. 4.2). Increase of concentration leads directly to increase in conductivity (Tab. 4.2). Thus, the conductivity of uni-univalent electrolyte solution is proportional to its ionic strength (Fig. 4.2).

5.1.3 Equivalent conductivity of solutions

An equivalent conductivity of any solution is defined as in Eq. (1.12.1). Conductivity of an electrolyte solution is proportional to its molar concentration. Normalizing the molar conductivity by the number of the ionic charge, the equivalent conductivity can be calculated. For the uni-univalent electrolyte, NaCl, since the number of the ionic charge is equal to 1, the molar conductivity therefore is equal to its equivalent conductivity. The equivalent conductivity varies significantly with the concentration of ions. It decreases as the ionic concentration increases (Eq. 1.12.4). This can be seen as the molar conductivities of NaCl dissolved in water at 25 °C shown in Tab. 4.3. The values of molar conductivities do decrease with increasing concentration [44]. However, this behavior appears only when ions are dissolve in water. If the solvent is not pure water (for example, blood plasma), an alteration in the molar conductivity of a solution will be observed. The viscosity of such solutions has to be taken into account as predicted by Walden (Eq. 1.12.9). The viscosity reduces the speed of moving ions, and consequently decreases in conductivity.

5.1.4 Viscosity of solutions

As already known from the Eq. 1.6.1a, viscosity of any solution decreases with increasing temperature. The results obtained in this study agree very well with the theory. However, if the concentration of the electrolyte is changed, the viscosity will be altered. This relation is known as Jones– Dole equation (1929) [99] expressed as:

$$\frac{\eta}{\eta_0} = 1 + A\sqrt{c} + Bc \qquad (5.1.1)$$

where η_0 and η refer respectively to the viscosity of pure water and that of the electrolyte, c is the concentration of the electrolyte. The coefficient A is related to electrostatic ionic interactions, including mobilities and charges of the ions, temperature, viscosity and dielectric constant of the solvent. B refers to hydration interactions, depending on the size of the hydrated ions, the orientation of water molecules in hydrate shells (predominantly in the first coordination sphere) and the relative change of the solvent structure in the first coordination sphere of the ion compared to that of the bulk solution. For ions which are dissolved in sucrose solutions, the mobilities will be reduced from those of ions dissolved in water. The decrease leads to an alteration of the parameter A in Eq. 5.1.1. Consequently, the second term of the Eq. (5.1.1) is switched from the properties of water to those of an experimental sucrose solution. The sucrose solution behaves like a non-electrolyte solution having mutual interactions and collisions of particles but sucrose is a very large and bulky molecule compared to water. The viscosity of sucrose solutions depends strongly on the molar volume fraction of solutes as described by Vand [100]. If the molar volume fraction of the dissolved components decreases, usually achieved by a decrease in its concentration, the viscosity will exponentially decrease [99-100]. Thus, the relations of viscosity over the concentrations of NaCl presented in Fig. 4.4 can be explained in terms of the findings of previous studies [99-100]. At low NaCl concentrations (lower than 150 mM), the major solvent present is sucrose because it has a high molar volume fraction. Increasing the ionic strength by adding of NaCl, the molar volume fraction contributed by sucrose decreases. This leads to an exponential decrease in viscosity of the solution as described above. At concentrations that are hypertonic to human blood, starting from 150 mM NaCl, where there is no sucrose added in, the trends in viscosity changes its sign to a trend for viscosities to increase to higher values. In solutions containing only NaCl, where the mutual interactions of sucrose molecules no longer apply, the ionic interactions increase. The dielectric constant of more concentrated pure NaCl solutions behaves differently to weaker solutions containing sucrose. The parameter B itself might also change its characteristics from that of pure water. This can be the reason for increasing viscosity at NaCl concentrations higher than 150 mM (Fig. 4.4).

5.1.5 A relation of molar conductivity to viscosity

In Fig. 4.5, the molar conductivities of all experimental solutions were plotted over conductivities. The experimental data were compared with the theoretical values obtained from [44]. Each experimental point was corrected with its viscosity. After the correction, the experimental points could be fitted with the theory only for the narrow concentration range of 2 mM to 10 mM or at conductivity range of 0.20 S/m to 1.00 S/m. At these conductivities, the effect of the buffer is effectively cancelled by the total ionic concentration of the solution. However, at concentrations of 0.16 mM, and at concentration of higher than 10 mM, deviations of the experimental data from the theoretical curve were observed. To explain the deviation at low ionic strength (concentration of 0.16 mM), the effect of the ionic composition of the buffer (a solution of Sodium phosphate salts) needs to be taken into account. The buffer posses the ionic strength of about 1.09 mM which is about the same value with that of the added NaCl. The ionic strength of the buffer participates in generating the higher than predicted molar conductivity at this experimental point. At concentrations higher than 10 mM, deviations of the measured points even after a correction for their viscosities were found. Also, since the solution has a high ionic concentration, the effect of buffer then can be minimized. The shift of experimental points from the predicted theory is caused by other reasons. One factor is the viscosity of the electrolyte itself. As we have shown in the Results section, if the ionic concentration is raised, the viscosity increases. The increase in viscosity directly influences on the speed at which ions can move through the solution. It will interfere to some extent with the effects of the inter-ionic force, especially at high concentrations. Therefore, there are very few electrolytes which can be regarded as completely dissociated at normal physiological concentrations. Consequently, the strict additivity which exists at great dilutions can not be expected to persist in salt solutions in the physiological range of concentrations. This seems to be the reason for the markedly lower dielectric constant of physiological solvents such as blood plasma. The properties of such a solvent must be profoundly modified by the presence of some substances which are totally different from that of water, for example sugars, zwitterionic organic compounds, soluble proteins etc. The theoretical predictions therefore can not be used in such media with significant ionic concentrations.

5.2 ER measurement

5.2.1 Effect of external conductivities on ER spectrum

The ER spectra of biological cells usually exhibit two strong, conductivity dependent rotation peaks. The two peaks located at lower and higher frequencies can be attributed to two distinct relaxation processes. The measured rotation spectra of HRBCs closely agree with the superposition of two Lorentzian peaks at low conductivities but deviate from this shape at conductivities above 0.4 S/m. This behaviour cannot be explained by the structural dispersions of a single shell model with frequency independent parameters. I believe that it is due to the molecular structure of the membrane and to cytoplasmic properties. In the Introduction we first introduced frequency dependent parameters for the cytoplasm of HRBCs [33]. An oblate spheroidal Laplace model with a confocal membrane thickness was fitted to the measuring points [33]. In this study, I increased the number of measuring points and apply a newer dielectric cell model [34]. In Figs. 4.7A and B the parameters published in [34] were introduced into this model, leading to slightly different theoretical curves. A thorough investigation of the reason for this deviation is still open. Nevertheless, these differences in the two models cannot explain the strong deviations of the fitted curves from the measuring points above 0.6 S/m. Introduction of frequency dependent cytoplasmic properties like in [34] only leads to a minor improvement. The generation of curves describing the theoretical peak behaviour (characteristic frequency and peak height) of the model is a complex problem. Nevertheless, the data suggests an increase in membrane conductivity and a capacitance decrease at higher external conductivities. Alas, frequency dependent parameters must also be assumed for the membrane. These would reflect molecular dispersions and lead to a more realistic dielectric HRBC model. Most probably the findings on HRBCs will be of a more general importance and may change our notion of the electric properties of biological cells at high frequencies.

5.2.2 Effect of temperature on ER spectrum

A moderate temperature increase led to a linear increase of the ER peak frequencies f_{c1} and f_{c2} accompanied by an increase in the rotation peaks R_1 and R_2. This behavior was reflected by the theoretical ER spectra calculated from the parameters of Tab. 4.6. These results confirm previous ER experiments performed without temperature control [31- 35, 98]. The largest contribution to the temperature dependence of the peak magnitudes arose from changes in the viscosity (Eq. 1.4.1a). The agreement of theory with experiment could be improved by introducing the cytoplasmic dispersion given by Eq. 4.2.1 especially for the 20 °C and 25 °C data [34]. However, Eq. 2.1.3 and Eq. 2.1.4 predicted higher R_1 and R_2 rotation peaks than experimentally found. To fit the points, a scaling factor was introduced to account for the additional friction in the vicinity of the chip surface. A factor of 2.6 was used for all temperatures and conductivities.

Different effects may be taken into account to explain the remaining deviations in the rotation speed. The hydrodynamic friction coefficient for the rotating biconcave cell in the vicinity of the glass surface of the experimental chamber is not known. In practice, the friction with the glass surface will depend on the distance of the surface and the shape of the cell. Both parameters depend on temperature and ionic strength, i.e. the external conductivity. For example, a more discocyte-shape, like what was observed at low conductivities, will give rise to an increase in the cell surface facing the chip and a subsequent increase in friction. Furthermore, changes in the ionic cell state, prior to, and during the measurements will alter the electric cell properties and subsequently, the induced torque. Ionic state changes are very complex and depend on the experimental solutions being used. They can hardly be fully controlled [60]. To reduce the effect of such changes no measurements were made later than 5 minutes after suspension of the cells in the experimental setup.

Experimentally, a decrease in the first rotation peaks was found at a conductivity of 0.5 S/m for temperatures above 25 °C. Generally, the cell volume was increased in the medium conductivities range (0.5 to 1.5 S/m) (microscopic observation). Volume changes may be related to a membrane phase transition resulting in a greater efficiency of water diffusion through the membrane [61]. In the classical view of behaviour of biological membranes, this diffusion would be related to the status of the membrane lipids. Diffusion is more efficient when the membrane lipids are in their fluidic and not the gel state. Volume alterations will alter the ionic, water, and protein concentrations in the cytoplasm as well as the hindrance factor of the ionic mobility [60]. Theoretically, a volume increase may therefore result in either an increase or decrease of the cytoplasmic conductivity depending upon the composition of the specific cell in question. I found that the first characteristic frequencies differ by a factor larger than four at very low external conductivities. An even larger frequency deviation was observed above 1 S/m at temperatures above 30 °C (Fig.4.10A). This is much larger than theoretically predicted. Alterations in the membrane capacitance have a pronounced effect on the first-characteristic-frequencies. Nevertheless, the explanation of the temperature effect at low conductivities by a corresponding decrease in the membrane capacitance would require unrealistic transitions in the molecular membrane structure.

In striking contrast to my results, Bao et al. [62] described a strong increase of the membrane capacitance by a factor of about two with temperature in the range from 25 °C – 35 °C. my results suggest a decrease by a factor of about four. An explanation for the strong spreading effect on my characteristic frequencies will probably require a combination of different effects, e.g. an increase in the cytoplasmic and membrane conductivities and a decrease in the membrane capacitance with temperature and frequency.

5.2.3 The anomalous rotation speed at 15 **°C**

Another interesting result is an anomalous increase in the rotation speed at a temperature of 15 °C (Fig. 4.11A). This effect vanishes at 10 °C and temperatures above 20 °C in the medium and high conductivity ranges. Interestingly, the anomalously rotation corresponds to data on the transmembrane-transport rate of ions changing just around 15 °C [63]. Brahm [described a deflection point in the Arrhenius plot of the anion transport at 15 °C. The point was persistent even after partial band 3 inhibition by DIDS. Different explanations for this behavior were proposed. Either the energy barrier of chloride transport decreases at a critical temperature, e.g. due to phase transitions of some membrane components or the chloride exchange is rate limited by different rate limiting steps in the transport process below and above 15 °C. According to Brahm [63], the rate limiting step above 15 °C would possess somewhat lower activation energy.

Probably, the transmembrane-mobility of anions is the major contribution to the AC-membrane conductance in HRBCs [59]. Nevertheless, the interpretation of my results by alterations in the membrane conductance requires the assumption of a more complex behavior of the membrane conductance with a minimum around 15 °C. A possible explanation was given by Prof. I. Bernhardt (personal communication) who proposed that the increase in the membrane conductance below 15 °C is due to the enhanced cation exchange at low temperatures (compare to [52]). My results with DIDS are hinting at a large role of the band 3 chloride transporter in these processes. DIDS-treatment increased the rotation speed at the first peak at various conductivities and temperatures (Fig.4.12). This DIDS-induced increase in the rotation speed resulted in an alignment of all measuring points with those measured for the control at 15 °C. These results are in line with a decrease in the membrane conductance as described before [59, 65]. These authors assume a decrease from 250 Sm^{-2} to 20 Sm^{-2} after DIDS inhibition of the band 3 chloride transporter leading to an increase in rotation speed by about 32% at 5 mS/m [59]. The assumption of a membrane conductance of 20 Sm^{-2} (dashed line in Fig.4.11A) could help explaining the anomalously high rotation speed of the control cells at 15 °C.

5.3 Cell volume and cell water of HRBCs

5.3.1 Effect of external media on cell volume and cell water

Changes in cell volume observed at both isotonic and hypertonic conditions are related to cell water (see Figs. 4.14A and B). At isotonic solutions, cell volume as well as cell water, increases as ionic strength of external solutions increase. Maximum volume and water content of the RBC cell were found at a conductivity of 0.50 S/m. At hypertonic solutions, however decrease in cell volume along with cell water was observed. It was concluded that change in cell volume depends mostly on water fluxes flowing into or out of the cell to balance the osmotic pressures, which may be altered by either changes in temperature or changes in the concentration gradient of ions across the membrane. However, the phenomena of volume change in isotonic and hypertonic solutions were totally different. The fundamentally different types of the behaviour therefore have to describe separately. In hypertonic solutions, there should be little or no net ion fluxes. Cell shrinkage would be caused only by water moving out of the cells [69,101]. For isotonic conditions, shrinkage resulted from a loss of osmotically active ions, usually K^+ and Cl^- [68-69, 101-103]. The most important factor in regulation of cell volume under an isoosmotic conditions is still unclear, and no simple answer has been offered, however if the rates of ion transport are not correctly matched, cells will inappropriately shrink or swell. The most important logical candidate for the process which is very sensitive to the cell volume to change is the $[Cl^-]$. It is known from the work of O' Neill [69] that under isoosmotic conditions, changes in $[Cl^-]$ is a more sensitive indicator of volume change than cell volume itself. That is if movements of Cl^- ions can account for one third of cellular anions and the cell loses one sixth of its cell volume via loss of $K^+ + Cl^-$, half of the Cl^- of the cell is lost and $[Cl^-]$ should theoretically decrease by 40 % (1/2 the original Cl^- content in 5/6 of the original volume). It is not surprising then that intracellular $[Cl^-]$ has important effects on volume-regulatory transporters. Normally, flowing of Cl^- through the cell membrane is mostly to achieve charge balance and to balance the osmotic pressures across the membrane. The parameter which can alter the balance of the system and drive net fluxes of Cl^- into or out of a cell is the pH of the external solution. Charges of organic molecules like hemoglobin are usually pH-dependent [66, 97]. Under physiological conditions, hemoglobin has its isoelectric point of 6.8. This isoelectric point will change according to the external *pH*. The relationship defining this process is:

$$Z_M = -Z_{MO}(pH - pH_{iso}) \qquad (5.3.1)$$

Near the isoelectric point ($pH = pH_{iso}$= 6.8 at 25°C) the total haemoglobin molecule is uncharged ($Z_M = 0$). Below this point ($pH < pH_{iso}$), Z_M becomes positive, and above it ($pH > pH_{iso}$), Z_M becomes negative. The buffer capacity of haemoglobin, Z_M, has a value of 10.5 eq/mol. In the present study, the cells were suspended in media with *pH* of 6 [33], and thus hemoglobin would have been positively charged. Because Na^+ and K^+ are relatively less permeate [97] than Cl^-, to balance the increased positive charges on the hemoglobin molecule, Cl^- would enter the cell and account for most of the charge-balancing required. Influx of Cl^- would increase the intracellular concentration of chloride. Water would then flow into the cell to balance the osmolarity and result in swelling of the cell. However, swelling of cells caused by pH alone cannot completely describe the overall of volume change. Other reasons should also be taken into the consideration. One should note that after net movement of Cl^- into the cell to balance the excess positive charge of hemoglobin, the cell itself would balance both iso-osmolarity and electroneutrality according to the new Donnan equilibrium. *In vivo*, HRBCs have charge concentrations of cations amounting to about +160 charges/litre cell water. Diffusible anions and phosphate compounds provide mobile negative charges of about -108 and -28 charges/litre cell water respectively. Haemoglobin has molecule concentration of 7 mol/litre cell water with charge concentration of -3.42 charge/mol provides charge concentrations of -24 charges/litre cell water under physiological pH conditions [104]. These charges are neutralized and the net charge in the cell becomes zero. However, when the cells were suspended in external medium with pH 6, the charges of haemoglobin become positive with a molecule concentration of +8.4 charges/molecule (calculated from Eq.5.3.1) giving charge concentration of +28.72 charges/litre cell water. These positive net charges result in the cell being out of neutrality with an excess charge concentration of +52.72 charges/litre cell water (+160 +28.72-108-28).

To neutralise these positive charges, Cl^- influx will occur leading to swelling of the cells. Unfortunately, since the concentrations of Cl^- outside the cell are lower than the interior exceeded positive charges, for example, they have respective concentrations of 1.6, 22.7 and 58.4 mmol/L for the external conductivities of 0.02, 0.2 and 0.5 S/m (see also Tab. 4.2). Thus, net movement of only Cl^- is not sufficient to neutralise the excess positive charge. Therefore, moble positive charges will need to leak out of the cell leading the cell to shrink. Since K^+ is the most permeable cation inside RBC most net movement of positive charge out of the cell will be K^+.

Normally, flowing of ions through the membrane will carry along a certain amount of water. K^+ flux will hold water molecules in a volume of approximately 150 $\overset{\circ}{A}{}^3$/ion whereas Cl^- flux carries a water volume of about 90 $\overset{\circ}{A}{}^3$/ion [66]. If both fluxes are driven to flow, each loss of K^+ ion will carry more water molecules out of the cell than is carried into the cell by each Cl^- entering the cell. This might be a reason for the cell shrinkage in low ionic strength observed in isotonic solutions. With increasing the ionic strength of the external media, the K^+ efflux is slowed by increases in the external [Na^+]. A small amount of water leaks out of the cell at a slow rate. In Fig. 4.13 we can see that the cells in isotonic solution initially swell after suspension in the experimental medium, but after 3 min of suspension, cell shrinkage is observed. From this behaviour we can infer that whether cells swell or shrink depends on the external ionic strength and there is more than one single process going on. At external conductivity of 0.02 S/m, the external charge concentration of Cl^- is very low, about 2 charges/litre cell water. Whereas on the other hand the internal charge concentrations of K^+ is very high compared to that outside, and since Cl^- can move faster than K^+ an electrical potential difference (+ve inside) will occur across the cell membrane. Only a small amount of water carried by Cl^- flows into the cell to neutralise this charge, but a big amount of water held by K^+ will leak out the cell as the intracellular K^+ decreases. With increasing the external ionic strength to 0.50 S/m, the external charge concentrations of Cl^-, which is about 21 charges/litre cell water higher than the first case, induces a bigger amount of water flowing into the cell. However, with increase external concentration, the K^+ efflux will be hindered by increasing external Na^+. The K^+ efflux in this case therefore is lower than that of the first case. Thus, at the same time of similar experiments at lower conductivities, a bigger volume was observed when the cells were suspended in external conductivity of 0.50 S/m. At an external conductivity of 1.50 S/m however, the charge concentration of Cl^- outside is about 150-charges/litre cell water which is higher than the interior positive charge +52.72 charges/litre cell water) resulting from the alteration of pH. Only Cl^- flows into the cell. The influx holds water only 90 $A^{\circ 3}$/ion which about 1.7 times lower than efflux of K^+. No significant cell swelling was observed for this external conductivity.

5.3.2 Effect of temperature on cell volume and cell water

Apart from the effect of external ionic solution, cell volume can also be disturbed by temperature as predicted by the Van't Hoff relation [66]. Changes in cell volume of HRBCs over temperature when suspended in different external conductivities are illustrated in Fig. 4.16. Their Arrhenius plots are shown in Fig. 4.17. Increase in cell volume according to temperature changes along with the amount of water content in the cell (please see also figs.4.14 A-B). An influence of temperature on water influx might caused by some of the following reasons. The first is an alteration of external hydrostatic pressure as predicted by the Van't Hoff relation. The hydrostatic pressure depends strongly on temperature and increases when the temperature is raised. The increase in external hydrostatic pressure will destroy the balance of the pressures between the two sides of the membrane. To re-balance the system, water moves down it's gradient and enters the cell. In this case, cell swelling will be observed. The second reason, as already been described in section 1.9, the decrease in viscosity with increasing temperature of external medium leads to a rise in the filtration coefficient and consequently generates the water flux flowing into the cell. The ions in this case also move to balance the iso-osmolarity and the electroneutrality conditions. A net flux of ions across membrane can be considered as the relation of flux ratio relating to an electric field which may exist across the membrane and to the thermal energy [66]. The general form of the relation is presented as:

$$\frac{J_i^i}{J_o^i} = e^{-(E_o - E_i)F/RT} \qquad (5.3.2)$$

where J_i^i and J_o^i are influx and efflux for ion *i*, respectively and the subscripts refer to the inside (i) and outside (o) of the cell. This is a form of the well-known Ussing-Teorell equation but modified for the case where the internal and external concentrations of the ions are very similar and so cancel out. The terms "$(E_o$-$E_i)F$" and "RT" respectively refer to electrical energy (as the electrical potential) and thermal energy. Theoretically, if $E_o = E_i$, in other words if the electrical potential is zero across the membrane) the flux ratio is equal to 1. The net flux across the membrane is nullified. No net energy is needed for the transportation of ions. If the difference between E_i and E_o gets large, the ions are off equilibrium. Eq. 5.3.2 gives no information on how quickly a new equilibrium state will be achieved. The diffusion of ions through the membrane to equilibrate the system need a certain critical activation energy. If a large amount of energy is required, the membrane permeability is low (see again the details in section 1.8), only a few molecules have the necessary energy to penetrate at any moment. Equilibration will be very slow. Raising the temperature increases the number of molecules with the required energy and thereby has an appreciable effect on diffusion rates. If a small amount of activation energy is used, the permeability is high. A greater fraction of the molecules possesses this minimal energy at any moment. An elevation of temperature therefore increases the speed of the molecules and causes an increase in the rate of diffusion and hence equilibrium will be achieved more quickly. In Fig. 4.18, the activation energies of ions fluxes across membrane of HRBCs suspended in different surrounding media are shown. The lowest activation energy of about 0.8 kJ was generated at the conductivity of 1.50 S/m which is very close to the conductivity of human blood plasma (about 1.48 S/m). The low energy implies a small difference of membrane potential generated by the charged molecules which relate to ion concentrations and the charge difference (Eq. 5.3.2). A membrane potential near to zero indicates a small flux ratio. The difference between influx and efflux is low. The membrane permeability in this case would be at its highest value. Thus, the system would in the balance of both concentration and charge differences across the membrane. At other concentrations, higher activation energies were calculated. A maximum value of about -8.5 kJ was found at the external conductivity of 3.0 S/m. This can be attributed to the larger difference in membrane potential caused by the ion concentration gradient and by charge of differences across the membrane. The ions therefore would not be in the equilibrium.

5.4 Influence of cell volume on cytoplasmic conductivity

According to the work of Pauly and Schwan [96], the internal conductivity of HRBCs is calculated based on the idea of that cytoplasm behaves like an electrolyte solution assuming the ions inside the cells experience neither relaxation nor electrophoretic effects. A calculated value of 1.44 S/m is obtained from the product of the ion concentrations in the cell and their molar conductivities (see column three in Tab.4.7). The ionic balance in the human red blood cell [96] is given in the first columns of Tab. 4.7. The second column gives limiting ionic conductance for all ions of interest [44, 89]. Nevertheless, the calculated value is 2.7 times higher than the measured value of 0.518 S/m [96]. They hypothesized this discrepancy that was due to a decrease in the mobility of ions in the cytoplasm. Unfortunately, at that time, the cytoplasmic viscosity of HRBC had not been considered. In addition, the cytoplasm of HRBC is not pure water but it is characterized as a non-aqueous solution [91, 96], switching of the ions from water to the non-aqueous solvent will alter their quantities of several magnitudes. The altered quantities including viscosity, dielectric constant of the medium, the distance of closest approach of the solvated ions, and the radii of the solvated ions result in changes of the mobility of the ions at infinite dilution and the concentration of free ions which causes the conductance behavior of an electrolyte to vary considerably.

To understand more about this phenomenon, in this study, Walden's law (Eq.1.12.9) has been taken into consideration. A relative viscosity of cytoplasm of HRBCs with a value of 5.91 mPa s at 37 °C [91] was applied. The viscosity hindered the mobility of ions, and consequently reduces the cytoplasmic molar conductivities from those at infinite dilution (see column five of Tab.4.3). The effective conductivities of cytoplasm influenced by viscosity are shown in column six of Tab. 4.3. The conductivities presented in column seven is the conductivity which diminished from the conductivity at infinite dilution. The diminution of the conductivity may be result of the reduction in magnitude of the molar conductivity according to an interionic interaction which reduces the conductivity to below that at infinite dilution (see more details in Section 1.12 and Eq. 1.12.2). Including all the necessary correction factors, a cytoplasmic conductivity of 0.53 S/m could be calculated. This value agrees well with the previous publications [33, 65, 96] and strongly confirms the predictions of Pauly and Schwan [96] that the discrepancy of internal conductivities obtained from the theoretical calculations and those obtained experimentally were due to the effects of viscosity. That is, the increased viscosity of the cytoplasm of the RBC leads to a decrease in ion mobility at infinite dilution.

Experimentally, as seen in Tab. 4.2 and Fig. 4.16, the cell volume can easily be changed by either an influence of external media or an effect of temperature. The changes in cell volume lead to alterations in cytoplasmic concentrations and consequently disturb the intracellular conductivity [78]. Cell swelling caused by either the external media or temperature result in a lowered conductivity. However, if the cell shrinks, higher conductivities will be obtained. An adjustment of ionic concentrations in the cell to balance the osmotic pressure when they are suspended in a new environment seems to be the best reason to describe this behavior. Theoretically, an internal osmotic pressure is given by the sum of the number of the penetrable ions (n_{ion}) and non-penetrable solutes (n_{Mol}) like hemoglobin. At equilibrium, the internal osmotic pressure is equal to that of the external medium [60].

$$\frac{n_{ion}}{V}+\frac{n_{Mol}}{V}=cont. \tag{5.4.1}$$

If the volume (V) decreases, the concentrations of the non-penetrant solutes (c_{Mol}) increases. However, Bobo and Solomon [104] showed that the increase in c_{Mol} leads to a decrease in the net charge of hemoglobin. In this case, only the concentrations of mobile ions (n_{ions}) play a role in balancing of the osmotic pressure. Thus, the increase in cytoplasmic conductivities of the shrinking cells can be attributed to the increase in c_{ion} to balance the net charges of hemoglobin. Inversely, if the cells swell, the concentrations of the c_{Mol} decreases leading to a rise of the net charges of hemoglobin, hence to adjust the external osmolarity, the concentration of mobile ions (c_{ions}) falls, and generates a lowered conductivity. The cytoplasmic conductivity therefore mostly resulted from the charges of hemoglobin.

5.4.1 Temperature coefficient of cytoplasmic conductivity

The temperature dependencies of cytoplasmic conductivities are presented in Fig. 4.20A. The data was fitted with the exponential relation for temperature dependent viscosity. A coefficient of 0.067/K was obtained for *in vivo* and for all experimental media except for the conductivity of 3.00 S/m where the apparent temperature coefficient had a value of 0.059/K. The temperature coefficient obtained from the experimental calculations is higher than that of water with a value of 0.02/K. The behavior may come from a different characterization of viscosity in the cytoplasm and that in water. The hemoglobin pigment/protein complex is composed of a long chain of carbon, which behaves like a globular polymer. For the ions to jump, they may need more activation energy than that required in water. To confirm this assumption, in second row of Tab. 4.9, activation energies of the cytoplasm of HRBCs suspended in different external conductivities obtained from the Arrhenius plots (Fig. 4.20B) were compared to the activation energy of water (value of -14.48 kJ) obtained from the Arrhenius plots of its viscosity. The activation energy of cytoplasm for all external media is effectively about 3.5 higher than that of water (see the data in the third row of Tab. 4.9). Interestingly, the effective value for the activation energy correlates very well with the effective temperature coefficient value (see the fifth row of tab. 4.4). Thus, this can be a reason why the temperature coefficient of the cytoplasm is higher than that of water. It is likely that ions moving in the cytoplasm need more energy to move than when moving in water. The activation energies may probably be used to break away from its surrounded molecules. Thus, increase in cytoplasmic conductivity may be predominately caused by temperature effects upon viscosity. Therefore, the obtained temperature coefficient of 0.067/K might perhaps be better regarded as a viscosity coefficient more than temperature coefficient of conductivity of the cytoplasm HRBC's. To explain the effect of temperature on viscosity, the effects of temperature upon the hydration shell of the solute and Brownian motion have to be considered. For solutions with mutual interactions and collision of particles, temperature dependent viscosity, η (T), can be described effectively by using an exponent (n) [100]:

$$\eta(T) = \eta(T_0)\left(\frac{\eta_{water}(T)}{\eta_{water}(T_0)}\right)^{n(\phi)-1} \quad (5.4.2)$$

where, T_0 is the reference temperature, term n depends on the molar volume fraction of the solute (ϕ) obtained from the molar volume of the dissolved component to the solvent [100] as:

$$n = 0.882 + \frac{1.493\phi}{1 - 1.05\phi} \quad (5.4.3)$$

$$\phi = \frac{wv}{wv + (1-w)v_{solvent}} \quad (5.4.4)$$

where, w is mass friction of the dissolved components, and v and v_{sovent} are the specific volumes of the dissolved component and solvent. Movement of water out of the cell, like in hypertonic solutions, yields a decrease in volume of the solvent and in the molar volume fraction (see also Eq. (5.4.4). These lead to a decrease of the exponential value of Eq. 5.4.2. This phenomenon might be a reason for obtaining the lower temperature coefficient of 0.059/K at the external conductivity of 3.00 S/m.

5.4.2 Cytoplasmic limiting molar conductivity of human red blood cells

Theoretically, temperature compensation of conductivity predominatedly arises from the limiting molar conductivity [93, 44]. For a simple ion moving in water such as Na^+, K^+ or Cl^-, the linear temperature compensation is about 0.02/K [93, 44]. For the cytoplasm, however, the limiting molar conductivity should be changed from the normal value for water since the cytoplasm has different properties, and this causes a change in the temperature coefficient. To obtain the limiting molar conductivities of cytoplasm, the molar conductivities were plotted over the square root of concentrations. The plots are illustrated in Fig. 4.21. Kohlrausch's law (Eq.1.12.2) was used to fit the data. The abscissa at the y-axis refers to a limiting molar conductivity value. To obtain the temperature compensation, the values were plotted over temperature presented in Fig. 4.22. The temperature coefficient of 0.067/K was given. The obtained value is equal to that of a viscosity. The results suggest that the temperature coefficient of the cytoplasmic conductivity is the temperature coefficient of cytoplasmic viscosity, and this can confirm that an increase in conductivities according to temperature is dominatingly due to the decrease in viscosity.

5.5 Influence of external media and temperatures on cell shape

Radii of the cells were microscopically measured via the monitor (see Materials and Methods). The experimental data are tabulated in Tab. 4.10. The relative changes in *a*-axes of the cell either due to both the external media and temperature were correlated to the cell volume; i.e. bigger volume resulted in a longer *a*-axis. Shorter *a*-axis values were obtained at smaller cell volumes resulting from water flows out of the cells which normally occur in hypertonic solutions. The cells under hyertonic conditions are echinocytes with asymmetrical spikes of uneven height. A volume calculation of this cell shape has been proposed [90], but the necessary measurement of the effective radius using an ordinary light microscope was rather complicated. Such measurements would be possible using a confocal microscope.

Practically, an average radius of the measured top of the spikes and the radius measured at the inner base of the spikes was performed. The minor (*c*) axes tabulated in column three of Tab. 4.10 were obtained from the determination of cell volume and the measured *a*-axes and *b*-axes. The depolarizing factor (n) [34, 101], an effective radius ($a_{infl.}$) and a normalized effective radius ($\xi = (a_{infl}/a) - 1$) were calculated according to [34]. With increasing temperature and external ionic strength, n and ξ decreased whereas a and a_{infl} increased. The relations of ξ with temperatures are presented in Fig. 4.26. The alterations of these parameters lead to a perturbation in characteristic points of the ER spectrum [34, 105]. The lower ξ was found when the temperature was raised.

Theoretically, decrease of ξ is caused by only a decrease in the *c*-axes. At conductivities lower than 1.50 S/m, the axes decreased dramatically. This behavior may be the result of an inflowing of water heaving the cell into a flat shape (rather like pushing in of a deflating soccer ball). The heavier cell collapses under the pressure to the surface with a larger area [101]. The flattened cell generates increased friction between surface of the cell and glass chip in the experimental setup. The friction would slow the rotation speed of the cell such as were observed at conductivities about 0.50 S/m for temperatures higher than 30 °C (compare to Fig. 4.11). At conductivities about and higher than 1.50 S/m, the *c*-axes seem to remain constant. The constant c-axes imply that the inner cell components such as hemoglobin behaves like a bead like solid retains the cell figure and so the shape of RBC are somewhat inelastic (analogy: a ball of dough in a plastic bag when compressed will retain its deflated soccer ball shape). The influence of temperature and external conductivities on both cell radii and shape factors extends on previous studies [33-34, 36, 60-62, 102, 106] where it was assumed that cell volume and cell radius did to not depend on either temperature or the external solution.

5.6 Cell parameters of human red blood cells obtained from the interpretation of the FEM

5.6.1 Cytoplasmic conductivity

In a previous publication [102] and the Section 5.2.1 and 5.2.2 of the present study, an increase in frequency peaks and rotation peaks according to temperature was hypothesized to be caused by changes in the cell properties. Assuming linear temperature dependent parameters and introducing them into the model of Gimsa and Wachner [34] under an assumption of no change in cell volume and cell radius, the experimental data could be fitted only for the external conductivities of 0.2 S/m to 0.4 S/m at temperature range of 20 °C to 25 °C. Under these conditions, the cell shape remains spheroid. The first- and the second-rotation peaks obtained from the experiment were faster than those obtained from theoretical calculations. Shifts of f_{c1}, f_{c2}, R_1 and R_2 that could not be interpreted within the basic arguments of the calculating model were hypothesized to be due to other effects, which have been omitted or incorrectly assumed to be constant. For example, cell volume and cell radius have been incorrectly assumed to not change under all experimental conditions [33-34, 98, 96].

Cytoplasmic conductivity was assumed to be independent from the external conductivity [33-34, 98, 60-62, 65] even though it has been known that it can easily be altered from changing of the environment of the cells such as changing the external ionic strengths of the bathing electrolyte and changing the temperature [65, 78, 68, 96, 101]. To access the cell parameters under actual experimental conditions, the ER spectra were directly fitted by the finite element presented method of Gimsa and Wachner [34]. The measured cell radius and the actual ξ presented in Tab. 4.10 were introduced into the fit. The cytoplasmic conductivities obtained from the fit presented in Fig. 4.27 are exponentially temperature dependent. The temperature coefficient of about 0.051/K was obtained from analyzing the data obtained for all the external solutions used in the present study. The results are consistent with those obtained from the volume calculations presented in Fig. 4.20A. In the present investigation, a temperature coefficient of about 0.067/K was found. The findings in the present study demonstrates that the internal conductivity of HRBCs is nonlinearly temperature dependent and also depends strongly on the external solution. The findings in the present study refutes two key assumptions made in earlier publications [33-34, 52, 56, 60-62, 98] where cytoplasmic conductivity was incorrectly assumed to be a constant independent of temperature and external ionic strength, whereas intracellular conductivity can be easily be altered by both temperature and external ionic strength.

To explain the unequal temperature coefficients values found in the present study using different experimental approaches, a picture of ionic movements as a diffusion process, and the activation energy should both be taken into the consideration [99, 107]. Firstly lets consider the simple case of temperature coefficients calculated from volume measurements. In this case a higher temperature coefficient was found. This temperature coefficient most likely simply reflects the movement of ions moving into or out of the cytoplasm. Such measurements were made without applying an external electric field. The movement performs a random walk in which all possible directions are equally likely for any particular step. The analysis of such a random walk indicated that the mean displacement of ions is zero. For such a random walk, they must posses a certain energy known as activation energy to break away only from their surrounding ions. When, however, the ions are situated in an electric field (in ER measurement), their movements are affected by the fact that they are charged. Positively charged particles will prefer to move to negative electrode; and negatively charged particles move to opposite direction. The walk is no longer quite random. The ions drift. If the ion is completely isolated (e.g., in vacuum), the electric field accelerates the ion to move indefinitely until it collides with the electrode.

In an electrolyte solution, however, the ion very soon collides with some other ion or solvent molecule which crosses its path. The collision introduces a discontinuity in its speed and direction. Hence, the motion of the ion is not smooth; it is as if the medium offers resistance to the motion of the ion. Thus, the ion stops and starts and consequently loses its activation energy. This behavior has known as Boltzmann's law of energy contribution which states that the energy of moving ions moving as a result of the thermic noise will be hindered if the ions are moving in an electric field since the energy of ions in the electric field opposes the energy of the thermic noise. Thus, if ions are moving in the medium without an applied of electric field, they can move more easily than when moving in the presence of an electric field consequently the calculated higher conductivity if the temperature is increased. This could be the reason of why the temperature coefficient obtained from the volume measurement is higher than that obtained from the fit by the finite element model in the ER experiments.

5.6.2 Cytoplasmic permittivity

Since the experimental solutions used in the present study were not pure water but contained NaCl and in the cases of the isotonic media, both Na, Cl and sucrose. To obtain the real value of the permittivity, the effects of the both solutes presented in [89] (see more details in the Appendix section 6.3) had to be taken into account. The data for all external solutions at different temperatures are presented in Tab. 4.11. Applying the experimentally determined value of external permittivity into the theoretical fit, the cytoplasmic permittivity of HRBCs for all experimental solutions were obtained and presented in Fig. 4.28. For all external solutions, the relative cytoplasmic permittivity of about 51 at 20 °C was obtained. The fit to the data is linearly temperature dependent with a small temperature coefficient of only 0.003/°C. The result agrees very well with the work of Jaspard and Nadi [50] who reported that at frequencies lower than 3 GHz, temperature dependent coefficient of human RBC cells remain constant. Therefore, because of the upper limitations of the frequency generator used in the present study which generated a maximum frequency of only 250 MHz, the frequency dependent cytoplasmic permittivity therefore could not be observed. The cytoplasmic permittivity value of about 50, which well known for HRBC, was then used as part of the model for all experimental external media. If frequencies higher than 1GHz had been possible in the present study, a dispersion of bulk water would been observable. A relative cytoplasmic permittivity smaller than 50 would then be obtained [43].

5.6.3 Membrane conductivity

Temperature dependent membrane conductivity could not be relationally accessed. However, the obtained data from the fit show that membrane conductivity is not constant as previous addressed. It also changes according to external conditions such as external conductivity and temperature. The obtained values give higher than 1µS/m for all conditions and intend to increase at low temperature and high external conductivities.

The higher membrane conductivity resulted from an increase of charge density of membrane as described in [60]. The charge density depends inversely on temperature and proportionally on the Debye-Hückel parameter known to vary with ionic strength [97]. Thus, from the experimental findings, not only is the cytoplasmic conductivity altered by temperature and the external environment of the cell but membrane conductivity is also influenced by the two conditions. This appears to be a new experimental finding for HRBC and other cells used for ER experiments especially when the cells were exposed to an electric field. Special care needs to be taken with regard to the experimental conditions used for ER experiments to access the real biological cell parameters.

5.6.4 Membrane permittivity

For all experimental conditions, the membrane permittivity value of about 9.04 was found. No temperature dependency was found which is consistent with the very low temperature coefficient of fatty acid-chain-like compounds [44].

5.7 Summary and Conclusions

In this study electrorotation was used to detect and analyse the temperature dependence of the electric HRBC parameters at the single cell level. However, it was found that the experimental data could only roughly be fitted by the model assuming the standard temperature coefficients for all media. Here, the major findings were the following:

1) The anomalously high rotation speed at the first peak at 15 °C and the DIDS-effects on the rotation speeds for all other temperatures, hint at a major role of the band 3 protein for the membrane conductance. The band 3 protein is known to be a chloride transport protein.
2) A temperature-spreading of the first characteristic frequencies was found to be much wider than predicted for standard temperature coefficients of the media. A corresponding change in the membrane capacitance seems to require unrealistic transitions in the molecular membrane structure. An explanation for this effect is still missing. It might include effects related to the capacitance of the protein areas in the membrane that probably possess a specific capacitance much higher (about 4.2 F/m^2) than those of the lipid areas (about 0.74 F/m^2; please see: [76]).
3) A dramatic increase was found in the first characteristic frequencies above 3 S/m especially for temperatures above 30 °C. A possible explanation might be the dispersion of membrane protein polarization leading to a decrease of the membrane capacitance around 3 MHz as already proposed [18].

These observations suggested that the interpretation of ER requires special attention to the experimental temperature and its careful monitoring and regulation. Therefore, temperature-dependent ER measurements on the HRBC model system were performed in order to obtain a better understanding of the electric properties of cytoplasm and membrane of HRBCs. These findings lead to further investigations of the cytoplasm conductivity affected by cell volume changes. At the present stage of this work, the following results were obtained:

1) A proportional increase in cell volume depending on the external ionic strengths was observed at low conductivity solutions. In hypertonic solutions, the volume decreases with increasing external ionic strengths.
2) With rising temperature, an increase of cell volume was found. This behaviour is due to an influx of water to balance the osmotic pressure as predicted by the Van't Hoff' relation.
3) An activation energy obtained from the Arrhenius plot of the cell volume indicates there is a difference of electrical potential across the membrane. The lowest activation energy obtained at conductivities near the physiological value indicates a very small difference of ions fluxes across the HRBC membrane. High activation energy shows a high ionic flux ratio across the HRBC membrane between the bathing electrolyte and the cytoplasm.
4) Change in cell shapes and cell radii were found to depend on external media and temperature. The length of the a-axis and ξ were found to increase and decrease respectively with increasing temperature.
5) The internal conductivity depends strongly on the external ionic strengths and temperature. It is exponentially related to temperature with a coefficient of 0.067/K for volume calculation and 0.059/K for the interpretation of ER spectrum by the finite element model. This finding is not surprising physiologically but it has not been adequately taken into account in ER modeling before.
6) The cytoplasmic permittivity from the interpretation of the model is linearly temperature dependent with a coefficient of 0.003/K. This is an unexpectedly low value.
7) No temperature dependency was found for membrane permittivity consistent with the known very low temperature coefficients of fatty-acid-chain-like compounds.
8) High values of membrane conductivities were obtained at high external conductivities at low temperature. The results are caused by an increase of charge density of the membrane which depends inversely on temperature and proportionally on the Debye-Hückel parameter.

Taken together, this work demonstrates that electrorotation is an elegant method for analysing the temperature dependency of the electric HRBC parameters. However, the temperature dependence of cytoplasmic conductivity of HRBC is exponentially related to temperature and this needs to be taken into account in ER studies, particularly in media with higher ionic strengths where Nernst heating during the course of an experiment is significant. The results provide new information about temperature compensation measuring conductivity of biological cells. These do not obey a linear relationship like that known for simple electroltye solutions. However, this temperature effect would be easy to allow for experimentally if the experimental temperature is carefully monitored. The results suggest that in future experiments on cellular mobility in strong electric fields special attention to the temperature will have to be made since a temperature increase will be induced by Joule heating, especially at high media conductivities.

6. Appendix

Basic knowledge for more information concerned

6.1 An introduction to dielectric theory

The passive electrical properties of a material held between two plane-parallel electrodes of area, *A* separated by a distance, *d* are completely characterised by the measured electrical capacitance C (in Farads) and conductance G (in Siemens) as defined in following equations:

$$G = A\sigma / d \qquad (6.1.1a)$$

$$C = A\varepsilon\varepsilon_0 / d \qquad (6.1.1b)$$

The conductivity σ is the proportionality factor between the electric current density and the electric field, and is a measure of the ease with which delocalised charge carriers can move through the material under the influence of the field. For aqueous biological materials, the conductivity arises mainly from the mobility of hydrated ions and other processes. ε_0 is the dielectric permittivity of vacuum, and has the value of 8.85×10^{-12} Fm^{-1}, while ε is the permittivity of material relative to that of vacuum. It is sometimes referred to as the dielectric constant. The permittivity is proportional to the ratio of the charge to the electric field, and reflects the extent to which localised charge distributions can be destroyed or polarised under the influence of the electric field. For biological materials, such charges are mainly associated with electrical double layers occurring at membrane surface or around solvated macromolecules, or with polar molecules, which possess a permanent dipole moment.

For an electric field with a circular frequency, equations 6.1.1a and b can be written in a form of complex admittance $Y*$:

$$Y* = G + j\omega C \qquad (6.1.2a)$$

$$= (A/d)(\sigma + j\omega\varepsilon_0\varepsilon) \qquad (6.1.2b)$$

where, ω is the angular frequency of the electrical field (in rad s^{-1}), and j is $(-1)^{1/2}$ from which is defined, the complex conductivity $\sigma*$ (sometimes called the admitivity or the specific admittance) of materials can be written as:

$$\sigma* = \sigma + j\omega\varepsilon\varepsilon_0 \qquad (6.1.3a)$$

Equivalently, the complex capacitance $C*$ can be defined as:

$$C* = Y*/ j\omega \qquad (6.1.3b)$$

which leads to the definition of the complex relative permittivity ε^*:

$$\varepsilon^* = \varepsilon' - j\varepsilon'' \qquad (6.1.3c)$$

$$= \varepsilon' - j\sigma / \omega\varepsilon_0 \qquad (6.1.3d)$$

The complex conductivity and permittivity are related by:

$$\sigma^* = j\omega\varepsilon^*\varepsilon_0 \qquad (6.1.4)$$

Only the two properties of conductivity and permittivity characterize the electrical characteristics of a material. Biological tissues contain a multitude of various cells of various sizes and geometries and intercellular clefts and so they are too complicated to be described the properties by a simple RC circuit, as defined above, since an enormous network of elementary RC elements, with different parameters, would be required to build an appropriate model to describe the system. For this reason, one uses the same simple RC circuit, with the expectation that the properties of resistor and the capacitor are now frequency dependent. ε^* and σ^* of various biological materials have been measured in a broad frequency range [109] and it was found that σ^* increased with increasing frequencies. The main reason for this is the increase of the membrane admittance. However, ε^* at low frequency has an enormous value up to the MHz range. These curves of ε^* and of σ^* over a range of frequencies do not continuously increase or decrease, but change in a characteristic step-wise fashion [43]. The reason for this, formally, are the properties of various kinds of RC circuits, which are included in the system. These frequency regions have normally been designated as α, b and γ dispersions. For most biological cells with a membrane as a dielectric barrier, β dispersion also exists. It is caused by a polarization of the cellular membrane with cytoplasm and extracellular media serving as access paths for the charging currents. Polarization caused by the structural inhomogeneity is known as the Maxwell-Wagner relaxation effect. With increasing frequencies, the γ dispersion caused by so-called Deybe relaxations of various molecular dipoles occurs. Since each type of polar or polarisable entity will exhibit its own characteristic response to an imposed electric field, a complex Debye function can be written as [108-109]:

$$\varepsilon^*(\omega) = \varepsilon_\infty + \frac{\varepsilon_s - \varepsilon_\infty}{1 + i\omega\tau} - \frac{\sigma_s}{i\omega} \qquad (6.1.5)$$

in which, ε_∞ is the permittivity measured at a frequency sufficiently high that the polar or polarisable entity is unable to respond to the electric field, ε_s is the limiting low-frequency permittivity (sometime calls static permittivity) where the polarisation is fully manifest, and τ is the characteristic response time or relaxation time. The real and imaginary parts of the complex permittivity can also be expressed in the form of Eq. 6.1.3c. In which the real part, ε', is given by:

$$\varepsilon'(\omega) = \varepsilon_\infty + (\varepsilon_s - \varepsilon_\infty)/(1+\omega^2\tau^2) \qquad (6.1.6)$$

The imaginary component, ε'', known as the dielectric loss, corresponding to the dissipative loss associated with the movement of polarizable charges in phase with the electric field and is given by:

$$\varepsilon''(\omega) = (\varepsilon_s - \varepsilon_\infty)(\omega\tau)/(1+\omega^2\tau^2) \qquad (6.1.7)$$

The ε'' may also be defined in terms of a frequency dependent conductivity as:

$$\varepsilon''(\omega) = \sigma(\omega)/\omega\varepsilon_0 = (\sigma_0 + \sigma_d(\omega))/\omega\varepsilon_0 \qquad (6.1.8)$$

where, σ_0 is the steady state conductivity arising from mobile ions and $\sigma_d(\omega)$ is the frequency dependent conductivity arising from dielectric polarisation.

6.2 A basic theory of interactions of a spherical particle with an electric field

6.2.1 Effective dipole moment

An effective dipole of a dielectric sphere in a dielectric medium was described by Jones (1995) [110]. An insulating dielectric sphere of radius R and permittivity ε_2 is suspended in a fluid of permittivity ε_1 and is subjected to a uniform z- directed electric field of magnitude E_0 (see Fig. 6.1). It is assumed at the outset that the electric field is uniform, that there is no free charge anywhere in the sphere or the dielectric liquid, and that the presence of the particles does not significantly disturb the system of source charges that create E_0.

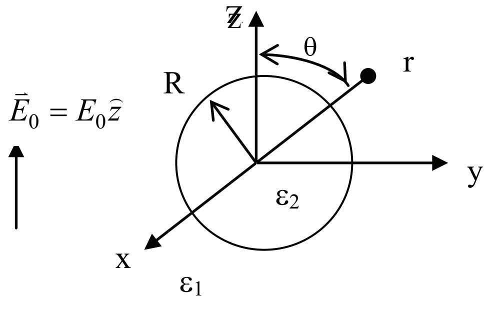

Fig. 6.1 Dielectric sphere of radius R and permittivity ε_2 immersed in a dielectric liquid of permittivity ε_1 and subjected to a uniform electric field of magnitude E_0.

The electrostatic potential satisfies Laplace's equation everywhere because of the divergence- and curl- free properties of the electrostatic field. The assumed solutions for the potential outside ϕ_1 and inside ϕ_2 the sphere take the form:

$$\phi_1(r,\theta) = -E_0 r\cos\theta + \frac{A\cos\theta}{r^2}, r > R \quad (6.2.1a)$$

$$\phi_2(r,\theta) = -Br\cos\theta, r < R \quad (6.2.1b)$$

where, A and B are known coefficients to be determined using the boundary conditions. θ and r are the polar angle and radial position in spherical coordinates, respectively. Note that the first term in Eq. 6.2.1a is the imposed uniform electrostatic field, while the second term is the induced dipole term due to the particle. The boundary conditions are applied at the surface of the particle, $r = R$. First, the electrostatic potential must be continuous across the particle-fluid boundary:

$$\phi_1(r = R,\theta) = \phi_2(r = R,\theta) \quad (6.2.2)$$

Second, the normal component of the displacement flux vector must be continuous across the boundary:

$$\varepsilon_1 E_{r1}(r = R,\theta) = \varepsilon_2 E_{r2}(r = R,\theta) \quad (6.2.3)$$

where, $E_{r1} = -\partial\phi_1 / \partial r$ and $E_{r2} = -\partial\phi_2 / \partial r$ are the normal electric field components in the fluid and the dielectric sphere, respectively. Combining Eq. 6.2.1a and b with Eq. 6.2.3, we obtain:

$$A = \frac{\varepsilon_2 - \varepsilon_1}{\varepsilon_2 + 2\varepsilon_1} R^3 E_0 \quad (6.224a)$$

$$B = \frac{3\varepsilon_1}{\varepsilon_2 + 2\varepsilon_1} E_0 \quad (6.2.4b)$$

For a particle suspended in a dielectric fluid subjected to an electric field, the field polarizes the effective dipole moment, $\vec{m}_{eff}$. The electrostatic potential ϕ_{dipole} due to the dipole moment in a dielectric medium of permittivity ε_1 is:

$$\phi_{dipole} = \frac{\vec{m}_{eff}\cos\theta}{4\pi\varepsilon_1 r^2} \quad (6.2.5)$$

Comparing Eq. 6.2.5 to the induced electric dipole term in Eq. 6.2.1a yields a useful general relationship between the effective moment and the coefficient A:

$$m_{eff} = 4\pi\varepsilon_1 A \quad (6.2.6)$$

For the special case of the homogeneous, dielectric sphere, the expression for the effective dipole moment is:

$$m_{eff} = 4\pi\varepsilon_1 K R^3 E_0 \quad (6.2.7)$$

where, K is known as the Clausius-Mossotti factor, providing a measure of the strength of the effective polarization of a spherical particle as a function of ε_1 and ε_2,

$$K(\varepsilon_2,\varepsilon_1)=\frac{\varepsilon_2-\varepsilon_1}{\varepsilon_2+2\varepsilon_1} \tag{6.2.8}$$

However, for more general cases of particles, an ohmic loss in a sinusoidal steady-state AC electric field will be found experimentally. A variety of dissipation mechanisms, including conduction and dielectric relaxation phenomena, influences the behaviour of real dielectric particles in an electric field. When loss is present, the dipole moment of a particle in a field exhibits either a time delay when the electric field is suddenly applied, or a phase shift lag when the electric field is a steady-state sinusoidal function of time. In such situations Eq. 6.2.8 now has become a function of a *complex* permittivity:

$$K^*(\varepsilon_2^*,\varepsilon_1^*)=\frac{\varepsilon_2^*-\varepsilon_1^*}{\varepsilon_2^*+2\varepsilon_1^*} \tag{6.2.9}$$

and the complex effective dipole moment $\vec{m}_{eff}$ can now be expressed as:

$$\vec{m}_{eff}=4\pi\varepsilon_1 K^* R^3 \vec{E}_0 \tag{6.2.10}$$

6.2.2 Theory for particle rotation

Consider a homogeneous sphere with radius R, permittivity ε_2, and conductivity σ_2 in a liquid of permittivity ε_1, conductivity σ_1, and dynamic viscosity η_1. The particle experiences a counter-clockwise rotating circularly polarized electric field $\vec{E}(t)$:

$$\vec{E}(t)=E_0(\hat{x}\cos\omega t+\hat{y}\sin\omega t) \tag{6.2.11}$$

where $\omega > 0$. Fig. 6.2 shows a simple arrangement of electrodes excited by poly AC phase voltages to create such a field. For convenience in the following analysis, we can rewrite the vector phase expression for $\vec{E}(t)$ as:

$$\vec{E}=E_0(\hat{x}+j\hat{y}) \tag{6.2.12}$$

The effective moment induced in the stationary particle by this rotating field is:

$$\vec{m}_{eff}=4\pi\varepsilon_1 K^*(\omega) R^3 E_0(\hat{x}-j\hat{y}) \tag{6.2.13}$$

where, $K^*(\omega)$ is given by Eq. 6.2.9. The Eq. 6.2.13 indicates that the effective moment vector of the particle, $\vec{m}_{eff}(t)$, rotating synchronously with the electric field vector, $\vec{E}(t)$, lags behind by the constant angle α, as illustrated in Fig.6.3. The phase factor associated with $K^*(\omega)$ in Eq. 6.2.13 is α. The value of α determines the magnitude and sign of the time-average torque.

The time-average torque in terms of the complex expressions for the dipole moment and the electric field phase can be expressed as:

$$\left\langle \vec{T}(t) \right\rangle = \frac{1}{2}\mathrm{Re}\left[\vec{m}_{eff}\ \vec{E} = \left|\vec{m}_{eff}\right| E_0 \sin\alpha\, \hat{z} \right] \qquad (6.2.14)$$

$$\alpha = -\sin^{-1}\left\{ \mathrm{Im}\left[K^*(\omega)\right] / \left|K^*(\omega)\right| \right\} \qquad (6.2.15)$$

where, E$_0$ is the magnitude of electric field. $\left|\vec{m}_{eff}\right|$ is the constant magnitude of the rotating effective moment vector. Combining Eq. 6.2.12 and 6.2.13 with Eq. 6.2.14 the result is:

$$\left\langle \vec{T}(t) \right\rangle = -4\pi\varepsilon_1 R^3\, \mathrm{Im}\left[K^*(\omega)\right] E_0^2 \hat{z} \qquad (6.2.16)$$

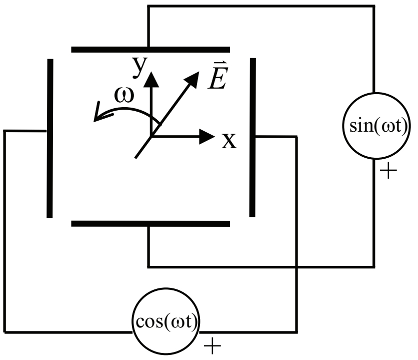

Fig. 6.2 Set of electrodes with polyphase AC excitation used to create a counter-clockwise rotating electric field. The vector of the electric field rotates with the angular frequency, *ω*.

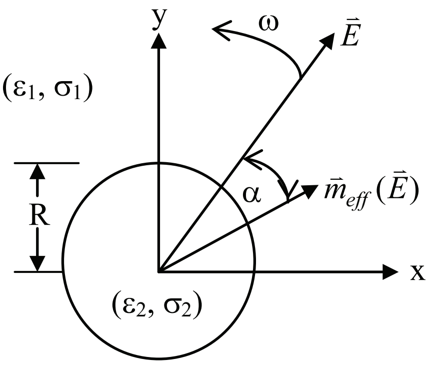

Fig. 6.3 Rotating electric field $\vec{E}$ and effective electric dipole moment $\vec{m}_{eff}$ vectors with lag angle α

The rotation of particles in a rotating electric field has been applied to investigate the dielectric properties of biological cells. To analyse and interpret the experimental results, a suitable model needs to be applied. The simplest biologically relevant model for consideration is a spherical single shell model covered by a homogeneous membrane. In this case, the radius of the cell and the membrane thickness as geometrical parameters are included in the corresponding equations, as well as the conductivities and the permittivities of the membrane, the cytoplasm, and the external medium. These model considerations indicated that the peak of the antifield rotation in its frequency position, and its amplitude, reflects the membrane properties of the cell. This first-characteristic-frequency is determined by the time constant of membrane charging. The maximum of the cofield rotation, i.e. the second-characteristic-frequency, indicates conductivity and permittivity of the cytoplasm in relation to that of the external milieu (bathing electrolyte).

Nevertheless, since most biological cells are not spherical, a development of a more proper model was then performed. The finite element model developed by Gimsa and Wachner [35] was used in the present study. For the details of this model as well as the definitions of the parameters please see in the theoretical section of Appendix 2.

6.3 Biological electrolytes

Mammals have a total water content amounting to some 65-70 % of their body mass, and apart from the effects of dissolved macromolecules and membrane surfaces, the dielectric properties of this water is largely influenced by the presence of dissolved ionic salts. The physical effects of such dissolved ions on the dielectric permittivity of biological fluids arise from more than just the volume effect of replacing polar water molecules by charged, but non-polar, ionic particles. In particular, the strong electric field around each ion has the effect of orienting the water molecules, reducing the way in which they can rotate in response to an applied field. The permittivity of dilute electrolytes (ε') and that of pure aqueous solvent (ε_1') in terms of a dielectric decrement is given by [89]:

$$\varepsilon' = \varepsilon_1' - \delta c \qquad (6.3.1)$$

where, c is concentration of the solution and δ is the sum of the decrements arising from the cations and anions present which is given by:

$$\delta = \delta^{+} + \delta^{-}. \qquad (6.3.2)$$

Values for δ^{+} and δ^{-} for various ions in water at a concentration (*c)* of 1 molar are given in Tab. 6.1. These values are sufficiently accurate to cover all biologically relevant cases except that of halophilic micro-organisms. KCl, for example, gives a total decrement of 11 (Tab.

6.1), and will reduce the permittivity of water ε_1' from 80 at 25 °C to 69. Thus, the relative permittivity of 1 M aqueous KCl and NaCl solutions at this temperature are both 69.

Cation	$\delta^{+}(\pm 1)$	Anion	$\delta^{-}(\pm 1)$
Na^{+}	8	Cl^{-}	3
K^{+}	8	F^{-}	5
Li^{+}	11	I^{-}	7
H^{+}	17	SO_4^{2-}	7
Mg^{2+}	24	OH^{-}	13

Tab. 6.1 Dielectric decrement values for some ions in aqueous solution [89]

As well as the effect of lowering the relative permittivity of the aqueous solvent, dissolved ions will generally decrease its relaxation time (protons are an exception). To a first approximation, this may be considered to result from the disruption by the solvated ions of the normal hydrogen-bond structure of pure water. For concentrations of dissolved ions less than 1 molar, this may be expressed in terms of a relaxation frequency increment (*f*) by the equation:

$$f = f_1 + c\delta f \qquad (6.3.3)$$

where,

$$\delta f = \delta f^{+} + \delta f^{-} \qquad (6.3.4)$$

and *f* represents the effects of cations and anions. Values of *f* are given in Tab. 2.2, and may be used to estimate how far the relaxation frequencies for various electrolytes differ from the value of 17.1 GHz accepted for pure water at 20 °C. Note in Tab. 6.2 that the behaviour of protons is quite different to other ions.

Cation	$\Delta f^{+}(\pm 0.2)$(GHz)	Anion	$\Delta f^{-}(\pm 0.2)$(GHz)
H^{+}	-0.33	OH^{-}	0.24
Li^{+}	0.34	Cl^{-}	0.44
Na^{+}	0.44	F^{-}	0.44
K^{+}	0.44	SO_4^{2-}	1.20
Mg^{2+}	0.44	I^{-}	1.65

Tab. 6.2 Relaxation frequency increment values for some ions in aqueous at 20°C [89]

The relaxation frequency is a parameter, which characterises the relaxation time (τ) of dispersion observed in biological materials. A simple physical model, which one may use to gain a mental picture of the processes occurring during the dielectric relaxation of a molecule with a permanent dipole moment, is one that considers the dipoles to be spheres whose rotation in response to the field is opposed by frictional interaction with the surrounding viscous medium. The relevant relaxation time for the orientation of such a sphere is given by:

$$\tau = \chi / 2kT \qquad (6.3.5)$$

where, χ is a molecular friction coefficient which relates the torque exerted on the dipolar molecule by the applied field to the molecule's angular velocity, k is Boltzmann's constant and T is the absolute temperature. Assuming the dipole to be equivalent to a rigid sphere of radius r turning in a Newtonian hydrodynamic fluid of macroscopic viscosity η, the Stokes-Einstein relation gives $\chi = 8\pi\eta r^3$ so that the relaxation time is:

$$\tau = 4\pi\eta r^3 / kT \qquad (6.3.6)$$

7 References

[1] R. Pethig, Dielectric and electronic properties of biological materials, Wiley Press, New York, (1979).

[2] J.C. Maxwell, A Treatise on electricity and magnetism, Clarendon Press, Oxford, (1873).

[3] K.W. Wagner, The after-effect in dielectrics. Archiv. Elektrotechnik, 2 (1914) 371–387.

[4] R. Pethig and G.H. Marx, Applications of dielectrophoresis in biotechnology.
Trends Biotechnol., 15 (1997) 426 –32.

[5] R. Pethig, Application of AC electrical fields to the manipulation and characterization of cells. Proceedings of the Fourth Toyota Conference, Amsterdam, Elsevier Press, (1990) 159–185.

[6] C.L. Davey and D.B. Kell, The low-frequency dielectric properties of biological cells. Bioelectrochemistry of Cells and Tissues, (1995) 159–207..

[7] K.R. Foster and H.P. Schwan, Dielectric properties of tissues and biological materials: a critical review, Critical reviews in biomedical engineering, CRC Press, (1989) 25–104.

[8] H.P. Schwan, Analysis of dielectric data. IEEE Trans. Elec. Insul., 20 (1985) 913–922.

[9] G. Cevc, Membrane electrostatics. Biochim. Biophys. Acta, 1031 (1990) 311– 382.

[10] L.E. Ferris, C.L. Davey, and D.B. Kell, Evidence from its temperature dependence that the dielectric dispersion of cell suspensions is not due solely to the charging of a static membrane capacitance. Eur. Biophys. J., 18 (1990) 267–276.

[11] J. Cheng, E. L. Sheldom, L. Wu, and M. J. Haller, Isolation of cultured cervical carcinoma cells mixed with peripheral blood cells on a bioelectronic chip. Anal. Chem. 70 (1998) 2321–2326.

[12] X.B. Wang, Y. Huang, P. R. Gascoyne, F. F. Becker, R. Holzel, and R. Pethig, Changes in Friend murine erythroleukemia cell membranes during induced differentiation determined by electrorotation. Biochim. Biophys. Acta, 1193 (1994) 330–344.

[13] G.N. Stewart, The relative volume or weight of corpuscles and plasma in blood. J. Physiol., 24 (1899) 356.

[14] E.H Grant, R.J. Sheppard, and G.P. South, Dielectric behavior of biological molecules in solution. Oxford University Press, Oxford, 1978.

[15] X.B. Wang, Y. Huang, R. Holzel, J.P.H. Burt, and R. Pethig, Theoretical and experimental investigations of the interdependence of the dielectric, dielectrophoretic, and electrorotational behaviour of colloidal particles. J. Phys. D Appl. Phys., 26 (1993) 312–22.

[16] H.P. Schwan, Determination of biological impedances. Physical techniques in biological research, Academic Press, New York, (1963) 323–407.

[17] J. Seidl, R. Knuechel, and L. A. Kunz-Schughart, Evaluation of membrane physiology following fluorescence activated or magnetic cell separation. Cytometry, 36 (1999) 102–111.

[18] H. Engel, C. Kleespies, J. Friedrich, M. Breidenbach, A. Kallenborn, T. Schondorf, H. Kolhagen, and P. Mallmann, Detection of circulating tumour cells in patients with breast or ovarian cancer by molecular cytogenetics. J. Cancer, 81 (1999) 1165–1173.

[19] P. Holmes and M. Al-Rubeai, Improved cell line development by a high throughput affinity capture surface display technique to select for high secretors. J. Immunol. Methods, 230 (1999) 141–147.

[20] O. Herault, P. Colombat, J. Domenech, M. Degenne, J.L. Bremond, L. Sensebe, M.C. Bernard, and C.A. Binet, Rapid single-laser flow cytometry method for discrimination of early apoptotic cells in a heterogeneous cell population. J. Haematol., 104 (1999) 530–537.

[21] X-B. Wang, M. P. Hughes, Y. Huang, F. F. Becker, and P. R. Gascoyne, Non-uniform spatial distributions of both the magnitude and phase of AC electric fields determine dielectric forces. Biochim. Biophys. Acta, 1243 (1995) 185–194.

[22] G. Quincke, Über Rotationen im constanten electrischen Felde, Wied. Ann. Phzs. 59 (1896) 417.

[23] A. Lampa, Über Rotationen im electrostatischen Drehfeld, Wiener. Ber. 115,.2a (1906) 1659.

[24] W.M. Arnold and U. Zimmermann, Rotating field induced rotation and measurement of the membrane capacitance of single mesophyll cells of Avena sativa, Z. Naturforsch. 37c (1982) 908-915.

[25] W.M. Arnold and U. Zimmermann, Rotation of an isolate cell in a rotating electric field. Naturwiss., 69 (1982) 297.

[26] W. M. Arnold, B. M. Geier, B. Wendt, and U. Zimmermann, The change in the electrorotation of yeast cells effected by silver ions. Biochim. Biophys. Acta, 885 (1986) 35.

[27] W. M. Arnold, R. K. Schmutzler, S. Al-Hasani, D. Krebs, and U. Zimmermann, Differences in membrane properties between unfertilized and fertilized single rabbit oocytes demonstrated by electrorotation. Comparison with cells from early embryoes, Biochim. Biophys. Acta, 979 (1989) 142.

[28] G. Fuhr, J. Gimsa, and R. Glaser, Interpretation of electrorotation of protoplasts I Theoretical considerations. Studia Biophysica, 108 (1985) 149.

[29] G. Fuhr, R. Glaser, and R. Hagedorn, Rotation of dielectrics in a rotating electric high-frequency-field. Model experiments and theoretical explanation of the rotation effect of living cells, Biophys. J., 49 (1986) 395.

[30] J. Gimsa, E., Donath, and R. Glaser, Evaluation of data of simple cells by electrorotation using square-topped fields. J. Physiol., 19 (1988) 389.

[31] J. Gimsa, P. Marszalek, U. Loewe, and T.Y. Tsong, Dielectrophoresis electrorotation of neurospora slime and murine myeloma cells, Biophys. J., 60 (1991) 749-760.

[32] S. Lippert and J. Gimsa, High resolution measurements of dielectric cell properties by a combination of AC-electrokinetic effects, in: P. Kostarakis (ed.), Proceedings of the 2nd International Workshop on Biological Effects of EMFs, Rhodes, Greece, (2002) 830-836.

[33] J. Gimsa , T. Mueller, T. Schnelle, and G. Fuhr, Dielectric spectroscopic of single human erythrocytes at physiological ionic strength: Dispersion of cytoplasm. Biophys. J., 71 (1996) 495-506.

[34] J. Gimsa and D. Wachner, A polarization model overcoming the geometric restrictions of the Laplace solution for spherical cells: Obtaining new equation for field- induced forces and transmembrane potential. Biophys. J., 77 (1999) 1316-1326.

[35] I. Turcu and C.M., Lucaciu, Electrorotation: a spherical shell model. J. Phys. A: Math. Gen. 22 (1989) 995-1003.

[36] V.L. Sukhorukov, H. Mussauer, and U. Zimmermann, The effect of electrical deformation forces on the electropermeabilization of erythrocyte membrane in low – and high – conductivity media. J. Membrane Biol., 163 (1998) 235-245.

[37] W.M. Arnold, and U. Zimmermann, Electrorotation: development of a technique for dielectric measurements on individual cells and particles. J. Electrostatics, 21 (1998) 151-191.

[38] J. Sudsiri, D. Wachner, J. Donath, and J. Gimsa, Can molecular properties of human red blood cells be accessed by electrorotation? Songklanakarin J. Sci. Technol. 24 (2002) 785-789.

[39] H. Geraed and L.D. Christopher, The dielectric properties of biological cells at radiofrequencies: Applications in biotechnology. Enzyme and Microbial Technology 25 (1999) 161-172.

[40] B. Adalberto, D.I. Vincenzo, P. Osvaldo and R. Gianfranco, Dielectric properties of the plasma membrane of cultured murine fibroblasts treated with a nonterpenoid extract of Azadirachta indica seeds. J. Membrane Biol. 215 (2007) 75-79.

[41] W.A. Wegener, V.J. Koester, and R.M. Dowben, A general ellipsoid cannot always serve as a model for the rotational diffusion of arbitrarily shaped rigid molecules. Proc. Natl. Acad. Sci., 76 (1979) 635-636.

[42] K. Maswiwat, M. Holtappels, and J. Gimsa, On the field distribution in electrorotation chambers- Influence of electrode shape. Electrochemica Acta, 51 (2006) 5215-5220.

[43] M. Simeonova, D. Wachner, J. Gimsa, Cellular absorption of electric field energy: the influence of molecular properties of the cytoplasm. Bioelectrochemistry
56 (2002) 215–218.

[44] D.R. Lide, CRC Handbook of chemistry and physics, 74th edition, CRC Press, Boca Raton, (1993).

[45] S.C. T. Xie and Y.Z. Lam, Investigation into the effects of haematocrit and temperature on the resistivity of mammalian blood using a four-electrode probe. Med. Biol. Eng., 36 (1998) 467-470.

[46] H.P. Schwan and R.F. Kenneth, RF-field interactions with biological system: electrical properties and biophysical mechanisms. Proceeding of the IEEE, 68 (1980) 104-113.

[47] G. F. Baker and P. Baker, Temperature dependence of the exchange of monovalent anions in human red blood cells. Biochim. Biophys. Acta, 1285 (1996) 192-202.

[48] M.S. Jaeger, T. Mueller, Th. Schnelle, N. Teuscher and A. Heilmann, A Thermometry in microfluidic systems during radio-frequency induced heating. The annual meeting of the German Biophysical Society. Dresden, Germany. September (2002).

[49] D. Mietchen, T. Schnelle, T. Mueller, R. Hagedorn, and G. Fuhr, Automated dielectric single cell spectroscopy-temperature dependence of electrorotation. J. Phys. D: Appl. Phys., 35 (2002) 1258-1270.

[50] F. Jaspard and M. Nadi, Dielectric properties of blood: an investigation of temperature dependence. Physiol. Meas., 23 (2002) 547-554.

[51] I. Bielinska and J. Terleski, Temperature dependence of the dielectric properties of blood. Folia Histochem. Cytobiol., 23(1-2) (1985) 33-42.

[52] A.L. Harris, CC. Guthe, F. van't Veer, and DF. Bohr, Temperature dependence and bi-directional cation fluxes in red blood cells from spontaneously hypertensive rats. Hypertension, 6 (1984) 42-48.

[53] A.C. Hall, and J.S. Willis, Differential effects of temperature on three components of passive permeability to potassium in rodent red cells. J. Physiol., 348 (1984) 629-643.

[54] J.S. Charnock, D.M. Dorty, and J.C. Russell, The effect of temperature on the activity of (Na+ +K+) ATPase. Arch. Biochem. Biophys., 142 (1971) 633-637.

[55] J.C. Ellory and J.S. Willis, Kinetic of the sodium pump in red cells of different temperature sensitivity. J. Gen. Physiol., 79 (1982) 1115-1130.

[56] S.L. Kimzey and J.S. Willis, Temperature adaptation of active sodium potassium transport and of passive permeability in erythrocytes of ground squirrels. J. Gen. Physiol., 58 (1971) 634-649.

[57] R. Glaser and J. Donath, Temperature and transmembrane potential dependence of shape transformations of human erythrocytes. Biochem. Bioenerg., 27 (1992) 429-440.

[58] J.O'M. Bockris, I. Reddy, and K.N. Amulya, Modern electrochemistry, 2nd edition, Plenum Publishing Corporation Press, New York, (1973).

[59] E. Donath and M. Egger, Dielectric behaviour of the anion-exchange protein of human red blood cells: Theoretical analysis and comparison to electrorotation data. Bioelectrochem. Bioenerg., 23 (1990) 337–360.

[60] J. Gimsa, Th. Schnelle, G. Zechel, and R. Glaser, Dielectric spectroscopy of human erythrocytes: investigations under the influence of nystatin. Biophys. J., 66 (1994) 1244-1253.

[61] J.Z. Bao, C.C. Davis, and M.L. Swicord, Microwave dielectric measurements of erythrocyte suspensions. Biophys. J., 66 (1994) 2173-2180.

[62] J.Z. Bao, C.C. Davis, and R.E. Schmukler, Frequency domain impedance measurement of erythrocytes: Constant phase angle impedance characteristics and a phase transition. Biophys. J., 61 (1992) 1427-1434.

[63] J. Brahm, Temperature-dependent changes of chloride transport kinetics in human red cells. J. Gen. Physiol., 70 (1977) 283-306.

[64] S. Despa, The influence of membrane permeability for ions on cell behaviour in an electric alternating field. Phys. Med. Boil., 40 (1995) 1399-1409.

[65] R. Georgiewa, E. Donath, J. Gimsa, U. Loewe, and R. Glaser, AC –field-induced KCl leakage from human red cells at low ionic strengths: Implication for electrorotation measurements. Bioelectrochem. Bioenerg., 22 (1989) 255-270.

[66] N. Sperelakis, Cell physiology, Academic Press, California, (1994).

[67] R. Mancinelli, A. Botti, F. Bruni and A. Ricci, Hydration of sodium, potassium, and chloride ions in solution and the concept of structure Maker/Breaker. J. Phys. Chem. B, 111 (2007) 13570-13577.

[68] I. Bernhardt, A.C. Hall, and J.C. Ellory, Effects of low ionic strength media on passive human red cell monovalent cation transport. J. Physiol., 434 (1991) 489-506.

[69] W. Charles O' Neill, Physiological significance of volume-regulatory transporters, J. Physiol., 276 (1999) C955-C1011.

[70] A. Katchalsky, and P.F. Curran, Nonequilibrium thermodynamics in biophysics, 2nd edition, Harvard University Press, London (1967).

[71] S. Munoz San Martin, J.L. Sebastian, M. Sancho, and J.M. Miranda, A study of the electric field distribution in erythrocyte and rod cells shape from direct RF exposure. Phys. Med. Biol., 48 (2003) 1649-1659.

[72] S.J. Rzoska and V.P. Zhelezny, Nonlinear dielectric spectroscopy of biological system: principle and application. Kluwer Academic Publishers, Netherlands, (2004) 335-344.

[73] A. Bonincontro, V. Di Ilio, O. Pedata, and G. Risuleo, Dielectric properties of the plasma membrane of cultured murine fibroblasts treated with a nonterpenoid extract of Azadirachta indica seeds. J. Membrane Biol., 215 (2007) 75-79.

[74] A.M. Zhivov and A.Y. Gyurova, Influence of cytoplasm concentration on Maxwell-Wagner polarization of bacteria E. coli. J. Phys. Chem. B, 113 (2009) 8375-8382.

[75] A. Herrmann, P. Müller, and R. Glaser, Shape transformation of erythrocyte ghosts depends on ion concentrations. Biosci. Rep., 5 (1985) 417-423.

[76] R. Glaser, T. Fujii, P. Müller, E. Tamura, and A. Hermann, Erythrocyte shape dynamics: influence of electrolyte conditions and membrane potential. Biomed. Biochim. Acta, 46 (1987) 327-333.

[77] R. Glaser, C. Gengnagel, and J. Donath, Membrane electric field and erythrocyte shape. Stud. Biophys., 127 (1988) 201-206.

[78] R. Glaser and J. Donath, Stationary ionic states in human red blood cells. Bioelectrochem. Bioenerg. 13 (1984) 71-83.

[79] M. Crose, S. Vrhovec, M. Brumen, S. Svetina, and B. Zesk, Low pH induced shape changes and vesiculation of Human erythrocytes. Gen. Physiol. Biophys., 15 (1996) 145-163.

[80] M.M. Gedde. E. Yang, and W.H. Huestis, Shape response of human erythrocytes to altered cell pH. Blood, 86 (1995) 1595-1599.

[81] M.M Gedde and W.H. Huestis, Membrane potential and human erythrocytes shape. Biophys J., 72 (1997) 1200-1233.

[82] R. Glaser, The shape of red blood cells as a function of membrane potential and temperature. J. Membrane Biol., 51 (1979) 217-228.

[83] J. Gimsa, Red cell echinocytogenesis is correlated to the recruitment of external band-3 conformations. Bioelectrochem. Bioenerg., 38 (1995) 99-103.

[84] D. G. Jay, Role of band-3 in homeostasis and cell shape. Cell, 86 (1996) 853-854.

[85] J. Gimsa, A possible molecular mechanism governing human erythrocyte shape. Biophys. J., 75 (1998) 568-570.

[86] E. Evans, Bending resistance and chemically induced moments in membrane bilayers. Biophys. J., 14 (1974) 923-931.

[87] G.V. Richieri, S. P. Akeson, and H. C. Mel, Measurement of biophysical properties of red blood cells by resistive pulse spectroscopy: volume, shape, surface area, and deformability. J. Biochem. Biophys. Methods, 11 (1985) 117-131.

[88] T.M. Fisher, C.W.M. Haest, M.S. Liesen, and H.S. Schönbein, The stress-free shape of the red blood cell membrane. Biophys., J. 34 (1981) 409-422.

[89] R. Pething and D.B. Kell, The passive electrical properties of biological systems: their significance in physiology, biophysics and biotechnology. Phys. Med. Biol., 32 (1987) 933-970.

[90] A. Iglic, A possible mechanism determining the stability of speculated red blood cells. J. Biomechanics, 30 (1996) 35- 40.

[91] G. R. Cokelet and H.J. Meiselman, Reological comparison of hemoglobin solutions and erythrocyte suspensions. Sci., 162 (1968) 275-277.

[92] A. Chiabrera, C. Nicolini, and H.P. Schwan, Interactions between electromagnetic fields and cells. Life Science, Plenum Press, New York, 97 (1985).

[93] L. K. Laidler and J. H. Meiser, Physical Chemistry, 2nd edition, Houghton Mifflin Company, Boston, Toronto, (1995).

[94] http://w3.whosea.org/haem/c10.htm [30/11/2010]

[95] D.R. Lide, CRC Handbook of chemistry and physics, 83th edition, CRC Press, Boca Raton (2002-2003).

[96] H. Pauly and H.P. Schwan, Dielectric properties and ion mobility in erythrocytes. Biophys. J., 6 (1966) 621-639.

[97] R. Glaser, Biophysics, 4th edition, Springer –Verlag, Berlin, (2000).

[98] J. Gimsa, R. Glaser, and G. Fuhr, Theory and application of the rotation of biological cells in rotating electric field (Electrorotation), Physical characterization of biological cells. Verlag Gesundheit GmbH, Berlin (1991).

[99] C. W. Davies, The conductivity of solutions, 2nd edition, Chapman & Hall, LTD, London (1933).

[100] W. Vand, Viscosity of solutions and suspension, I Theory. J. Phys. Coll. Chem., 52 (1984) 314-321.

[101] G.V. Richieri, S.P. Akeson, and H.C. Mel, Measurement of biophysical properties of red blood cells by resistive pulse spectroscopy: volume shape, surface area, and deformability. J. Biochem. Biophys. Methods, 11 (1985) 117-131.

[102] J. Sudsiri, D. Wachner, and J. Gimsa, On the temperature dependence of the dielectric membrane properties of human red blood cells. Bioelectrochemistry, 70 (2007) 134-140.

[103] V.I. Sukhorukov, H. Mussauer, and U. Zimmermann, The effect of electrical deformation forces on the electropermeabilization of erythrocyte membranes in low-and high-conductivity media. J. Membrane Biol., 163 (1998) 235-245.

[104] G.M. Gary-Bobo and A.K. Solomon, Properties of hemoglobin solutions in red cells. J. Gen. Physiol., 52 (1968) 825-853.

[105] K. Asami, Y. Takahashi, and S. Takashima, Dielectric properties of mouse lymphocytes and erythrocytes. Biochim. Biophys. Acta, 1010 (1989) 49-55.

[106] I. Turcu and C. M. Lucaciu, Electrorotation: a spherical shell model. J. Phys. A: Math. Gen., 22 (1989) 995-1003.

[107] H. S. Harned and B. B. Owen, The physical chemistry of electrolytic solutions, 3rd edition, Reinhold Publishing Corporation, New York, (1958).

[108] C. Polk and E. Postow, Biological effects of electromagnetic fields, 2nd edition, CRC press, Boca Raton, Florida, (1996).

[109] R. S. Cole and R. H. Cole, Dispersion and absorption in dielectrics I. Alternating current characteristics. J. Chem. Phys., 9 (1941) 341-351.

[110] T.B. Jones, Electromechanism of particles, 1st edition, Cambridge University Press, USA, (1995).

8 Acknowledgments

It was a great opportunity to perform my PhD study under the supervision of Prof. Dr. Jan Gimsa at the Rostock University in Rostock, Germany. I would like to thank all those who have provided guidance and support while I worked in pursuing my degree.

First and foremost, I must thank Prince of Songkla University, Thailand, who gave me the financial support for four years of my study.

Thanks go also to the Forschungsgemeinschaft Funk, Germany for the one year additional financial support, without which much of this would have been possible.

I wish to express my deepest thanks to my supervisor Prof. Dr. Jan Gimsa for his inspiring and encouraging guidance to a deeper understanding of the electrical properties of cells. I would also like to thank Prof. Dr. Dieter G. Weiss, Promotionsbeauftragter for the Department of Biological Sciences, Rostock University for his valuable suggestions whenever needed for solving the problems during work on this dissertation and for his fruitful discussions, encouragement and for always being willing to help.

I am indebted to Dr. Raymond Ritchie, Sydney University, Australia for providing valuable information; valuable suggestions and kind help and especially for the meticulous correction of my manuscript. I would also like to acknowledge Assoc. Prof. Dr. Pikul Wanichapichart, Prince of Songkla University, Thailand, for her encouragement, support even when I was at my most stressed.

I would like to thank Derk Wachner, the co-author of most of my publications, for everything he has done for me. Thanks for the helpful discussions, answering my questions, kind help with my computer accidents. I have learned so much from you (too much to list here).

I would like to give my special thanks to Jutta Donath for her advice and excellent technical assistance. Lutz Haberland and Werner Baumann are acknowledged for their assistance.

I would also like to thank the International Postgraduate Program (IPP), University of Rostock and especially Prof. Eberhard Burkel and Prof. Anka Köhler who enabled me to take part in the 3rd Regional Symposium on Membrane Science and Technology (MST) 2005 (Bundung, Indonesia) and in the XVIII International Symposium on Bioelectrochemistry and Bioenergetics of the Bioelectrochemical Society (BES) and the 3rd Spring Meeting Bioelectrochemistry of the International Society of Electrochemistry (ISE), 2005 (Coimbra, Portugal).

I would like to give my special thanks to The Abteilung für Transfusionsmedizin Blutspende, University of Rostock for kindly providing the human red blood cells for all my experiments.

Thanks also to all of the members at the Chair of Biophysics for providing me a pleasant working atmosphere and enormous amount of support over the past four years.

Last but certainly not least, I would like to say thank all of my family in Thailand. They were always understanding, supportive and have made many sacrifices in order to help me in my project. Special thanks to my husband, Major Suriya Chuaibamrung, for putting up with me when I was totally stressed, for everlasting love, encouragement and support and for everything great or small he has done to help me.

9 Curriculum vitae

Particulars

Name: Jutiporn Sudsiri
Date of birth: September 1st 1972
Place of birth: Trang, Thailand

Status

Married; married name Jutiporn Chuaibamrung

Home address

30 Moo 5 Surat – Nasan Road
Ampor Maung
Surattani Province
84100, Thailand
Tel: +6677355675 Fax: +6677355448

Current address

Faculty of Sciences and Industrial Technology,
Prince of Songkla University - Suratthani Campus,
Muang District, Suratthani Province 84100, Thailand
Tel: +6677355453 Fax: +6677355453

Schooling

1979-1984	Banpikulloy primary school in Trang, Thailand
1985-1987	Lumpuraraungwit pre-secondary school in Trang, Thailand
1986	Lumpuraraungwit school prize in Thai Dancing
1988-1990	Saparachinee secondary school in Trang, Thailand
1989	Staff member of Saparachinee school's science club

University studies

1991-1995	Physics Major at Prince of Songkla University, Pattani, Thailand
1991	Certification as boyscout leader
1992	Chair of electronics club in Prince of Songkla University, Patani, Thailand
1993	Staff member in the "Science Camp", Southern Thailand
1994	Supervisor of a practical course in physics at the Dachapattanayanukul High School, Pattani, Thailand
1995-1998	Masters in Physics (specialization in Biophysics) at Prince of Songkla University, Songkla Province, Thailand

Academic Qualifications

1998	M.Sc. (Physics), Prince of Songkla University, Songkla Province, Thailand
1995	B.Sc. (Education in Physics), Prince of Songkla University, Pattani, Thailand

Career Synopsis

1998 Lecturer at the Department of Science and Technology, Prince of Songkla University, Surattani, Thailand

1999 Chair of academics club of Prince of Songkla University, Surattani, Thailand

2000 Chair assistance at the department of Science and Technology, Prince of Songkla University, Surattani, Thailand

2001 Chair of physics laboratory of department of Science and Technology, Prince of Songkla University, Surattani, Thailand

2001 Invited teacher of physics at the Surattani School, Surattani, Thailand

March 2002– August 2002 Scientist employed, University of Rostock, Germany, supported by Forschungsgemeinschaft Funk

October 2002 – Dec. 2006 Doctoral Fellow at the Institute of Biological Sciences, University of Rostock

2006- Lecturer at the Faculty of Sciences and Industial Technology, Prince of Songkla University, Surattani, Thailand

Prizes and stipends

1989	Prize in the “Southern Thailand – Poetry” Competition
1995	Prizes and grants stipend from the National Science and Technology Development Agency, Thailand
2002	Grant stipend from the Forschungsgemeinschaft Funk, Germany.
2002-2006	Grant stipend from the Prince of Songkla University, Thailand.

Research fields

- AC field frequencies for dielectrophoretic separation of five marine phytoplankton species
- Dielectrophoretic investigations of Chlorella sp. for detecting the heavy metal content in water

Fields of interest

-Electric properties of cells
-Dielectrophoresis and Electrorotation of single cells
-Electromagnetic effects on biological cells

Publication list

Original refereed papers (including refereed Meetings Proceedings)

1. J. Sudsiri, P. Wanichapichart and T. Mahaworasilpa. 1998. AC Electric field frequencies for isolating five marine phytoplankton. Songklanakarin J. Sci. Technol. 21: 214-219

2. J. Sudsiri, D. Wachner, J. Donath, and J. Gimsa. 2002. Can molecular properties of human red blood cells be accessed by electrorotation ? Songklanakarin J. Sci. Technol. 24: 785-789

3. J. Sudsiri, D. Wachner, M. Simeonova, J. Donath, and J. Gimsa. 2006. Effect of temperature on the electrorotation behavior of human red blood cells. J. of Technology Malaysia. 44(F): 1-12.

4. J. Sudsiri, D. Wachner, and J. Gimsa.2007. On the temperature dependence of the dielectric membrane properties of human red blood cells. Bioelectrochemistry. 70:134-140.

5. J. Chuaibamrung. 2009. Influence of cell shape and cell volume on cytoplasmic conductivity of human red blood cells. Journal of Microscope Society of Thailand. 23(1): 1-6.

6. J. Sudsiri and R.J. Ritchie. 2011. Effect of temperature on internal conductivity of human red blood cells. Bioelectrochemistry, (submitted)

Other Publications

1. J. Gimsa, M. Simeonova, D. Wachner, J. Sudsiri, and L. Haberland. 2002. On the influence of molecular properties on the subcellular absorption of electric field energy. Internet publication. Final Report on the Project COST281 - Potential Health Implications from Mobile Communication Systems. http://www.COST281.org/documents.php

2. J. Sudsiri, D. Wachner, J. Donath, and J. Gimsa. January 2003. Accessing molecular membrane properties of human red blood cells by electrorotation. Proceedings of the 1st Regional Symposium on Membrane Science and Technology. pp. P1-2. ISBN 974-644-342-9

Abstracts of Posters and Oral Presentations

1. J. Sudsiri, D. Wachner, M. Simeonova, J. Donath, and J. Gimsa. 2004. Effect of temperature on the electrorotation behavior of human red blood cells. Abstract of the 2nd Regional Symposium on Membrane Science and Technology. pp 103.

2. J. Sudsiri, D. Wachner, and J. Gimsa. 2005. Effect of temperature on the electrorotation behavior of human red blood cells: Implications for a transition in ion transport around 15°C. Abstract of the 3rd Regional Symposium on Membrane Science and Technology, 2005. Institut Teknologi, bundung, Indonesia, 26th-27th April.

3. J. Sudsiri, D. Wachner, and J. Gimsa. 2005. On the temperature dependence of electrorotation of human red blood cells-rotation speed transition around 15°C. Abstract of the Bioelectrochemistry and Bioenergetics of the Bioelectrochemical Society (BES) and 3rd Spring Meeting Bioelectrochemistry of the International Society of Electrochemistry (ISE), 2005, Coimbra, Portugal, 19th –24th June.

4. J. (Sdusiri) Chuaibamrung and J. Gimsa. 2008. Effect of temperature on cell volume and internal conductivity of human red blood cells. Abstract of Siam Physics Congress, 2008, Khao Yai, Nakorn Ratchasima, Thailand, 20th -22nd March.

5. J. (Sdusiri) Chuaibamrung. 2008. Temperature effect on international conductivity and cell volume of human red blood cells. Abstract of the 1st PSU Phuket Research Conference, Phuket, Thailand, 19th -21st November.

6. J. (Sdusiri) Chuaibamrung. 2009. Influence of cell shape and cell volume on cytoplasmic conductivity of human red blood cells. Proceeding of the 26th MST Annual Conference, Chiangmai, Thailand, 28th -30th January.

Seminars, Conferences, Workshops attended

1. 15th Congress on Biotechnology of Thailand, January 1996. Phuket, Thailand
2. Workshop in bioscience at The University of Science, April 1997. Penung, Malaysia
3. 25th Congress on Science and Technology of Thailand, October 1999. Pitsanulok, Thailand
4. J. Sudsiri and P. Wanichapichart. 1997. AC field frequencies for isolating five marine phytoplankton. poster presentation at the 23rd Congress on Science and Technology of Thailand, Changmai, Thailand
5. J. Sudsiri, P. Wanichapichart and D. Chukerd. 2001. Dielectrophoresis of chlorella sp. for detecting heavy metal content in water. 27th Congress on Science and Technology of Thailand, Songkla, Thailand. Oral presentation.
6. M. Simeonova, D. Wachner, J. Sudsiri, and J. Gimsa. October 2002. On the influence of the molecular composition of cellular membrane and cytoplasm on the subcellular absorption of electric field energy. 2nd international workshop on biological effects of electromagnetic fields. Rhodes. Greece. **Poster.**
7. J. Gimsa, M. Simeonova, D. Wachner, J. Sudsiri, and L. Haberland. November 2002. On the influence of molecular properties on the subcellular absorption of electric field energy. 3rd MCM and workshop “Subtitle temperature effects of RF-EMF”, COST 281, London. Great Britain. **Oral presentation.**
8. J. Sudsiri, D. Wachner, J. Donath, and J. Gimsa. January 2003. Can molecular properties of human red blood cells be accessed by electrorotation ?. 1st Regional Symposium on Membrane Science & Technology, Songkla, Thailand. **Poster.**
9. J. Sudsiri, J. Donath, and J. Gimsa. April 2004. Effect of temperature on the electrorotation behavior of human red blood cells. 2nd Regional Symposium on Membrane Science & Technology, Johor Bahru, Malaysia. 21st-25th April. **Oral presentation.**
10. J. Sudsiri, D. Wachner, M. Simeonova, J. Donath, and J. Gimsa. 2004. Effect of temperature on the electrorotation behavior of human red blood cells. Proceedings of the 2nd Regional Symposium on Membrane Science and Technology.2004. Putari Pan Pacific Hotel, Johor Bahru, Johor, Malaysia, 21st-25th April. CD
11. J. Sudsiri, D. Wachner, and J. Gimsa. April 2005. Effect of temperature on the electrorotation behavior of human red blood cells: Implications for a transition in ion transport around 15°C. 3rd Regional Symposium on Membrane Science and Technology. Institut Teknologi, bundung, Indonesia. 26th-27th April. **Oral presentation.**
12. J. Sudsiri, D. Wachner, and J. Gimsa. 2005. Effect of temperature on the electrorotation behavior of human red blood cells: Implications for a transition in ion transport around 15°C. Proceedings of the 3rd Regional Symposium on Membrane Science and Technology.2005. Institut Teknologi, bundung, Indonesia, 26th-27th April. CD.

13. J. Sudsiri, D. Wachner, and J. Gimsa. June 2005. On the temperature dependence of electrorotation of human red blood cells-rotation speed transition around 15°C. Abstract submitted to the BES-ISE 2005: XVIII International Symposium on Bioelectrochemistry and Bioenergetics-3rd Spring Meeting Bioelectrochemistry, Coimbra, Portugal, 19th-24th. **Poster presentation**

14. J. Chuaibamrung and J. Gimsa. 2008. Effect of temperature on cell volume and internal conductivity of human red blood cells. Abstract submitted to Siam Physics Congress, 2008, Khao Yai, Nakorn Ratchasima, Thailand, 20th -22nd March. **Oral presentation.**

15. J. Chuaibamrung. 2008. Temperature effect on international conductivity and cell volume of human red blood cells. Abstract submitted to the 1st PSU Phuket Research Conference, Phuket, Thailand, 19th -21st November. **Oral presentation.**

16. J. Chuaibamrung. 2009. Influence of cell shape and cell volume on cytoplasmic conductivity of human red blood cells. The 26th MST Annual Conference, Chiangmai, Thailand, 28th -30th January. **Oral presentation.**

Conference Certificates obtained

1. Certificate of presentation at the 27th Congress on Science and Technology of Thailand, Songkla, Thailand. 2001.

2. Certificate of attendance at the 2nd Regional Symposium on Membrane Science & Technology 2004, Johor Bahru, Malaysia, 23rd – 25th April 2004.

3. Certificate of presentation at the 3rd Regional Symposium on Membrane Science & Technology 2005, Bundung, Indonesia, 26th – 27th April 2005.

4. Certificate of presentation at the 26th MST Annual Conference, Chiangmai, Thailand, 28th -30th January 2009.

Language Certificates obtained

1. Certificate for the successful completion of the Basic course in German, Language Center, University of Rostock, 11. July 2002.

2. Certificate for the successful completion of the Basic course “B” in German, Language Center, University of Rostock, 08. April 2003.

3. Certificate for the successful completion of the intermediate course in German, Language Center, University of Rostock, 26. January 2004.

4. Certificate for the successful completion of the Contemporary issues in America, Language Center, University of Rostock, 8. February 2004.

5. Certificate for the successful completion the Intermediate English course for International Students, Language Center, University of Rostock, 14 July 2004.

6. Certificate for the successful completion of the Intermediate Academic English course, Language Center, University of Rostock, 21 July 2004.

Selbständigkeitserklärung

Hiermit erkläre ich, dass ich die vorliegende Arbeit selbständig und ohne fremde Hilfe verfasst und nur unter Verwendung der angegebenen Literatur und Hilfsmittel angefertigt habe.

Datum: 15 January 2011

Unterschrift:

julipom Suchiri